Study of Kerr-AdS5 spacetime from the quasi-normal modes and the catalytic effect of the vacuum decay

古賀, 一成

出版情報：Kyushu University, 2022, 博士（理学）, 課程博士
バージョン：
権利関係：

Ph.D. Dissertation

Study of Kerr-AdS$_5$ spacetime from the quasi-normal modes and the catalytic effect of the vacuum decay

Issei Koga

Department of Physics, Faculty of Science,
Kyushu University

December, 2022

Abstract

Modern cosmology can effectively explain the development of spacetime from just after the creation of the universe to the present day, in a manner consistent with many observations. On the other hand, the standard model of elementary particle theory describes some of the fundamental interactions of nature, including the strong, weak, and electromagnetic forces, and can successfully explain the high-energy phenomena observed in accelerator experiments. Although modern physics has succeeded in describing things from the microscopic scale of subatomic particles to the macroscopic scale of the current universe, there are still unsolved problems and interesting theoretical predictions.

One of these unsolved problems is the theory of quantum gravity. This has not yet been established within the framework of modern physics, although "Superstring Theory" and "Loop Quantum Gravity" have been discussed as candidates. Quantum gravity is important when considering the inflation theory, which claims that our universe was created by quantum fluctuations that produced a finite and very small spacetime, and this created spacetime was immediately expanded exponentially and rapidly. To discuss the very begging of the universe, quantum gravity is necessary because the spacetime itself is quantum in nature.

Superstring theory has been actively studied as the most promising candidate for quantum gravity theory. However, the vacuum structure of the theory is complicated, and it is difficult to construct an accelerating expanding four-dimensional (4D) de Sitter spacetime supported by observations. As one of the solutions, a method called a "bubble universe" was proposed to effectively construct a 4D de Sitter spacetime based on the vacuum decay (phase transition) of a five-dimensional (5D) spacetime. A metastable 5D anti-de Sitter (AdS) spacetime (AdS_5) is required to construct this bubble universe. In this thesis, we theoretically investigate the possibility of a metastable 5D AdS spacetime from two viewpoints: a classical analysis using quasi-normal modes and quantum analysis of the catalytic effects of vacuum decay.

We analyzed the scalar perturbations of the Kerr-AdS_5 as quasi-normal modes in a wider range using the Heun's equation. Previous study showed in the limited parameter range that there are unstable modes (amplitude of

perturbation diverge in time evolution) when the black hole mass is small. The analysis using quasi-normal modes revealed that the instability against perturbations increases when the spin parameters are asymmetric. In addition, the asymptotic behavior of the discretely distributed quasi-normal modes reveals the existence of two new types of quasi-normal modes, one of which is a resonance between the black hole horizon and AdS boundary, corresponding to the instability of the system. The other has imaginary parts aligned at intervals proportional to the temperature of the black hole, reflecting its thermodynamic properties.

In relation to the catalytic effects of vacuum decay, the presence of an object such as a black hole in a metastable vacuum promotes the vacuum decay. In this thesis we investigate the catalytic effect of the Kerr-AdS$_5$ and find that the vacuum decay is enhanced by rotation. By comparing these results with those of the above-mentioned instability studied using quasi-normal modes, it is possible to compare two time scales: the divergence time scale of the perturbation, which is a classical instability, and the lifetime of spacetime in the vacuum decay, which is a quantum phenomenon. We show that for the example parameter sets, quantum instability is larger and "bubble universe" scenario is possible even though there is a classical instability.

Acknowledgements

First I would like to thank my supervisor, Prof. Koji Harada. I would not be able to obtain my Ph.D. without his help. Discussions with him and his pointed questions have greatly advanced my research. I am also very grateful to Dr. Oshita Naritaka. He was very enthusiastic in discussing our joint research. I learned much from him, including how to behave as a researcher, and working with him was an invaluable experience.

I also express my gratitude to Prof. Yutaka Ookochi. He gave me the opportunity to begin researching the catalytic effects of vacuum decay, and I thank him for teaching me during my master and the first year of my Ph.D. studies. I am very thankful to Prof. Hiroshi Suzuki, who led the preliminary examination and gave me useful comments.

I would like to thank Mr. Kazushige Ueda for the daily discussions and the opportunity to collaborate with Dr. Oshita. While there were no colleagues in our laboratory, Mr. Ueda entered Kyushu University's Ph.D. program with a similar research theme, and we were able to spend meaningful time together discussing our work, as well as other things.

I thank other members of the Theory of Subatomic Physics and Astrophysics laboratory, including Prof. Kentaro Kojima, Prof. Shuichiro Tao, and Prof. Ken'ichiro Nakazato. The members have a wide range of research topics, and I appreciate the advice from different perspectives. In particular, I would like to thank Prof. Kojima for his support and advice on matters other than research.

I am very grateful Dr. Fumika Funatsu who provided regular counseling and was always accommodating. She supported me to the point where I was able to lead a normal research life when I was at the bottom of my condition due to the stress caused by the COVID-19 pandemic and other factors. Thank you very much.

I appreciate the financial support from the "Kuroda Scholarship Founda-

tion." They supported me for nine years from the time that I entered Kyushu University as an undergraduate student. Their support allowed me to concentrate on my research without worrying about daily life. They gave me friendly advice when I was struggling and were concerned about the progress of my research. At the regular workshop, I was able to listen to various research presentations, which stimulated and motivated me in my own research. I would like to express my gratitude once again.

Finally, I express my utmost appreciation to my entire family for helping and encouraging me in various ways related to my research and daily life.

Contents

List of Figures

List of Tables

Chapter 1

Introduction

Gravity, as one of the fundamental interactions of nature, is described by the general theory of relativity, which enables us to deal with the physics of spacetime. Modern cosmology, which has been developed based on general relativity, has been able to effectively explain the development of spacetime from the early universe to the present day, in a manner that is consistent with many observations. On the other hand, the standard model of elementary particles describes some of the fundamental interactions of nature, including the strong, weak, and electromagnetic forces, and can successfully explain the high-energy phenomena observed in accelerator experiments. Among the elementary particles proposed in the standard model, the Higgs boson was finally discovered in 2012, validating the standard model as an established theory. However, despite the successes in modern physics in terms of experiments, observations, and theories, there are still unsolved problems and interesting theoretical predictions.

The cosmic microwave background (CMB) observations by the Planck satellite[1] and other observations show us that the universe is uniformly isotropic and very flat on a macroscopic scale. To explain these observed facts, inflation is thought to have occurred[3, 4, 5, 6]. Inflation is the theory that the universe was created as a finite, very small spacetime as a result of quantum fluctuations, which exponentially expanded immediately after the creation of the universe. Although a new type of inflation has been proposed [7, 8, 9], and various models have been suggested, e.g., [10, 11, 12, 13], no one has yet reached a conclusion, which is one of the open questions of modern

[1]The paper [2] is the final result of the Planck satellite's observations.

physics. Furthermore, at the moment that the seed of the spacetime that caused the inflation to emerge, it is believed that the spacetime itself had a quantum characteristic. Thus, this spacetime is inevitably treated with a theory beyond general relativity, i.e., quantum gravity. Therefore, it is necessary to discuss the very beginning of the universe based on the quantum gravity theory, but it has not yet been established within the framework of modern physics. "Superstring theory" and "loop quantum gravity" are discussed as candidates.

Superstring theory has been actively studied as the most promising candidate for the quantum gravity theory, but the vacuum structure of the theory is complicated and difficult to use in constructing an accelerated expanding four-dimensional (4D) de Sitter spacetime that is supported by observations [14, 15]. In addition, some studies suggest the existence of a tremendous number of vacuua [16, 17]. Therefore, it is believed that "something" is needed to connect string theory and our universe. Several models such as KKLT [18] and large volume scenarios (LVS) [19] have been considered, and recently there has been much discussion on the topics of the "Swampland program," e.g., the distance conjecture, weak gravity conjecture, de Sitter conjecture, and trans-Planckian censorship conjecture [20, 21, 22, 23, 24], but the issue has not yet been settled. As "something" is needed to connect string theory and our universe, a proposal was made to construct a 4D deSitter spacetime starting with a 5D metastable anti-de Sitter (AdS_5) spacetime through the vacuum decay (i.e., pjase transition) of this 5D spacetime, instead of creating a 4D de Sitter spacetime from the beginning [25]. The vacuum decay begins with the appearance of a bubble filled with a true vacuum in a metastable spacetime, and the decay proceeds as the bubble expands.

The surface of the bubble in 5D spacetime has four dimensional, and the equation explaining how this bubble expands is determined by the Israel junction conditions [26], which successfully connect spacetime before and after the decay. The "bubble spacetime" was proposed because the equation of motion that this bubble follows has the same form as the Friedman equation for the de sitter spacetime, and the spacetime that is an accelerated expansion in four dimensions can be created effectively on the surface of the bubble in this way.

A metastable AdS_5 is required to construct this bubble spacetime, and the original setup of this bubble spacetime [25] assumes the existence of black holes and a cloud of strings. In addition, a pure AdS spacetime is known to be non-linearly unstable and is eventually believed to form a black hole

[27, 28], so the vacuum decay with black hole is a realistic situation and also in general, black hole can be rotating. For these reasons, we theoretically investigate the possibility of the AdS_5 spacetime, which is the premise of the bubble spacetime setup, with a rotating black hole from two viewpoints: a classical analysis using quasi-normal modes and a quantum analysis of the catalytic effect of vacuum decay.

1.1 Quasi-Normal Modes of Black Holes

Because the AdS spacetime has a potential barrier at infinity, a black hole in it can be regarded as being trapped inside a box. On the other hand, it is known that a rotating black hole has the property of superradiance [29, 30, 31, 32], in which an incident wave is amplified by the black hole. Therefore, if we consider a perturbation of a rotating black hole in AdS spacetime, the perturbation is amplified by the black hole. It is then reflected at the AdS boundary (the surface of the box), amplified again by the black hole, and so on. It is known that this process will eventually cause the amplitude of the wave produced by the perturbation to diverge, and spacetime itself will become unstable to the perturbation [33]. In particular, we introduce a rotating black hole in a 5D AdS spacetime (Kerr-AdS_5) and investigate the perturbation of a scalar field with respect to this spacetime using the method of quasi-normal modes. In the case of a black hole with a small mass and limited parameter range, the quasi-normal modes of Kerr-AdS_5 are known to have unstable modes (modes that grows indefinitely in time) [34, 35, 36, 37, 38], but we have analyzed them in a wider region using the Heun equation method [39]. Quasi-normal modes have an infinite number of discrete eigenfrequencies and satisfy the boundary conditions. Whether or not the spacetime is stable against perturbation can be determined by the sign of the imaginary part of the complex quasi-normal frequency.

As a theoretical feature of quasi-eigenfrequencies, it is known that the real part of the quasi-eigenfrequencies of 4D black holes asymptotically approaches a certain value [40, 41]. It has been suggested that this value is related to the area quantization of the black hole [42]. Furthermore, the relationship between this value and loop quantum gravity has been discussed [43, 44]. Regarding the ADS/CFT correspondence [45, 46], it has also been shown that there is a correspondence between the periodicity of the quasi-normal modes of a BTZ black hole, a rotating black hole solution in a three-

dimensional (3D) AdS spacetime, and the pole of Green's function of the dual CFT [47]. Thus, various studies have suggested that quasi-normal modes are not only an aspect of simple perturbation solutions, but are also related to modern physics problems such as the quantum gravity theory. In this thesis, we discuss not only the stability of spacetime, but also these theoretical features.

1.2 Catalysis Effect of the Vacuum Decay

A metastable vacuum, which is a local minimum of potential, is known to decay into a true vacuum in finite time [48, 49, 50], and the existence of an object such as a black hole in this metastable vacuum enhances the vacuum decay, which is the so-called catalytic effect of the vacuum decay. This phenomenon was first discussed for a non-rotating Schwarzschild black hole in 4D spacetime [51, 52, 53, 54], and has been extended to the case of a rotating black hole in four dimensions [55, 56] and rotating black hole in three dimensions [57]. In relation to the 4D aspects of catalysis, the instability of a Higgs vacuum has been discussed in some papers [58, 59, 60]. In this thesis, we first extend the analysis of the catalytic effects of the vacuum decay to a 5D case and investigate the catalytic effects of black holes and a cloud of strings [61], the existence of which were assumed in the bubble spacetime setup [25]. We also discuss the catalysis by quintessence in five dimensions [62]. Then, we investigate the catalytic effect of a rotating black hole in the AdS_5 spacetime, which is used in the bubble spacetime setup, and find that the rotation enhances the vacuum decay [63].

1.3 Organization of This Thesis

The thesis is organized as follows. In Chap. 2, we provide a review of the vacuum decay and catalysis effect, showing the Schwarzschild catalysis in four dimensions. We also briefly review the bubble universe setup. In Chap. 3, we also provide a review of the quasi-normal modes and use of Heun's equation method to solve the perturbation. Then, Chap. 4 shows how we investigated the catalysis of black holes, including a Kerr-AdS_5 black hole, cloud of strings, and a time-varying scalar field. Chap. 5 shows how we studied the quasi-normal modes of Kerr-AdS_5, instability due to superradiance, and thermal

and other properties of quasi-normal modes. Finally, we conclude this thesis in Chap. 6.

Chapter 2

Catalytic Effect of Vacuum Decay

This chapter reviews vacuum decay and catalytic effect. We start with the decay in one-dimensional quantum mechanics, which is extended to field theory and finally to the case with gravity. The rate of a vacuum decay can be estimated by the WKB method, i.e., through the Euclidean on-shell action. Then, we include a black hole and evaluate the catalytic effect of the black hole and reproduce the known results [51, 52, 53, 54]. Then, we consider the case in five dimensions. We simply consider the junction surface of five-dimensional decay and derive the equation of motion of a bubble universe from the junction conditions. We also confirm that the effective cosmological constant for the bubble universe can be positive, and the equation has terms that correspond to those for the radiation and matter contributions in the Friedmann equation.

2.1 Tunneling in One-dimensional Quantum Mechanics

As a first step to explain the vacuum decay, it is useful to start with the tunneling from a false vacuum to a true vacuum in one-dimensional quantum mechanics. Here we assume that the Hamiltonian is give by:

$$H = \frac{p^2}{2m} + V(q), \tag{2.1.1}$$

where the potential is assumed to have the shape shown in Fig. 2.1, and particle energy E is lower than the maximum point of the potential. In classical mechanics, a particle never penetrates the potential when the energy is lower than maximum value of the potential. However, a particle can penetrate the potential in quantum mechanics. The transition rate of this penetration is computed using a semi-classical approximation called the WKB approximation, where the rate Γ can be expressed as follows:

$$\Gamma = Ae^{-B/2}, \qquad B = 2\int_{q_1}^{q_2} \sqrt{2m\left(V(q) - E\right)}, \tag{2.1.2}$$

where q_1 and q_2 are the classical turning points that satisfy the relation $V(q_1) = V(q_2) = E$, and pre-factor A has the dimension of the inverse time and is not determined by a semi-classical approximation. Loop corrections and zero modes contribute to this factor.

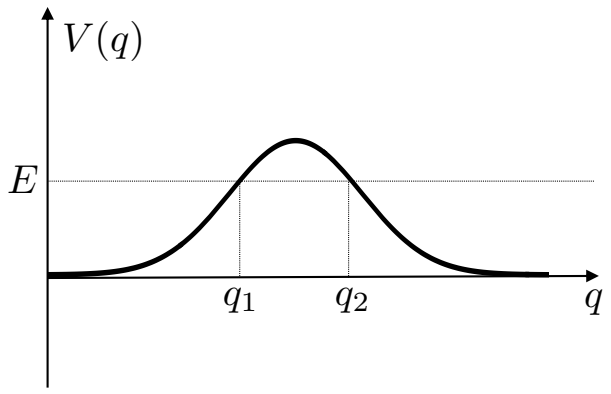

Figure 2.1: Plot of one-dimensional potential with potential barrier, where q_1 and q_2 are points $V(q_1) = V(q_2) = E$.

2.2 Tunneling in Many Degrees of Freedom

This subsection extends the one-dimensional case to a case with many degrees of freedom. When the system has N degrees of freedom and the coordinates

are expressed as $q_1, q_2 \cdots, q_N$, the Lagrangian is given by:

$$\begin{aligned} L &= \frac{1}{2}\sum_{i=1}^{N}\left(\frac{dq^i}{dt}\right)^2 - V(q_1, q_2, \cdots, q_N) \\ &= \frac{1}{2}\left(\frac{d\mathbf{q}}{dt}\right)^2 - V(\mathbf{q}). \end{aligned} \tag{2.2.1}$$

In the one-dimensional case, a unique tunneling path is determined. However, in the case with many degrees of freedom, a path that maximizes the tunneling rate is selected from a tremendous number of candidate paths that connect the initial and final points [64, 65]. To investigate this path, we here introduce a parameter s for the path $\mathbf{q}(s)$, with the definition:

$$ds^2 = \sum_{i=1}^{N}(dq^i)^2 \equiv d\mathbf{q}^2. \tag{2.2.2}$$

The initial and final tunneling points are expressed as $\mathbf{q}_i = \mathbf{q}(0)$ and $\mathbf{q}_f = \mathbf{q}(s_f)$, respectively, and the path dependent tunneling factor is found as follows:

$$B_{\text{path}} = 2\int_0^{s_f} ds\sqrt{2\left(V(\mathbf{q}(s)) - E\right)}. \tag{2.2.3}$$

It is difficult to find the path that minimizes this factor for the N variables case, but Coleman showed that the Euclidean action is useful for solving this problem [48]. The Euclidean action is derived by replacing time variable t with imaginary time τ,

$$t \to i\tau. \tag{2.2.4}$$

Then, under this coordinate change, the action is transformed to:

$$S_E = \int_{\tau_0}^{\tau_f} d\tau \left(\frac{1}{2}\left(\frac{d\mathbf{q}}{d\tau}\right)^2 + V(\mathbf{q})\right), \tag{2.2.5}$$

where subscript E denotes that it is Euclidean. The equation of motion for this Euclidean action is as follows:

$$\frac{d^2 q_i}{d\tau^2} = \frac{\partial V}{\partial q_i}. \tag{2.2.6}$$

This equation can be used to obtain the following:

$$\frac{d}{d\tau}\left(\frac{d\bar{q}_i}{d\tau}\right)^2 = 2\frac{\partial V}{\partial \tau} \tag{2.2.7}$$

$$\left(\frac{d\bar{q}_i}{d\tau}\right)^2 = 2\left(V(\bar{q}_i) - V(q_0)\right) = 2\left(V(\bar{q}_i) - E\right) \tag{2.2.8}$$

where $E = V(q_0), (dq_i/d\tau)|_{\tau=\tau_0} = 0$ and $\bar{\mathbf{q}}(s)$ is the solution of the equation, which we call a bounce solution. Then, we substitute the solution (2.2.8) into the Euclidean action (2.2.5) and obtain the on-shell action:

$$\begin{aligned} S_E|_{\mathbf{q}=\bar{\mathbf{q}}} &= \int_{\tau_0}^{\tau_f} d\tau \left(V(\bar{\mathbf{q}}) - V(\mathbf{q}_0)\right) + V(\mathbf{q}) \\ &= \int_{\tau_0}^{\tau_f} d\tau 2\left(V(\bar{\mathbf{q}}) - V(\mathbf{q}_0)\right) + \int_{\tau_0}^{\tau_f} d\tau V(\mathbf{q}_0) \\ &= \int_{\tau_0}^{\tau_f} d\tau \sqrt{\left(\frac{d\bar{\mathbf{q}}}{d\tau}\right)^2}\sqrt{2\left(V(\bar{\mathbf{q}}) - V(\mathbf{q}_0)\right)} + \int_{\tau_0}^{\tau_f} d\tau V(\mathbf{q}_0) \\ &= \int_0^{s_f} ds \sqrt{2\left(V(\bar{\mathbf{q}}) - V(\mathbf{q}_0)\right)} + \int_{\tau_0}^{\tau_f} d\tau V(\mathbf{q}_0). \end{aligned} \tag{2.2.9}$$

Based on the principle of least action, the first term in (2.2.9) is the integration of the path that minimizes it, and this is the desired path for (2.2.3). Based on this, we denote the minimum tunneling factor, $B_{\min} = B$, as the bounce action:

$$B = S_E|_{\mathbf{q}=\bar{\mathbf{q}}} - \int_{\tau_0}^{\tau_f} d\tau V(\mathbf{q}_0), \tag{2.2.10}$$

In this way, using the Euclidean action, we can easily find the desired path, and the tunneling factor is derived by evaluating the Euclidean on-shell action.

2.3 Decay in Field Theory

The last two sections reviewed the decay in quantum mechanics. This section will consider the decay in the field theory. Here, weconsider a 4D scalar theory with the Lagrangian:

$$\mathcal{L} = \frac{1}{2}\partial_\mu \phi \partial^\mu \phi - V(\phi), \tag{2.3.1}$$

where the potential has two minima, as seen in Fig. 2.2, with the lower one called the true vacuum and the other called the false vacuum. The false

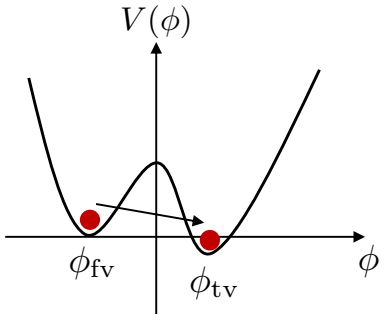

Figure 2.2: Plot of potential $V(\phi)$ with two minima. The lower minimum is called the true vacuum and the other the false vacuum. The false vacuum decays to the true vacuum via a tunneling process.

vacuum decays into the true vacuum via a tunneling process, and we can discuss the tunneling phenomena using an analogy to the previous quantum mechanics case. In particular, in the field theory, the decay rate is evaluated using the Euclidean on-shell action:

$$\Gamma = Ae^{-B}, \qquad B = S_E(\phi) - S_E(\phi_{\rm fv}), \qquad S_E = \int d^4x \frac{1}{2}(\partial_\mu \phi)^2 + V(\phi), \tag{2.3.2}$$

where $S_E(\phi)$ is the on-shell Euclidean action and

$$S_E(\phi_{\rm fv}) = \int dx^4 V(\phi_{\rm fv}). \tag{2.3.3}$$

These formulas correspond to those derived in the last section, (2.2.10). The equation of motion of the scalar field is written as follows:

$$\left(\frac{\partial^2}{\partial \tau^2} + \nabla^2\right)\phi - \frac{dV}{d\phi} = 0. \tag{2.3.4}$$

The classical solution for this equation which satisfies the boundary conditions:

$$\lim_{\tau \to \pm\infty} \phi(\tau, \mathbf{x}) = \phi_{\rm fv}, \qquad \lim_{|\mathbf{x}| \to \infty} \phi(\tau, \mathbf{x}) = \phi_{\rm fv}, \tag{2.3.5}$$

is called the bounce solution. The first condition corresponds that the initial and final state of the solution is $\phi_{\rm fv}$, and the second condition is used to make the potential energy finite at all the tunneling paths measured from the false vacuum. In addition, the kinetic energy of the field is zero at the initial and final points, and at turning point $\tilde{\tau}$:

$$\frac{\partial\phi}{\partial\tau}|_{\tau_i,\tau_f,\tilde{\tau}} = 0. \tag{2.3.6}$$

Based on the conditions (2.3.5), the bounce solution has O(4) invariance, and we imposes the O(4) symmetry on the solution[1]. The action can be express using one parameter, ρ:

$$S_E = 2\pi^2 \int_0^\infty d\rho\rho^3 \frac{1}{2}(\phi')^2 + V(\phi), \qquad \rho = \sqrt{r^2 + x^2}. \tag{2.3.7}$$

Fig. 2.3 shows a schematic representation of the O(4) symmetric bounce solution. The boundary condition (2.3.5) and field constraint (2.3.6) are

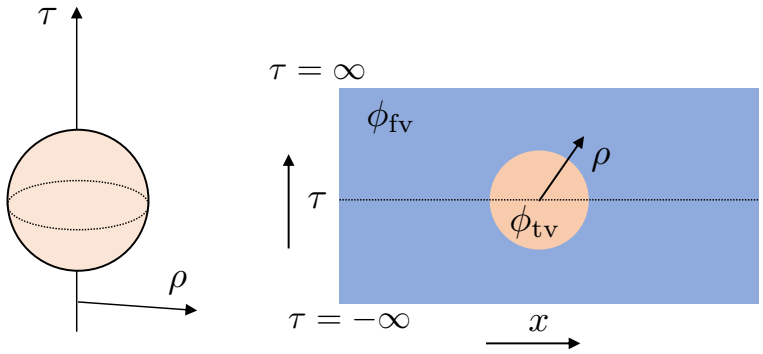

Figure 2.3: A schematic picture of O(4) symmetric bounce. It may be viwed as a ball in EUcledean spacetime.

reduced to:

$$\phi(\infty) = \phi_{\rm fv}, \quad \phi'(0) = 0, \tag{2.3.8}$$

where prime denotes the derivative with respect to ρ. Then, the equation of motion is shown as follows:

$$\phi'' + \frac{3}{\rho}\phi' - \frac{dV}{d\phi} = 0. \tag{2.3.9}$$

[1]Indeed the bounce solution is shown to always be O(4) symmetric [66].

Fig. 2.4 shows the classical solution of this Euclidean equation of motion. Here, we assume that the potential is derived from even function $V_0(\phi)$, plus

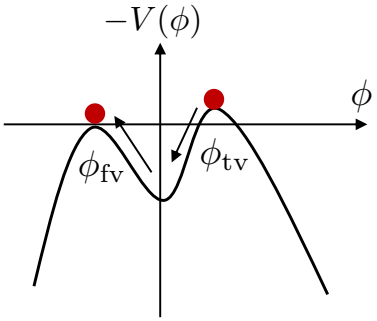

Figure 2.4: Plot of $-V(\phi)$ and the motion of the classical solution of Euclidean equation of motion. It starts at the true vacuum. At a certain instant, it begins to move along the potential slope and stops at the false vacuum.

the small energy difference, ϵ, between the true and false vacua:

$$V(\phi) = V_0(\phi) + O(\epsilon), \tag{2.3.10}$$

where ϵ is the energy difference, as seen in Fig. 2.5:

$$V(\phi_{\rm fv}) - V(\phi_{\rm tv}) = \epsilon. \tag{2.3.11}$$

If the potential barrier between the false and true vacua is sharp enough

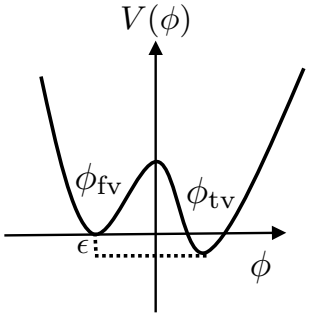

Figure 2.5: Plot of the double well potential (2.3.11), where the difference between two local minima is ϵ.

for the field to move quickly, the time scale for the field transition is much

shorter than the time that the field stays at the initial state. In this situation, the second term $3\phi'/\rho$ in (2.3.9) is negligible and the field is regarded to start at true vacuum ($\phi(0) = \phi_{\rm fv}$). Then, the equation of motion is obtained at the 0-th order of ϵ,

$$\phi'' - \frac{dV_0}{d\phi} = 0, \tag{2.3.12}$$

and integrating this equation produces:

$$\left(\frac{1}{2}\phi'^2 - V_0\right)' = 0. \tag{2.3.13}$$

The boundary condition at the true and false vacua gives the integration constant:

$$\frac{1}{2}(\phi')^2 - V_0(\phi) = -V_0(\phi_{\rm tv}) = -V_0(\phi_{\rm fv}), \tag{2.3.14}$$

which can be used to obtain:

$$\phi' = \Big[2\left(V_0(\phi) - V_0(\phi_{\rm fv})\right)\Big]^{1/2}. \tag{2.3.15}$$

Integrating this we obtai:

$$\int_{(\phi_{\rm fv}+\phi_{\rm tv})/2}^{\phi} d\phi \Big[2\left(V_0(\phi) - V_0(\phi_{\rm fv})\right)\Big]^{-1/2} = \rho - R, \tag{2.3.16}$$

where R is the point where the field seems to vary rapidly from the false to true vacuum and satisfies the following condition: $\phi(R) = (\phi_{\rm fv} + \phi_{\rm tv})/2$. Again the assumption just before (2.3.12) is interpreted as R being sufficiently large compared to the length scale of the transition of ϕ. In the Euclidean spacetime, this transition (bounce solution) is seen as a thin wall that separates two regions, the false and true vacua. This assumption is called the "thin-wall approximation." Let us return to the bounce action, (2.3.2) and (2.3.3), which can be divided into three parts, outside the wall, inside the wall, and the wall itself:

$$B_{\rm outside} = 0, \tag{2.3.17}$$

$$B_{\rm inside} = \frac{\pi^2}{2}R^4(V(\phi_{tv}) - V(\phi_{fv})) = -\frac{\pi^2}{2}R^4\epsilon, \tag{2.3.18}$$

$$B_{\rm wall} = 2\pi^2 R^3 \int d\rho \Big[\frac{1}{2}\phi'^2 + V_0(\phi) - V_0(\phi_{\rm fv})\Big] = 2\pi^2 R^3\sigma, \tag{2.3.19}$$

where we define the wall tension σ as:

$$\sigma = 2\int d\rho\Big[V_0(\phi) - V_0(\phi_{\rm fv})\Big] = \int_{\phi_{\rm tv}}^{\phi_{\rm fv}} d\phi\Big[2\left(V_0(\phi) - V_0(\phi_{\rm fv})\right)\Big]^{1/2}. \quad (2.3.20)$$

The bounce action is derived by summing these three parts:

$$B = -\frac{\pi^2}{2}R^4\epsilon + 2\pi^2 R^3\sigma. \quad (2.3.21)$$

The minimum value of this action is obtained by solving:

$$\frac{dB}{dR} = -2\pi R^3\epsilon + 6\pi^2 R^2\sigma = 0. \quad (2.3.22)$$

Then, the bounce action takes the minimum value at

$$R = 3\sigma/\epsilon, \quad (2.3.23)$$

and the minimum value is derived as follows:

$$B_{\rm min} = \frac{27\pi^2\sigma^4}{2\epsilon^3}. \quad (2.3.24)$$

This result indicates that when the energy difference, ϵ, is fixed at a small value, the potential information in the bounce action can be expressed by one parameter, σ. Here, we consider an example potential:

$$V(\phi) = V_0(\phi) + \epsilon\frac{\phi + a}{2a} \quad (2.3.25)$$

$$V_0(\phi) = \frac{\lambda}{4}(\phi^2 - a^2)^2, \quad (2.3.26)$$

where $-a = \phi_{\rm fv}, a = \phi_{tv}, V_0(\pm a) = 0$, and (2.3.15) is solved as follows:

$$\frac{d\phi}{d\rho} = \pm\sqrt{\frac{\lambda}{2}}\left(\phi^2 - a^2\right). \quad (2.3.27)$$

On the basis of the boundary condition, the lower sign is the right choice. Then, the solution is obtained as follows:

$$\phi(\rho) = -a\tanh\left(\sqrt{\frac{\lambda}{2}}a(\rho - R)\right), \quad (2.3.28)$$

where R is the integration constant determined by the condition $\phi(R) = (\phi_{fv} + \phi_{tv})/2$. Thus, the solution behaves as follows:

$$\phi(\rho) = \begin{cases} a & (0 < \rho \ll R) \\ \phi(\rho) & \rho \approx R \\ -a & R \ll \rho \end{cases} . \tag{2.3.29}$$

Where the solution is constant except for a small region around $\rho \approx R$. We draw the potential and the solution for several values of parameters in Fig. 2.6. We see that when the potential has a sharp barrier, the solution rapidly changes and the thin-wall approximation is good.

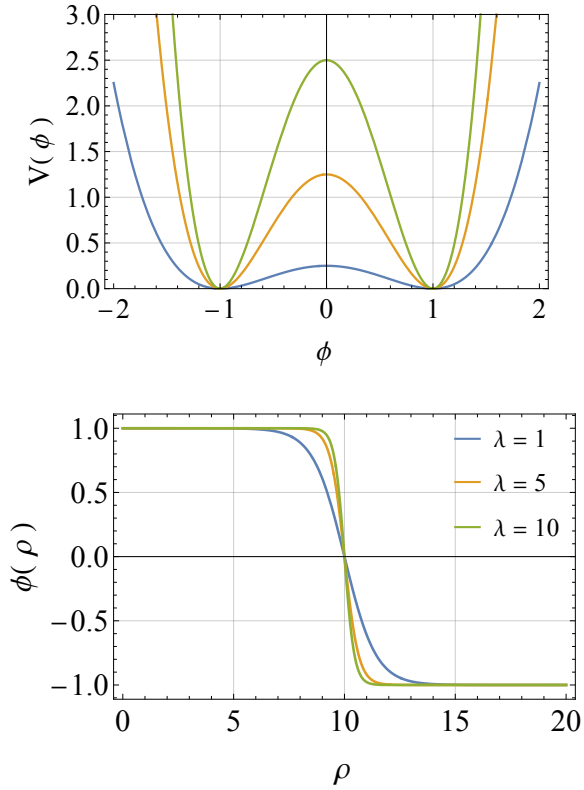

Figure 2.6: Plot of the potential and the bounce solution for several values of parameters. Parameters are set to $a = 1, R = 10$, and $\lambda = 1, 5, 10$. Note that the selection of these values does not necessarily reflect the realistic situations.

2.3.1 Wall Dynamics after Tunneling

We discussed the tunneling rate based on the field theory, and here we look at the tunneling from the viewpoint of Minkowski spacetime. The bounce solution has O(4) symmetry in Euclidean space, and we assume that the thin-wall bubble materializes in Minkowski spacetime at $t = 0$. We need to analytically continue from Euclidean space to Minkowski spacetime and we choose the point where the field satisfies the following conditions:

$$\frac{\partial\phi}{\partial\tau} = 0, \quad \frac{\partial\phi}{\partial t} = 0. \tag{2.3.30}$$

Then, after it materializes in Minkowski spacetime, the O(4) symmetry is reduced to O(3,1), and the wall trajectory is hyperboloid as seen in Fig. 2.7,

$$R^2 = -t^2 + |x|^2. \tag{2.3.31}$$

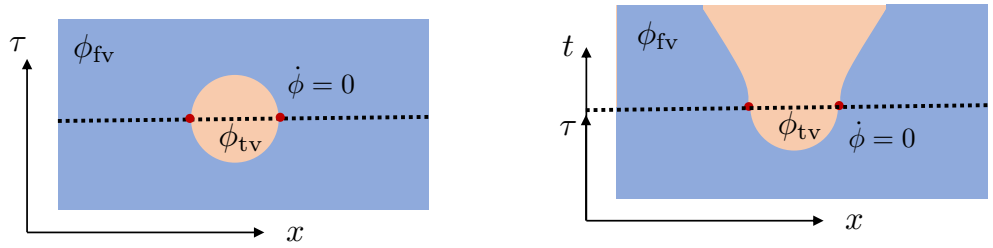

Figure 2.7: An Euclidean O(4) symmetric bounce solution of Fig. 2.3 is analytically continued to a Lorentzian one at the time where $\partial\phi/\partial\tau = \partial\phi/\partial t = 0$. The trajectory of the wall is hyperboloid after the continuation.

2.4 Decay with Gravity

So far we have discussed the vacuum decay using quantum mechanics and field theory, and found that the Euclidean action method is useful for estimating its decay rate. In this section, we focus on the decay with gravity. The most significant difference that arises in the presence of gravity is related to the vacuum energy. In a theory without gravity, the relative values of the two vacua are meaningful, but in the case with gravity, the vacuum energy

itself is coupled to gravity and thus important. The Lagrangian with gravity is shown as follows:

$$S(\phi, g_{\mu\nu}) = \frac{1}{16\pi G}\int dx^4\sqrt{-g}\,(R-2\Lambda) + \int dx^4\sqrt{-g}\left(-\frac{1}{2}g^{\mu\nu}\partial_\mu\phi\partial^\nu\phi - V(\phi)\right), \tag{2.4.1}$$

$$= \frac{1}{16\pi G}\int dx^4\sqrt{-g}\,(R-2\Lambda) + \int dx^4\sqrt{-g}\mathcal{L}_m(g_{\mu\nu},\phi) \tag{2.4.2}$$

where R is the Ricci scalar, $g_{\mu\nu}$ is the spacetime metric, g is the determinant of the metric, and $\mathcal{L}_m$ is the Lagrangian of the matter field. The Einstein equation for this action is derived as follows:

$$R_{\mu\nu} - \frac{1}{2}Rg_{\mu\nu} + \Lambda g_{\mu\nu} = 8\pi G T_{\mu\nu}, \tag{2.4.3}$$

where Λ is the cosmological constant. We consider the decay from the false vacuum to the true vacuum, where the bubble wall that separates the two vacua acts as a junction surface between the two geometries because the vacuum energy is related to the spacetime geometry, and the inside and outside geometries are quite different.

2.4.1 Junction of spacetime

Before evaluating the Euclidean action, we introduce the junction condition of spacetimes [26]. Here, we assume that there are two spacetimes which are spherically symmetric, $x^\mu = \{t, r, \theta, \phi\}$,

$$ds_\pm^2 = g_{\mu\nu\,\pm}dx_\pm^\mu dx_\pm^\nu = -f_\pm(r_\pm)dt^2 + \frac{dr_\pm^2}{f_\pm(r_\pm)} + r_\pm^2 d\Omega_{2\pm}^2, \tag{2.4.4}$$

where $d\Omega_{2\pm}^2 = d\theta_\pm^2 + \sin\theta_\pm^2 d\phi_\pm^2$. The two different spacetimes are separated by a thin wall, Σ:

$$\Sigma = \{x^\mu : t = T(\lambda),\ r = R(\lambda)\}, \tag{2.4.5}$$

where the subscripts $\pm$ denote the two different spacetimes inside $(-)$ and outside $(+)$ of wall respectively, and λ is the proper time on the wall. Then, the induced metric γ_{ij} on the wall is found as follows:

$$ds_\Sigma^2 = \gamma_{ij}dy^i dy^j = \Big[-f_\pm(R)\left(\frac{dt_\pm}{d\lambda}\right)^2 + \frac{1}{f_\pm(R)}\left(\frac{dr_\pm}{d\lambda}\right)^2\Big]d\lambda^2 + R^2(\lambda)d\Omega_2^2. \tag{2.4.6}$$

The junction condition known as the "Israel Junction condition" is derived from the requirement that the Einstein equation be satisfied even on the wall:

$$\gamma_{ij}{}_{+} = \gamma_{ij}{}_{-} = \gamma_{ij}, \qquad \text{(First junction condition)}, \tag{2.4.7}$$

$$K_{ij}{}_{+} - K_{ij}{}_{-} = -8\pi G\left(S_{ij} - \frac{1}{2}\gamma_{ij}S\right) \qquad \text{(Second junction condition)}, \tag{2.4.8}$$

where $K_{ij}{}_{\pm}$ is the extrinsic curvature of each surface of the wall, and S_{ij} is the reduced energy momentum tensor defined on the wall,

$$\lim_{\delta\to 0}\int_{R-\delta}^{R+\delta} T_{ij}dr = S_{ij}. \tag{2.4.9}$$

We normalize the induced metric,

$$f_{\pm}(R)\left(\frac{dt_{\pm}}{d\lambda}\right)^2 - \frac{1}{f_{\pm}(R)}\left(\frac{dr_{\pm}}{d\lambda}\right)^2 = 1, \tag{2.4.10}$$

and introduce the normal vector on the wall,

$$n_{\pm\mu} = \left(\mp\frac{dR}{d\lambda}, \pm\frac{dt}{d\lambda}, 0, 0\right) = (\mp\dot{R}, \pm\dot{t}, 0, 0), \tag{2.4.11}$$

where the extrinsic curvature is expressed using this n_{μ},

$$K_{ij}{}_{\pm} = \frac{\partial x^{\alpha}_{\pm}}{\partial y^{i}}\frac{\partial x^{\beta}_{\pm}}{\partial y^{j}}\nabla_{\alpha}n_{\beta}{}_{\pm}, \tag{2.4.12}$$

with ∇ being a covariant derivative. Explicitly $K_{\theta\theta}$ is written as:

$$K_{\theta\theta}{}_{\pm} = \frac{\partial x^{\alpha}_{\pm}}{\partial\theta}\frac{\partial x^{\beta}_{\pm}}{\partial\theta}\nabla_{\alpha}n_{\beta}{}_{\pm} \tag{2.4.13}$$

$$= \frac{\partial n_{\theta}{}_{\pm}}{\partial\theta} - \Gamma^{\lambda}_{\eta\eta}n_{\lambda}{}_{\pm} \tag{2.4.14}$$

$$= f_{\pm}(R)R\dot{t}_{\pm}. \tag{2.4.15}$$

Next, we substitute this formula into the second junction condition (2.4.8), and obtain:

$$\frac{1}{R}\left(f_{+}(R)\dot{t}_{+} - f_{-}(R)\dot{t}_{-}\right) = -4\pi G_4\sigma, \tag{2.4.16}$$

where we define the wall as having uniform tension,

$$S_{ij} = -\gamma_{ij}\sigma. \tag{2.4.17}$$

Then, combining (2.4.10) and (2.4.16), we obtain:

$$\left(\frac{\dot{R}}{R}\right)^2 = 4\pi^2 G^2\sigma^2 - \frac{f_+(R)+f_-(R)}{2R^2} + \frac{\left(f_+(R)-f_-(R)\right)^2}{32\pi^2G^2\sigma^2R^2}, \tag{2.4.18}$$

where we used:

$$4\pi^2G^2\sigma^2 = \frac{1}{4}(-4\pi G\sigma)^2 = \frac{1}{4R^2}(f_+(R)\dot{t}_+ - f_-(R)\dot{t}_-)^2. \tag{2.4.19}$$

Equation (2.4.18) can be regarded as an equation of motion of the bubble wall:

$$\dot{R}^2 + V_{\text{eff}}(R) = 0, \tag{2.4.20}$$

where $V_{\text{eff}}(R)$ is the effective potential of the wall,

$$V_{\text{eff}}(R) = -4\pi^2G^2\sigma^2R^2 + \frac{f_+(R)+f_-(R)}{2} + \frac{\left(f_+(R)-f_-(R)\right)^2}{32\pi^2G^2\sigma^2}. \tag{2.4.21}$$

Thus, we have obtained the equation of motion of the spherical symmetric bubble that separates the two spacetimes, and the next step is to analyze the wall dynamics in Euclidean spacetime.

2.4.2 Thin-wall Dynamics in Euclidean Spacetime

In the last section, we derived the equation of motion of the bubble wall in the spherical symmetric spacetime, but the metric was not specified. That is, $f_\pm(r_\pm)$ was not specified. In this section, we specify the false and true vacuum metric. Then, by performing a coordinate change from $t \to i\tau$, we obtain the equation of motion for the Euclidean. Under this transformation, other variables also change: $\dot{R}^2 \to -\dot{R}_E^2$, $\dot{t} \to \dot{\tau}$. Thus, the equation of motion, (2.4.20), is transformed as follows:

$$\dot{R}^2 - V_{\text{eff}}(R) = 0. \tag{2.4.22}$$

We choose the vacuum metric:

$$f_{\pm}(r) = 1 - \frac{\Lambda_{\pm} r^2}{3}, \tag{2.4.23}$$

where $\Lambda_{\pm}$ is the cosmological constant of each vacuum. It corresponds to the potential energy of the scalar field, and satisfies the relation $\Lambda_- < \Lambda_+$. Note that there is a cosmological horizon at $r = \sqrt{3/\Lambda_{\pm}}$. Then, substituting the metric into (2.4.21), we obtain the equation of motion:

$$\left(\frac{d\tilde{R}}{d\tilde{\lambda}}\right)^2 = 1 - \tilde{R}^2, \tag{2.4.24}$$

where we introduce the following parameters for notational simplicity:

$$\bar{\sigma} = 2\pi G\sigma, \quad l^2 = \frac{3}{\Lambda_+ - \Lambda_-}, \quad \gamma = \frac{4\bar{\sigma} l^2}{1 + 4\bar{\sigma}^2 l^2}, \tag{2.4.25}$$

$$\alpha^2 = 1 + \frac{3\Lambda_- \gamma^2}{3}, \quad \tilde{R} = \frac{\alpha R}{\gamma}, \quad \tilde{\lambda} = \frac{\alpha \lambda}{\gamma}, \quad \tilde{\tau} = \frac{\alpha \tau}{\gamma}. \tag{2.4.26}$$

We want to evaluate the Euclidean action, where the equation of the bubble wall is

$$\left(\frac{d\tilde{R}_E}{d\tilde{\lambda}}\right)^2 = \tilde{R}_E^2 - 1. \tag{2.4.27}$$

The solution of (2.4.27) is $\tilde{R} = \cos\tilde{\lambda}$, which is the bounce solution for this case. Once we obtain the bounce solution, we can evaluate the Euclidean action and derive the bounce action. The action can be divided into four parts: those near the horizon ($\mathcal{H}$), at the wall itself ($\mathcal{W}$), and inside and outside the region ($\mathcal{M}_+$ and $\mathcal{M}_-$, respectively).

$$S_E = S_{\mathcal{W}} + S_{\mathcal{H}} + S_{\mathcal{M}_+} + S_{\mathcal{M}_-}, \tag{2.4.28}$$

where

$$S_{\mathcal{M}_\pm} = -\frac{1}{16\pi G_5}\int_{\mathcal{M}_\pm} dx^4\sqrt{g}R - \int_{\mathcal{M}_\pm} dx^4\sqrt{g}\mathcal{L}_m + \frac{1}{8\pi G}\int_{\mathcal{W}} dx^3\sqrt{\gamma}K_\pm, \tag{2.4.29}$$

$$S_{\mathcal{W}} = -\int dx^4\sqrt{g}\mathcal{L}_m = -\int_{\mathcal{W}} dx^3\sqrt{\gamma}\Big\{\lim_{\delta\to 0}\int_{R-\delta}^{R+\delta}\mathcal{L}_m dr\Big\} = \int_{\mathcal{W}} dx^3\sqrt{\gamma}\sigma. \tag{2.4.30}$$

Here we added the Gibbons Hawking boundary terms. The action near the horizon is difficult to treat in Euclidean spacetime, but Gregory et al. showed that the contribution of the horizon is replaced by that of its area [53]:

$$S_{\mathcal{H}} = -\sum_i \frac{\mathcal{A}_i}{4G}, \tag{2.4.31}$$

where $\mathcal{A}_i$ is the area of the horizon. In de Sitter spacetime, there is only one horizon, the cosmological horizon. Using Arnowitt-Deser-Misner (ADM) decomposition [67] the bulk part of the action, (2.4.29), is reduced to:

$$S_{\mathcal{M}_\pm} = -\frac{1}{16\pi G}\int_{\mathcal{M}} dx^4\sqrt{g}(R + 16\pi G\mathcal{L}_m) + \frac{1}{8\pi G}\int_{\mathcal{W}} dx^3 K_\pm \tag{2.4.32}$$

$$= -\frac{1}{16\pi G}\int_0^\beta d\tau \int_{\Sigma_\tau} dx^3\sqrt{\gamma}\left({}^{(3)}R - K^2 + K_{ij}K^{ij} + 16\pi G\mathcal{L}_m\right) + \frac{1}{8\pi G}\int_{\mathcal{W}} dx^3\sqrt{\gamma}n_{\pm\alpha}u_\pm^\mu\nabla_\mu u_\pm^\alpha u^\nu + \frac{1}{8\pi G}\int_{\mathcal{W}} dx^3\sqrt{\gamma}K \tag{2.4.33}$$

$$= \frac{1}{8\pi G}\int_{\mathcal{W}} dx^3\sqrt{\gamma}n_{\pm\alpha}u_\pm^\mu\nabla_\mu u_\pm^\alpha + \frac{1}{8\pi G}\int_{\mathcal{W}} dx^3\sqrt{\gamma}K_\pm, \tag{2.4.34}$$

where the first term in (2.4.33) vanishes as a result of the Hamiltonian constraint, n is the normal vector defined by (2.4.11), and u is the normal vector on a constant τ surface,

$$u_{\pm\mu} = (f_\pm, 0, 0, 0)\,. \tag{2.4.35}$$

Then, summing all parts of the action (2.4.28),

$$S_E = \frac{1}{8\pi G}\int_{\mathcal{W}} dx^3\sqrt{\gamma}n_{\pm\alpha}u_\pm^\mu\nabla_\mu u_\pm^\alpha + \frac{1}{8\pi G}\int_{\mathcal{W}} dx^3\sqrt{\gamma}K + \int_{\mathcal{W}} dx^3\sqrt{\gamma}\sigma - \sum_i \frac{\mathcal{A}_i}{4G} \tag{2.4.36}$$

$$= -\frac{1}{16\pi G}\int_{\mathcal{W}} dx^3\sqrt{\gamma}\left(f_+'\dot{\tau}_+ - f_-'\dot{\tau}_-\right) - \frac{1}{2}\int_{\mathcal{W}} dx^3\sqrt{\gamma}\sigma - \sum_i \frac{\mathcal{A}_i}{4G} \tag{2.4.37}$$

$$= \frac{1}{16\pi G}\int_{\mathcal{W}} dx^3\sqrt{\gamma}\left(\left(\frac{2f_+}{R} - f_+'\right)\dot{\tau}_+ - \left(\frac{2f_-}{R} - f_-'\right)\dot{\tau}_-\right) - \sum_i \frac{\mathcal{A}_i}{4G} \tag{2.4.38}$$

where we use the following relations:

$$n_{\alpha\pm}u^{\mu}_{\pm}\nabla_{\mu}u^{\alpha}_{\pm} = n_{\alpha\pm}u^{\tau}_{\pm}\Gamma^{\alpha}_{\tau\tau}u^{\tau}_{\pm} = \mp\frac{\dot{\tau}_{\pm}f'_{\pm}}{2}, \tag{2.4.39}$$

$$\frac{1}{R}\left(f_{+}(R)\dot{t}_{+} - f_{-}(R)\dot{t}_{-}\right) = -4\pi G_4\sigma. \tag{2.4.40}$$

We want to calculate the bounce action,

$$B = S_E(\phi) - S_E(\phi_{\rm fv}), \tag{2.4.41}$$

where $S_E(\phi)$ is given by (2.4.38), and $S_E(\phi_{\rm fv})$ is the contribution of the horizon alone:

$$S_E(\phi_{\rm fv}) = -\sum_i \frac{\mathcal{A}_i^{\rm fv}}{4G}. \tag{2.4.42}$$

Then, the bounce action is derived as follows:

$$B = \frac{1}{16\pi G}\int_{\mathcal{W}} dx^3\sqrt{\gamma}\left(\left(\frac{2f_+}{R} - f'_+\right)\dot{\tau}_+ - \left(\frac{2f_-}{R} - f'_-\right)\dot{\tau}_-\right) + \sum_i \frac{(\mathcal{A}_i^{\rm fv} - \mathcal{A}_i)}{4G}. \tag{2.4.43}$$

Next, we assume that the false vacuum is de Sitter spacetime ($\Lambda_+ > 0$), and the true vacuum is Minkowski spacetime ($\Lambda_- = 0$), and we evaluate the bounce action. In this case, there is only one cosmological horizon, thus the contributions from the horizons cancel each other $\sum_i(\mathcal{A}_i^{\rm fv} - \mathcal{A}_i) = 0$. By substituting the metric,

$$f_+(r) = 1 - \frac{\Lambda_+ r^2}{3}, \quad f_-(r) = 1, \tag{2.4.44}$$

into (2.4.43), we obtain

$$B = \frac{1}{8\pi G}\int_{\mathcal{W}} dx^3\sqrt{\gamma}\left(\frac{1}{R}\dot{\tau}_+ - \frac{1}{R}\dot{\tau}_-\right) \tag{2.4.45}$$

$$= \frac{\gamma^2}{2G}\int_{-\pi/2}^{\pi/2} d\tilde{\lambda}\tilde{R}\left(\dot{\tilde{\tau}}_+ - \dot{\tilde{\tau}}_-\right) \tag{2.4.46}$$

$$= \frac{\pi}{2G}(2l^2 - \gamma^2 - 2l\sqrt{l^2 - \gamma^2}) \tag{2.4.47}$$

$$= \frac{\pi l^2}{G}\frac{16\bar{\sigma}^4 l^4}{(1 + 4\bar{\sigma}^2 l^2)^2} \tag{2.4.48}$$

where we use the following relations:

$$\dot{\tilde{\tau}}_+ = \sqrt{\frac{1}{f_+} - \frac{\dot{\tilde{R}}}{f_+^2}} = \frac{1}{f_+}\sqrt{f_+ - \dot{\tilde{R}}} = \frac{\tilde{R}}{1-\tilde{R}^2/l^2}\sqrt{1-\frac{\gamma^2}{l^2}} \tag{2.4.49}$$

$$\dot{\tilde{\tau}}_+ = \sqrt{\frac{1}{f_-} - \frac{\dot{\tilde{R}}}{f_-^2}} = \frac{1}{f_-}\sqrt{f_- - \dot{\tilde{R}}} = \tilde{R}. \tag{2.4.50}$$

The bounce action, (2.4.48), is called the "Coleman-de-Luccia (CDL) instanton" [50], and gives the decay rate in the gravity case. To check this formula is consistent with the no-gravity case, we take the limit $G \to 0$,

$$\frac{\pi l^2}{G}\frac{16\bar{\sigma}^4 l^4}{(1+4\bar{\sigma}^2 l^2)^2} = \frac{\pi l^2}{G}\frac{16\times 16\pi^4 G^4\sigma^4 l^4}{(1+16\pi^2 G^2\sigma^2 l^2)^2} \tag{2.4.51}$$

$$\approx \frac{\pi l^2}{G} 256\pi^4 G^4\sigma^4 l^4 \tag{2.4.52}$$

$$= 256\pi^5 G^3\sigma^4 \left(\frac{3}{8\pi G\epsilon}\right)^3 \tag{2.4.53}$$

$$= \frac{27\pi^2\sigma^4}{2\epsilon^3}, \tag{2.4.54}$$

where we use the following relations:

$$\epsilon = V(\phi_{\rm fv}) - V(\phi_{\rm tv}), \quad \frac{\Lambda_+}{8\pi G} = \epsilon. \tag{2.4.55}$$

Equation (2.4.54) gives the same value as (2.3.24). Thus, we confirmed that our result is consistent with the non-gravity case.

2.5 Decay Induced by Black Hole

Some studies have shown that a black hole in a false vacuum plays a role as a nucleation site, which means the black hole enhances the decay rate [51, 52, 53]. In the previous section, we focused on the decay from de Sitter spacetime to Minkowski spacetime. In this section, we consider the decay from Schwarzschild-de Sitter spacetime (de Sitter spacetime in the presence of a Schwarzschild blackhole) to Schwarzschild-de Sitter spacetime. The presence of a black hole changes the shape of the effective potential, and the

bounce solution no longer has O(4) symmetry but has O(3) symmetry only, as seen in Fig. 2.9. In addition, Schwarzschild-de Sitter spacetime has two horizons, an event horizon and a cosmological horizon. The bounce action can be evaluated in a similar manner as in the previous section. We can use the effective potential, (2.4.21), and bounce action, (2.4.43), which is derived for a generic metric. We just substitute the preferable metric into these formulas to obtain the effective potential and bounce solution. The metric of Schwarzchild-de Sitter is given as follows:

$$ds_\pm^2 = g_{\mu\nu\pm} dx_\pm^\mu dx_\pm^\nu = -f_\pm(r_\pm)dt^2 + \frac{dr_\pm^2}{f_\pm(r_\pm)} + r_\pm^2 d\Omega_{2\pm}^2, \tag{2.5.1}$$

$$f_\pm(r) = 1 - \frac{2GM_\pm}{r} - \frac{\Lambda_\pm r^2}{3}. \tag{2.5.2}$$

First, we substitute these into (2.4.21) and plot them. Fig. 2.8 shows an effective potential plot for the decay from Schwarzschild-de Sitter ($0 < \Lambda_+, 0 < M_+$) to Minkowski ($\Lambda_- = 0, M_- = 0$), where we consider various values of the mass parameter M_+. We normalize the mass using Nariai mass $M_N = 1/3\Lambda_+ G$, for which the event horizon and the cosmological horizon match [68, 69]. Fig. 2.9 shows the Euclidean effective potential. As seen in this figure, there are two types of bounce solutions: (b) shows an oscillating solution between $r_{\min}$ and $r_{\max}$, and (c) shows a stationary solution that stays at $r_{\rm st}$. In addition to these solutions, for (d) there is no classical solution. Here, $r_{\min}$ and $r_{\max}, (r_{\min} < r_{\max})$ satisfy the relations $V_{\rm eff}(r_{\min}) = V_{\rm eff}(r_{\max}) = 0$, and we define M_+ in (b) as the critical value $M_{\rm crit}$. If $M_{\rm crit} < M_+$, there is no Euclidean solution (d).

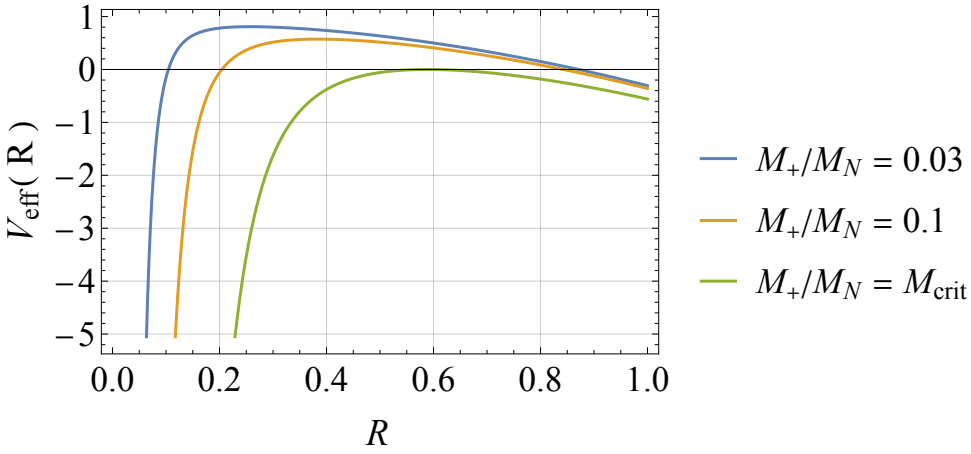

Figure 2.8: Plot of $V_{\text{eff}}(R)$, where parameters are set to $M_- = 0, \Lambda_- = 0, \bar{\sigma} l = 0.3$, and $M_+ = 0.03, 0.1, M_{\text{crit}}$. Here, $M_{\text{crit}} = 0.359595$ for this parameter choice. This figure shows the effective potential changes under the variation of M_+.

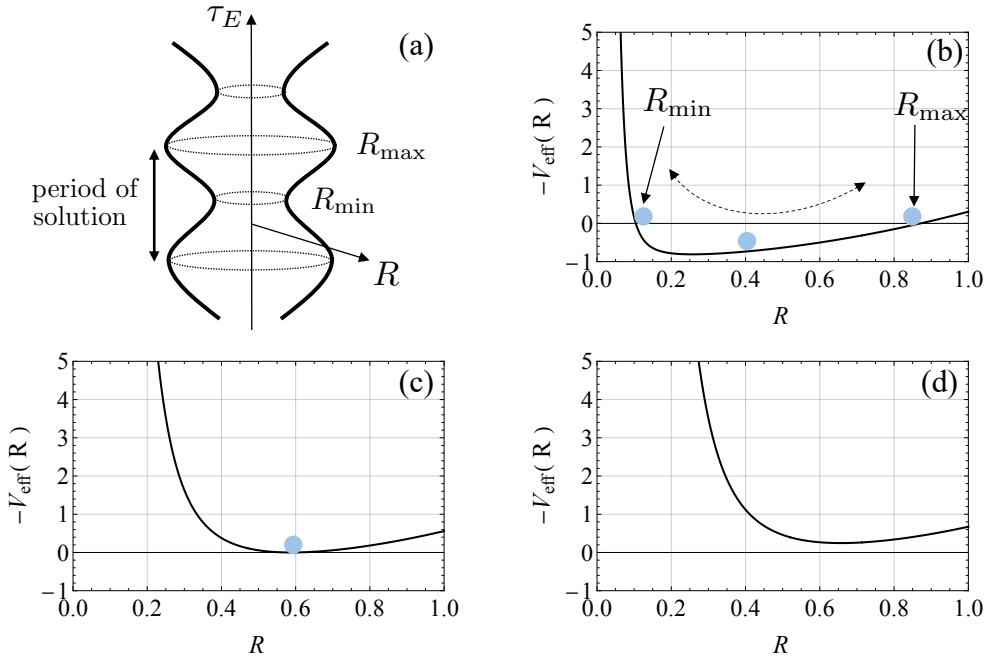

Figure 2.9: (a) Picture of an O(3) symmetric bounce solution, where solution oscillates for the period of the solution. (b)(c)(d) Plots of $-V_{\rm eff}(R)$, where the parameters are set to $M_- = 0, \Lambda_- = 0, \bar{\sigma} l = 0.3$, and M_+ takes different values for each plot. (b) $M_+/M_N = 0.03$ and classical Euclidean solution oscillates between the points $r_{\min}, r_{\max}$. These points satisfy $V_{\rm eff}(R_{\min}) = V_{\rm eff}(R_{\max}) = 0$ and $R_{\min} < R_{\max}$. (c) $M_+ = M_{\rm crit}$ and classical solution do not oscillate but remain steady. (d) $M_+/M_N = 0.03$ no Euclidean solution exists for this parameter.

Next, we use the metric in (2.4.43),

$$B = \frac{1}{16\pi G}\int_{\mathcal{W}} dx^3\sqrt{\gamma}\left(\frac{1}{R}\left(2-\frac{6GM_+}{R}\right)\dot{\tau}_+ - \frac{1}{R}\left(2-\frac{6GM_-}{R}\right)\dot{\tau}_-\right) + \sum_i \frac{(4\pi r_{h+}^2 + 4\pi r_c^2 - 4\pi r_{h-}^2 - 4\pi r_c^2)}{4G} \tag{2.5.3}$$

$$= \frac{1}{4G}\Big[\int_{\mathcal{W}} d\lambda\left((2R-6GM_+)\,\dot{\tau}_+ - (2R-6GM_-)\,\dot{\tau}_-\right) + 4\pi\left(r_{h+}^2 - r_{h-}^2\right)\Big], \tag{2.5.4}$$

where $r_{h\pm}^2$ is the event horizon of the black hole, and r_c^2 is the cosmological horizon. Note that the contribution of this black hole horizon is nothing but the Beckenstein-Hawking entropy [70, 71, 72]. One can easily reproduce the previous result, (2.4.45), by taking $M_\pm = 0$. Now we get the bounce solution from the effective potential, and evaluate the bounce action. Fig. 2.10 shows a plot of the bounce action for the decay from Schwarzschild-de Sitter spacetime to Schwarzschild or Minkowski spacetime, where $B/B_{CDL} < 0$ shows that the presence of the black hole enhances the decay. Because the decay rate is estimated as $\Gamma \sim e^{-B}$ and the ratio $B/B_{\rm CDL} < 1$ means the presence of the black hole decrease the bounce action compared to the action without the blackhole, this ratio indicates an enhancement of the decay rate. In Fig. 2.10, each plot has a turning point where the bounce action changes from a decrease to an increase. Before this point, $M_- = 0$ is the dominant process, whereas after this point, the process in which the bounce solution becomes stationary is dominant, and M_- is determined by this condition. The results discussed in this section can be summarized as follows.

- The symmetry of the bounce solution is reduced from O(4) to O(3).
- A black hole plays a role as a bubble nucleation site, and the decay rate around the black hole is enhanced.
- The process in which the Euclidean solution becomes stationary gives the most probable solution.

2.6 Bubble Universe Derived from AdS_5

In the previous section, we reviewed the vacuum decay in four dimensions and showed that the Euclidean on-shell action is useful for evaluating the vacuum

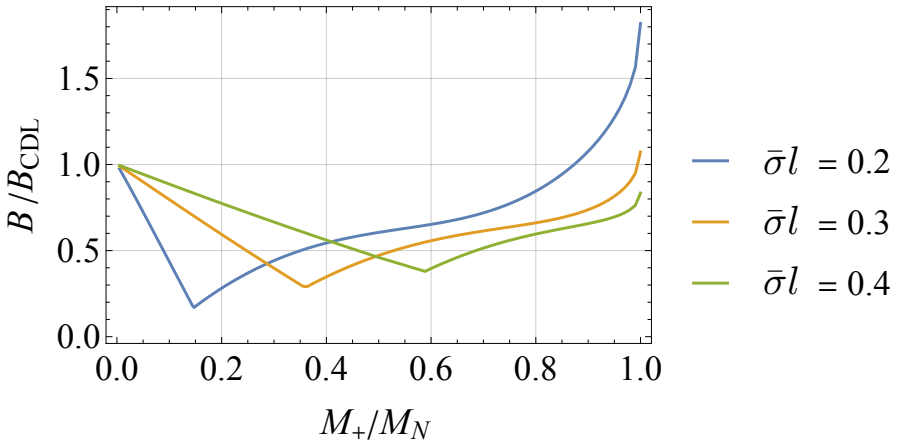

Figure 2.10: Plot of bounce action ratio $B/B_{CDL} < 1$ for different $\bar{\sigma}$. The ratio that satisfies B/B_{CDL} shows the catalysis. It can also be seen that each plot has a minimum bounce action point, which corresponds to the maximum decay rate and stationary bounce solution.

decay rate. In this section, we consider the decay in five dimensions and the bubble wall dynamics, and briefly review the setup of a bubble universe.

This bubble universe was proposed in the context of string theory [25]. In the string theory, vacuum structure is complicated and still not understood well. Thus, it is difficult to construct a 4D de-Sitter spacetime (the difficulties are explained in a review [73]). This empirical rule is known as the so-called "de Sitter conjecture" [22, 23]. We need a novel way to connect the string theory to our universe. In order to solve this problem, Danielsson et al. suggested a bubble universe [25]. In the bubble universe formalism, we start with metastable AdS_5 spacetime. We saw that the vacuum decay occurs as the bubble it is inside is a true vacuum and is nucleated in a false vacuum. Then, the decay proceeds as the bubble expands. In the decay in five dimensions, the bubble wall that separates the two vacua is four-dimensional. Thus, we can effectively construct a 4D de Sitter universe on this bubble wall. This is the idea of a bubble universe, which will be reviewed in the following subsection.

2.6.1 Formalism

A cloud of strings

Before constructing the bubble universe, we here introduce the cloud of strings whose presence is assumed in the original setup [25]. The origin of the cloud of strings is the uniform distributed strings extending to the radial directions, and this has been known as one of the solutions of Einstein equations [74, 75]. The solution of a cloud of strings in five dimensions was studied by [76], and we here review this derivation. We start with the action in the presence of N strings:

$$S = \frac{1}{16\pi G_5}\int \sqrt{-g}R + S_m, \tag{2.6.1}$$

$$S_m = -\frac{1}{2}\sum_{i=1}^{N} T_i \int d^2\xi \sqrt{-h} h^{\alpha\beta}\partial_\alpha X^\mu \partial_\beta X^\nu g_{\mu\nu}, \tag{2.6.2}$$

where T_i is the tension of the i-th string, $g_{\mu\nu}$ is the metric of five-dimensional spacetime, and $h_{\alpha\beta}$ is the induced metric on the string world sheet. Einstein equation for this action can be written as follows:

$$R_{\mu\nu} - \frac{1}{2}Rg_{\mu\nu} + \Lambda^{(5)}g_{\mu\nu} = 8\pi G_5 T_{\mu\nu} \tag{2.6.3}$$

$$T^{\mu\nu} = -\sum_{i=1}^{N} T_i \int d\xi^2 \frac{1}{\sqrt{|g|}}\sqrt{|h|}h^{\alpha\beta}\partial_\alpha X^\mu \partial_\beta X^\nu \delta_i^{(5)}(X - x_i) \tag{2.6.4}$$

Then, we choose the static gauge, $\xi^0 = t$, $\xi^1 = r$, and assume that the number of strings, N, is large enough to regard the distribution as spherically symmetric. With this assumption, the metric is written as:

$$ds^2 = g_{00}(r)dt^2 + g_{11}(r)dr^2 + r^2 d\Omega_3^2. \tag{2.6.5}$$

In addition, the induced metric on the world sheet of the string is shown as:

$$h_{\alpha\beta} = g_{\mu\nu}\frac{\partial x^\mu}{\partial \xi^\alpha}\frac{\partial x^\nu}{\partial \xi^\beta}. \tag{2.6.6}$$

In the static gauge,

$$h_{00} = g_{00}, \quad h_{11} = g_{11}. \tag{2.6.7}$$

Using these equations, the energy momentum tensor of (2.6.4) is found to be:

$$T^{00} = -\frac{ag^{00}}{r^3}, \qquad T^{11} = -\frac{ag^{11}}{r^3}, \tag{2.6.8}$$

where we assume that the string tension is uniform and we define the density of the tension as follows:

$$a(x) = T\sum_i \delta_i^{(3)}(X_- - x_i) \tag{2.6.9}$$

$$a = \frac{1}{V_3}\int dx^3 a(x) = \frac{T}{V_3}\sum_i^N \int dx^3 \delta^{(3)}(X - x_i) = \frac{TN}{V_3}. \tag{2.6.10}$$

Then, the solution of Einstein equation in the presence of the cloud of strings is found as follows:

$$ds^2 = -f(r)dt^2 + \frac{dr^2}{f(r)} + r^2 d\Omega_3^2 \tag{2.6.11}$$

$$f(r) = 1 - \frac{\Lambda^{(5)} r^2}{6} - \frac{2a}{3r}. \tag{2.6.12}$$

Next, the spherically symmetric 5D spacetime metric with a black hole and a cloud of string is[76] shown as follows:

$$f_\pm(r) = 1 - \frac{\Lambda_\pm^{(5)} r^2}{6} - \frac{8G_5 M_\pm}{3\pi r^2} - \frac{2a_\pm}{3r}, \tag{2.6.13}$$

and we consider the decay in this spacetime[2].

Bubble spacetime

Here, we briefly review the bubble spacetime that Danielsson et al. proposed [25, 77]. The method is the same as that in the 4D case, where we start with the false and true vacuum metrics in the presence of a black hole and a cloud of string:

$$f_\pm(r) = 1 - \frac{\Lambda_\pm^{(5)} r^2}{6} - \frac{8G_5 M_\pm}{3\pi r^2} - \frac{2a_\pm}{3r}. \tag{2.6.14}$$

[2]The catalysis effect of a cloud of strings in four dimensions and its application to the instability of a Higgs vacuum is presented in [60].

The induced metric is the same as that in the 4D case:

$$ds_\Sigma^2 = \gamma_{ij}dy^i dy^j = -d\lambda^2 + R^2(\lambda)d\Omega_3^2. \tag{2.6.15}$$

Next, we substitute this metric into the equation derived from the junction condition, (2.4.16), but the right hand side of this formula needs to be modified for the 5D case[3]:

$$\frac{1}{R}\left(f_+(R)\dot{t}_+ - f_-(R)\dot{t}_-\right) = -\frac{8\pi G_5 R\sigma}{3}, \tag{2.6.16}$$

$$\left(\frac{\dot{R}}{R}\right)^2 = \left(\frac{4\pi G_5\sigma}{3}\right)^2 - \frac{f_+(R)+f_-(R)}{2R^2} + \frac{\left(f_+(R)-f_-(R)\right)^2}{16R^4}\left(\frac{3}{4\pi G_5\sigma}\right)^2. \tag{2.6.17}$$

Then, we get:

$$\sigma = \frac{3}{8\pi G_5}\left(\sqrt{\frac{1}{l_-^2} + \frac{1+\dot{R}^2}{R^2} - \frac{8G_5M_-}{3\pi R^4} - \frac{2a_-}{3R^3}}\right. \\ \left. - \sqrt{\frac{1}{l_+^2} + \frac{1+\dot{R}^2}{R^2} - \frac{8G_5M_+}{3\pi R^4} - \frac{2a_+}{3R^3}}\right), \tag{2.6.18}$$

where $l_\pm = \sqrt{-6/\Lambda_\pm^{(5)}}$, and we consider the decay from a metastable AdS_5 to more stable AdS_5. This situation may be expressed as

$$\Lambda_-^{(5)} < \Lambda_+^{(5)} < 0, \qquad l_- < l_+. \tag{2.6.19}$$

Assuming that a sufficiently expanded bubble corresponds to the universe, the square roots in (2.6.18) are expanded by using the following conditions:

$$l_\pm \ll R,\ l_\pm \ll \frac{\dot{R}}{R}. \tag{2.6.20}$$

Then, we get the following:

$$\sigma = \frac{3}{8\pi G_5}\left[\frac{1}{l_-}\left(1 + \frac{l_-^2}{2R^2} + \frac{l_-^2\dot{R}^2}{2R^2} - \frac{8G_5M_-l_-^2}{6\pi R^4} - \frac{2a_-l_-^2}{6R^3}\right)\right. \\ \left. - \frac{1}{l_+}\left(1 + \frac{l_+^2}{2R^2} + \frac{l_+^2\dot{R}^2}{2R^2} - \frac{8G_5M_+l_+^2}{6\pi R^4} - \frac{2a_+l_+^2}{6R^3}\right)\right]. \tag{2.6.21}$$

[3] $2\pi G_4\sigma$ is replaced by $4\pi G_5/3$ in the 5D case.

Reorganizing the terms in (2.6.21), the equation of motion of the bubble is derived as follows:

$$\frac{\dot{R}^2}{R^2} = -\frac{1}{R^2} + \frac{\Lambda^{(4)}}{3} + \frac{8\pi G_4}{3}\left(\frac{M_+ l_+ - M_- l_-}{2\pi^2 R^4} + \frac{a_+ l_+ - a_- l_-}{8\pi G_5 R^3}\right), \tag{2.6.22}$$

where we assume:

$$\Lambda^{(4)} = 8\pi G_4\left(\frac{3}{8\pi G_5}\left(\frac{1}{l_-} - \frac{1}{l_+}\right) - \sigma\right), \qquad G_4 = \frac{2G_5}{l_+ - l_-}. \tag{2.6.23}$$

These formulas show the relations between the 4D cosmological constant and gravitational constant derived in order to match (2.6.21) to the Friedmann equation. Remembering the Friedmann equation in four dimensions,

$$\frac{\dot{a}^2}{a^2} = -\frac{1}{a^2} + \frac{\Lambda^{(4)}}{3} + \frac{8\pi G_4}{3}\left(\frac{\rho_{rad}}{a^4} + \frac{\rho_{mat}}{a^3}\right), \tag{2.6.24}$$

and comparing (2.6.22) and (2.6.24), we can regard the terms proportional to $1/R^4$ and $1/R^3$ in (2.6.21) as the radiation and matter energy density, respectively. These correspondences imply that on the bubble spacetime nucleated between the spacetime with the metric (2.6.14), a black hole and a cloud of strings may be viewed as the radiation and matter. In addition, if the tension of bubble σ satisfies the following relation:

$$\sigma < \sigma_{\rm crit}, \qquad \sigma_{\rm crit} = \frac{3}{8\pi G_5}\left(\frac{1}{l_-} - \frac{1}{l_+}\right) = \frac{3}{4\pi G_5}\bar{\sigma}_{\rm crit}, \tag{2.6.25}$$

the cosmological constant on the bubble universe becomes positive, and the bubble spacetime can effectively be regarded as de Sitter spacetime.

In this setup, the bubble itself obeys the Friedmann-like equation, and on the bubble surface, one can see that matter, radiation, and a positive cosmological constant are realized, although there are some problems we need to resolve to identify this bubble spacetime as our universe. One of the problem is the localization of matter on the bubble universe. Just thinking about the bubble nucleated in AdS_5 spacetime, matter is not localized on the bubble surface and does not match our universe, unlike the well-known brane world scenario of Randall-Sundrum [78, 79]. Danielsson et al. proposed that the strings that spread in five dimensions and end at the bubble can be used to resolve this problem [80]. They also discussed gravitational waves in the

bubble cosmology [81]. The other problems are the realization of the inflation and reproduction of the thermal history of our universe. Although these problems are very challenging and seem difficult to resolve, some directions have been proposed [82, 83, 84, 85]. This thesis does not discuss these problems in detail, but focuses on the instability of AdS_5 spacetime, which is necessary for the setup of a bubble universe, from the classical as well as quantum pointis of view.

Chapter 3

Quasi-normal Modes of Black hole

In this section, we review the quasi-normal modes of a black hole. The quasi-normal modes are the black hole perturbation solutions with a infinite numbers of complex frequencies, and are obtained as infinite discrete numbers. The following sections review some of the properties of quasi-normal modes. Then, we focus on Heun's equation method to derive quasi-normal modes and show the result for a static 4D Schwarzschild black hole in de Sitter spacetime.

3.1 Quasi-normal Modes as Perturbation

In this section, we review the black hole perturbation, known as quasi-normal modes for the 4D Schwarzschild black hole case. We consider the perturbation $h_{\mu\nu}$ with the following background metric:

$$ds^2 = g^0_{\mu\nu} dx^\mu dx^\nu \tag{3.1.1}$$

$$= -\left(1 - \frac{2M}{r}\right) dt^2 + \left(1 - \frac{2M}{r}\right)^{-1} dr^2 + r^2 \left(d\theta^2 + \sin^2\theta d\phi^2\right). \tag{3.1.2}$$

The perturbed solution $g_{\mu\nu}$ is given by:

$$g_{\mu\nu} = \ g^0_{\mu\nu} \ + \ h_{\mu\nu}. \tag{3.1.3}$$

Then, we assume the following ansatz:

$$h_{\mu\nu} \sim e^{-i\omega t} R_\ell(r) Y_{\ell m}(\theta, \phi), \tag{3.1.4}$$

where ω is the quasi-normal frequency. An infinite number of discrete frequencies are obtained by solving the perturbation with appropriate boundary conditions. From the ansatz formula, (3.1.4), the real part of the quasi-normal frequency, $\mathrm{Re}(\omega)$, corresponds to the normal frequency, and the imaginary part of quasi-normal frequency, $\mathrm{Im}(\omega)$, corresponds to the damping of the oscillation if $\mathrm{Im}(\omega) < 0$. The equation for the perturbation is reduced to the Regge-Wheeler equation [86]:

$$\left(-\frac{d^2}{dr_*^2} + V(r)\right) R(r,\omega) = \omega^2 R(r,\omega), \tag{3.1.5}$$

$$V(r) = \left(1 - \frac{2M}{r}\right)\left(\frac{l(l+1)}{r^2} - \frac{6M}{r^3}\right), \tag{3.1.6}$$

where r_* is the tortoise coordinate,

$$r_* = r + 2M\log(r - 2M)/2M. \tag{3.1.7}$$

Fig. 3.1 shows a plot of the Regge-Wheeler potential of (3.1.6), where it can

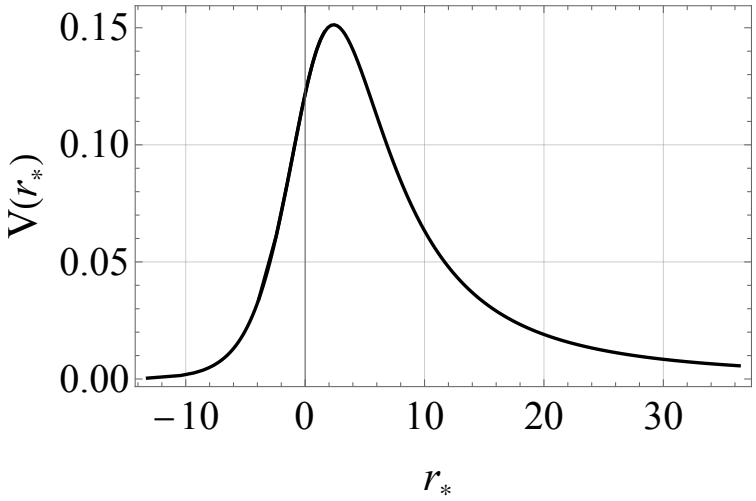

Figure 3.1: Plot of Regge-Wheeler potential. The parameters are set to $M = 1, l = 2$. The potential has a barrier and vanishes at each boundary ($r_* = \pm\infty$).

be seen that the potential barrier exists. Thus, solving (3.1.5) corresponds to solving the scattering problem for this potential. Because the potential,

(3.1.6), vanishes at the horizon ($r_h = 2M, r_* = -\infty$) and at the infinity ($r = \infty, r_* = \infty$), (3.1.5) is reduced to,

$$\left(\frac{d^2}{dr_*^2} - \omega^2\right) R(r,\omega) = 0, \tag{3.1.8}$$

near the horizon and infinity, and the general solution of this asymptotic equation is given by:

$$R(r,\omega) = Ae^{-i\omega r_*} + Be^{i\omega r_*}. \tag{3.1.9}$$

By combining this with the exponential term of the ansatz, (3.1.4), and obtain the following:

$$e^{-i\omega t}R(r,\omega) \sim Ae^{i\omega(r_*-t)} + Be^{-i\omega(r_*+t)}, \tag{3.1.10}$$

where the first term corresponds to the outgoing mode, and the second term is the ingoing mode. Here, we consider the boundary condition at the event horizon and at infinity:

$$R(r,\omega) \sim e^{-i\omega r_*} \sim (r-2M)^{-2iM\omega} \quad \text{as} \quad r \to r_h, \tag{3.1.11}$$

and

$$R(r,\omega) \sim e^{i\omega r_*} \sim e^{i\omega r} r^{2iM\omega} \quad \text{as} \quad r \to \infty. \tag{3.1.12}$$

These boundary conditions mean that there is nothing from the event horizon and no energy coming from the infinity. Thus, there are only the ingoing mode at the horizon and outgoing mode at the infinity. Then, the problem is reduced to finding the ω that satisfies the boundary conditions.

From here we review the method of the continued fraction given by Leaver [87]. The general solution of (3.1.5) that satisfies the boundary conditions is given as a power series:

$$R(r,\omega) = (r-2M)^{2iM\omega} r^{-4iM\omega} e^{-i\omega(r-2M)} \sum_{n=0}^{\infty} a_n \left(\frac{r-2M}{r}\right)^n, \tag{3.1.13}$$

where the convergence for $r \to \infty$ of this series is not clear, so we investigate the coefficients for $r \to \infty$. The coefficient of the series, a_n, obeys the recurrence formula:

$$c_0(n,\omega)a_n + c_1(n,\omega)a_{n-1} + c_2(n,\omega)a_{n-2} = 0 \tag{3.1.14}$$

$$a_0 = 1, \ a_{-1} = 0, \tag{3.1.15}$$

where

$$c_0(n,\omega) = n^2 + 2i\tilde{\omega}, \tag{3.1.16}$$
$$c_1(n,\omega) = -2n^2 - (8i\tilde{\omega} - 2)n + 8\tilde{\omega}^2 + 4i\tilde{\omega} - l(l+1) + 3, \tag{3.1.17}$$
$$c_2(n,\omega) = n^2 + (4i\tilde{\omega} - 2)n + 8\tilde{\omega}^2 + 4i\tilde{\omega} - 3, \tag{3.1.18}$$
$$\tilde{\omega} = 2\omega M. \tag{3.1.19}$$

We want to calculate the solution that converges at $r = \infty$, and Gautschi showed that this kind of solution satisfies the following relation [88]:

$$\frac{a_n}{a_{n-1}} = \cfrac{-c_2(n+1,\omega)}{c_1(n+1,\omega) - \cfrac{c_0(n+1,\omega)\times c_2(n+2,\omega)}{c_1(n+1,\omega) - \cfrac{c_0(n+1,\omega)\times c_2(n+3,\omega)}{c_1(n+3,\omega) - \cdots}}}. \tag{3.1.20}$$

For $n = 0$, the left-hand side of (3.1.20) becomes infinite, so that the denominator of the right-hand side is zero,

$$0 = c_1(1,\omega) - c_0(1,\omega)\cfrac{c_2(2,\omega)}{c_1(2,\omega) - c_0(2,\omega)\cfrac{c_2(3,\omega)}{c_1(3,\omega) - \cdots}}. \tag{3.1.21}$$

This is the equation that gives us the desired quasi-normal frequencies, ω. Leaver numerically solved it for up to $n = 60$, where the parameters were $l = 2, 3$ and $M = 1/2$, and showed the asymptotic value (large n)[87]:

$$\omega = 0.15 - \left(\frac{1}{2}n + 0.2\right)i \quad \text{for } l = 2, \tag{3.1.22}$$
$$\omega = 0.16 - \left(\frac{1}{2}(n-1) + 0.13\right)i \quad \text{for } l = 3. \tag{3.1.23}$$

From this result, the real parts of the quasi-normal modes seem to approach a non-zero value for each l, and they are slightly different for $l = 2$ and $l = 3$. However Nollert improved the behavior for large n and showed that the asymptotic value is independent of l [40]:

$$\omega = 0.0874247 - \frac{i}{2}\left(\frac{1}{2}n + 0.5\right) + O[(n+1)^{-1/2}]. \tag{3.1.24}$$

In Appendix A we give an explanation of this asymptotic value.

3.2 Quasi-normal Modes as Heun's Equation

We introduced the quasi-normal modes in Sec. 3.1 and reviewed the continued fraction method for the Schwarzschild black hole. In this section, we extend it to the Kerr-de Sitter black hole and review Heun's equation method to calculate the quasi-normal frequencies [89, 90]. We start with Kerr-de Sitter metric:

$$ds^2 = -\frac{\Delta_r}{(1+\alpha)^2\rho^2}\left(dt - a\sin^2\theta d\phi\right)^2 + \frac{\Delta_\theta \sin^2\theta}{(1+\alpha)^2\rho^2}\left[adt - \left(r^2+a^2\right)d\phi\right]^2 + \frac{\rho}{\Delta_r}dr^2 + \frac{\rho^2}{\Delta_\theta}d\theta^2, \tag{3.2.1}$$

where

$$\alpha = \frac{\Lambda a^2}{3}, \quad \rho =^2 + a^2\cos^2\theta, \tag{3.2.2}$$

$$\begin{aligned}\Delta_r &= (r^2+a^2)\left(1-\frac{\Lambda}{3}r^2\right) - 2Mr \\ &= -\frac{\Lambda}{3}(r-r_-)(r-r_+)(r-r'_-)(r-r'_+),\end{aligned} \tag{3.2.3}$$

$$\Delta_\theta = 1 + \alpha\cos^2\theta. \tag{3.2.4}$$

The equation$\Delta_r = 0$ has four roots, and r_+ and r'_+ correspond to the black hole horizon and the cosmological horizon, respectively. We consider the perturbation of a massless field with spin s on Kerr-de Sitter background. We conside the following separation-of-variables ansatz:

$$\Psi = e^{-i\omega t + im\phi}R(r)S(\cos\theta). \tag{3.2.5}$$

The perturbation equation is reduced to Tuekolsky equations for the angular and the radial parts [91]:

$$\left[\frac{d}{dx}(1+\alpha x^2)(1-x^2)\frac{d}{dx} + \lambda - s(1-\alpha) - 2\alpha x^2 + \frac{(1+\alpha)^2}{1+\alpha x^2}\left(c^2x^2 - 2csx - c^2 + 2cm + \frac{4\alpha}{1+\alpha}smx - \frac{(m+sx)^2}{1-x^2}\right)\right]S(x) = 0, \quad (3.2.6)$$

$$\left[\Delta_r^{-s}\frac{d}{dr}\Delta_r^{s+1}\frac{d}{dr} + \frac{(1+\alpha)^2K^2 - is(1+\alpha)K\Delta_r'}{\Delta_r} + 4is(1+\alpha)\omega r - \frac{2\alpha}{a^2}(s+1)(2s+1)r^2 + 2s(1-\alpha) - \lambda\right]R(r) = 0, \quad (3.2.7)$$

where $x = \cos\theta, c = a\omega$, $K(r) = \omega(r^2+a^2) - am$, and λ is the separation constant determined by the condition that $S(x)$ is regular at $x = -1$ and $x = 1$. The equation is difficult to solve. However, by performing the following transformations:

$$x \to u \equiv \frac{(1 - i/\sqrt{\alpha})(x+1)}{2(x - i/\sqrt{\alpha})}, \quad (3.2.8)$$

$$S(x) \to S(u) \equiv u^{A_1}(u-1)^{A_2}(u-u_a)^{A_3}(u-u_\infty)y_a(u), \quad (3.2.9)$$

$$r \to z \equiv \frac{(r_+' - r_-)(r - r_+)}{(r_+' - r_+)(r - r_-)}, \quad (3.2.10)$$

$$R(r) \to R(z) \equiv z^{B_1}(z-1)^{B_2}(z-z_r)^{B_3}(z-z_\infty)^{2s+1}y_r(z), \quad (3.2.11)$$

(3.2.6) and (3.2.7) are reduced to Heun's differential equations:

$$y_a''(u) + \left(\frac{2A_1+1}{u} + \frac{2A_2+1}{u-1}\frac{2A_3+1}{u-u_a}\right)y_a'(u) + \frac{\rho_+\rho_-u + u_0}{u(u-1)(u-u_a)}y_a(u) = 0, \quad (3.2.12)$$

$$y_r''(z) + \left(\frac{2B_1+s+1}{z} + \frac{2B_2+s+1}{z-1} + \frac{2B_3+s+1}{z-z_r}\right)y_r'(z) + \frac{\sigma_+\sigma_-z + v}{z(z-1)(z-z_r)}y_r(z) = 0, \quad (3.2.13)$$

where we have introduced the following parameters:

$$u_a \equiv -\frac{(1-i/\sqrt{\alpha})^2}{4i/\sqrt{\alpha}}, \qquad u_\infty \equiv \frac{1-i/\sqrt{\alpha}}{2}, \tag{3.2.14}$$

$$A_1 = \frac{m-s}{2}, \qquad A_2 = -\frac{m+s}{2}, \qquad A_3 = \frac{i}{2}\left(\frac{1+\alpha}{\sqrt{\alpha}}c - m\sqrt{\alpha} - is\right), \tag{3.2.15}$$

$$A_3^* = -\frac{i}{2}\left(\frac{1+\alpha}{\sqrt{\alpha}}c - m\sqrt{\alpha} + is\right), \tag{3.2.16}$$

$$\rho_+ = 1, \qquad \rho_- = 1 - s - im\sqrt{\alpha} + ic\left(\sqrt{\alpha} + \frac{1}{\sqrt{\alpha}}\right), \tag{3.2.17}$$

$$u_0 = -\left[\frac{i\lambda}{4\sqrt{\alpha}} + \frac{1}{2} + A_1 + \left(m + \frac{1}{2}\right)(A_3 - A_3^*)\right], \tag{3.2.18}$$

$$z_r = \frac{(r'_+ - r_-)(r'_- - r_+)}{(r'_+ - r_+)(r'_- - r_-)}, \qquad z_\infty = \frac{r'_+ - r_-}{r'_+ - r_+}, \tag{3.2.19}$$

$$B_1 = \frac{i(1+\alpha)K(r_+)}{\Delta'_r(r_+)}, \quad B_2 = \frac{i(1+\alpha)K(r'_+)}{\Delta'_r(r'_+)}, \quad B_3 = \frac{i(1+\alpha)K(r'_-)}{\Delta'_r(r'_-)}. \tag{3.2.20}$$

The coordinate transformation, (3.2.8) and (3.2.10), maps the boundaries of Fig .3.2:

$$x : (-1, 1) \to u : (0, 1), \qquad r : (r_+, r'_+) \to z : (0, 1). \tag{3.2.21}$$

Thus, we consider the quasi-normal modes between 0 and 1. The general form of Heun's equation is

$$y''(z) + \left(\frac{\gamma}{z} + \frac{\delta}{z-1} + \frac{\epsilon}{z-a}\right)y'(z) + \frac{\alpha\beta z - q}{z(z-1)(z-a)}y(z) = 0, \tag{3.2.22}$$

and the general solution is derived at each singular point, $z = 0, 1, a, \infty$[1]. The solutions we need are those at event horizon $r = r_+(z = 0)$ and cosmological horizon $r = r'_+(z = 1)$ for the radial part, and at $x = -1(u = 0)$ and $x = 1(u = 1)$ for the angular part. The general solutions for $z = 0$ and $z = 1$ are found to be:

$$\begin{aligned} y(z) =& a_1 H\ell(a, q; \alpha, \beta, \gamma, \delta; z) \\ &+ a_2 z^{1-\gamma} H\ell\left(a, (a\delta + \epsilon)(1-\gamma) + q; \alpha + 1 - \gamma, \beta + 1 - \gamma, 2 - \gamma, \delta; z\right), \end{aligned} \tag{3.2.23}$$

[1]The solutions at the singular points can be found at https://dlmf.nist.gov/31.

$$
\begin{aligned}
y(z) =& a_3 H\ell(1-a, \alpha\beta - q; \alpha, \beta, \delta, \gamma; 1-z) \\
&+ a_4 (1-z)^{1-\delta} H\ell(1-a, ((1-a)\gamma + \epsilon)(1-\delta) + \alpha\beta - q; \\
&\qquad \alpha + 1 - \delta, \beta + 1 - \delta, 2 - \delta, \gamma; 1-z),
\end{aligned} \tag{3.2.24}
$$

where a_1, a_2, a_3, a_4 are arbitrary constants, and $H\ell(a, q; \alpha, \beta, \gamma, \delta; z)$ is the local solution of Heun's equation at $z = 0$, which can be normalized as:

$$
H\ell(a, q; \alpha, \beta, \gamma, \delta; 0) = 1. \tag{3.2.25}
$$

In the following sections, we consider the solutions for the radial and angular equations.

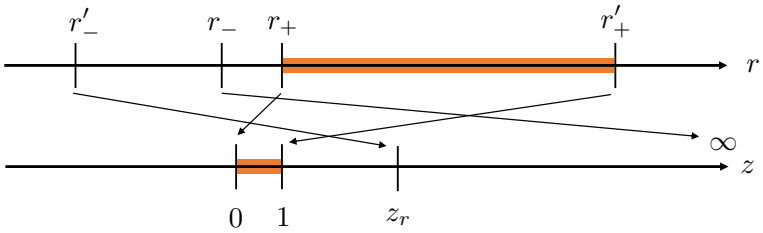

Figure 3.2: Schematic picture showing the mapping of the radial coordinates (3.2.10). In general $4! = 24$ choices of mapping, although here we adopt the mapping shown, especially mapping the boundaries, $r = r_+, r'_+$ to $z = 0, 1$.

3.2.1 Radial Part

There are solutions at each point, and the boundary conditions determine the desired solution. The boundary conditions are the same as (3.1.11) and (3.1.12), with only the ingoing mode at the event horizon and only outgoing mode at the cosmological horizon. The solutions at the event horizon are derived by identifying the parameters:

$$
\begin{aligned}
R_1(z) &\equiv z^{B_1}(z-1)^{B_2}(z-z_r)^{B_3}(z-z_\infty)^{2s+1} H\ell(a, q; \alpha, \beta, \gamma, \delta; z) \\
&\sim (r - r_+)^{i\omega {r_+}^2/\Delta'_r(r_+)},
\end{aligned} \tag{3.2.26}
$$

$$
\begin{aligned}
R_2(z) &\equiv z^{B_1}(z-1)^{B_2}(z-z_r)^{B_3}(z-z_\infty)^{2s+1} \\
&\qquad \times z^{1-\gamma} H\ell\left(a, (a\delta + \epsilon)(1-\gamma) + q; \alpha + 1 - \gamma, \beta + 1 - \gamma, 2 - \gamma, \delta; z\right) \\
&\sim (r - r_+)^{-s - i\omega {r_+}^2/\Delta'_r(r_+)},
\end{aligned} \tag{3.2.27}
$$

where we take $a = 0$ for simplicity, and $R_2(z)$ satisfies the boundary condition. The solutions at the cosmological horizon are derived as follows:

$$\begin{aligned} R_3(z) &\equiv z^{B_1}(z-1)^{B_2}(z-z_r)^{B_3}(z-z_\infty)^{2s+1} \\ &\qquad \times H\ell(1-a, \alpha\beta - q; \alpha, \beta, \delta, \gamma; 1-z) \\ &\sim (r'_+ - r)^{i\omega {r'_+}^2/\Delta'_r(r'_+)}, \end{aligned} \tag{3.2.28}$$

$$\begin{aligned} R_4(z) &\equiv z^{B_1}(z-1)^{B_2}(z-z_r)^{B_3}(z-z_\infty)^{2s+1} z^{1-\gamma} \\ &\quad \times (1-z)^{1-\delta} H\ell(1-a, ((1-a)\gamma + \epsilon)(1-\delta) + \alpha\beta - q; \\ &\qquad\qquad \alpha + 1 - \delta, \beta + 1 - \delta, 2 - \delta, \gamma; 1-z) \\ &\sim (r'_+ - r)^{-s - i\omega {r'_+}^2/\Delta'_r(r'_+)}. \end{aligned} \tag{3.2.29}$$

$R_3(z)$ satisfies the boundary condition. The radial solution at each boundary is found as follows:

$$R(z) \sim \begin{cases} R_2(z) & (z \sim 0) \\ R_3(z) & (z \sim 1) \end{cases} \tag{3.2.30}$$

where these local solutions are valid for $a \neq 0$. Next, we derive the solution of the angular part using the same procedure.

3.2.2 Angular Part

The angular Heun's equation, (5.2.18), also has two solutions at each singular point, and we need the solutions of $u = 0, 1$ for the regularity condition. Here, we identify the parameters as follows:

$$a = u_a, \qquad q = -u, \qquad \alpha = \rho_+, \qquad \beta = \rho_-, \tag{3.2.31}$$

$$\gamma = 2A_1 + 1, \qquad \delta = 2A_2 + 1, \qquad \epsilon = 2A_3 + 1. \tag{3.2.32}$$

Then, the solutions for $z = 0$ ($x = 0$) are found as follows:

$$\begin{aligned} S_1(u) &\equiv u^{A_1}(u-1)^{A_2}(u-u_a)^{A_3}(u-u_\infty) H\ell(a, q; \alpha, \beta, \gamma, \delta; u) \\ &\sim (1+x)^{(m-s)/2}, \end{aligned} \tag{3.2.33}$$

$$\begin{aligned} S_2(u) &\equiv u^{A_1}(u-1)^{A_2}(u-u_a)^{A_3}(u-u_\infty) \\ &\qquad \times u^{1-\gamma} H\ell\left(a, (a\delta + \epsilon)(1-\gamma) + q; \alpha + 1 - \gamma, \beta + 1 - \gamma, 2 - \gamma, \delta; u\right) \\ &\sim (1+x)^{-(m-s)/2}, \end{aligned} \tag{3.2.34}$$

we need to distinguish by the value of s, m. For $s < m$, $S_1(u)$, and for $m < s$, $S_2(u)$ is preferable. The solutions for $z = 1$ ($x = -1$) are found as follows:

$$\begin{aligned} S_3(u) &\equiv u^{A_1}(u-1)^{A_2}(u-u_a)^{A_3}(u-u_\infty)H\ell(1-a, \alpha\beta - q; \alpha, \beta, \delta, \gamma; 1-u) \\ &\sim (1-x)^{-(m+s)/2}, \end{aligned} \tag{3.2.35}$$

$$\begin{aligned} S_4(z) &\equiv u^{A_1}(u-1)^{A_2}(u-u_a)^{A_3}(u-u_\infty) \\ &\times (1-u)^{1-\delta}H\ell(1-a, ((1-a)\gamma + \epsilon)(1-\delta) + \alpha\beta - q; \\ &\qquad \alpha + 1 - \delta, \beta + 1 - \delta, 2 - \delta, \gamma; 1-u) \\ &\sim (1-x)^{(m+s)/2}, \end{aligned} \tag{3.2.36}$$

For $s + m < 0$, $S_3(u)$, and $0 < m + s$, $S_2(u)$ is preferable. Then, the angular solutions are derived as follows:

$$S(u) \sim \begin{cases} S_1(u) & (z \sim 0, s < m) \\ S_2(u) & (z \sim 0, m < s) \\ S_3(u) & (z \sim 1, 0 < s + m) \\ S_4(u) & (z \sim 1, s + m < 0) \end{cases} \tag{3.2.37}$$

The solutions around the boundaries are derived, and the perturbation problem is reduced to finding the quasi-normal frequency, ω, and separation constant, λ, while simultaneously ensuring that the solutions around the boundary are linearly dependent. In the next section we calculate the quasi-normal modes of Schwarzschild-de Sitter black hole as a simple example.

3.3 Quasi-normal Modes for Schwarzschild dS

In this section, we numerically calculate the quasi-normal modes for Schwartzschild-de Sitter using the *Mathematica* function "`HeunG`$[a, q, \alpha, \beta, \gamma, \delta, z]$"[2] and finding quasi-normal frequency ω. The Schwarzschild metric is obtained from the Kerr metric by setting the rotation parameter $a = 0$. In this case, the angular equation become trivial, and the separation constant, λ, is derived analytically:

$$\lambda = l(l+1) - s(s+1). \tag{3.3.1}$$

[2]The specifications of this function are found at https://reference.wolfram.com/language/ref/HeunG.html

The boundary condition is used to derive the radial solutions, (3.2.30). However, these solutions are only regular either around $z = 0$ or $z = 1$. We want to obtain the ω with which the solution is regular around both singular points. This condition is reduced to a linear dependence problem, which is addressed by the Wronskian of two solutions. The Wronskian tells us the linear dependence of the functions, and in this case it is written as follows:

$$W[R_2(z), R_3(z)]_{z=1/2} = R_2 R_3' - R_2' R_3 = 0, \tag{3.3.2}$$

where we choose the evaluation point as the midpoint between the two singularities. See Fig. 3.3. Fig. 3.4 shows a contour plot of $\log_{10} |W[R_2(z), R_3(z)]|$, where the zeros of Wronskian correspond to the quasi-normal modes, and there are some number of singular points are lined. Then, we use the function `FindRoot` to identify the location of the quasi-normal modes. The upper part of Fig. 3.5 shows a plot of the first forty quasi-normal modes, and the lower part shows a contour plot and identifies the quasi-normal modes. It can be seen that the points in Fig. 3.5 correspond to the quasi-normal modes and match the pole in Fig. 3.4. We list the first four quasi-normal frequencies in Table 3.1, and these values agree with the results derived using the WKB approximation and approximation by the Pöshl-Teller potential [1].

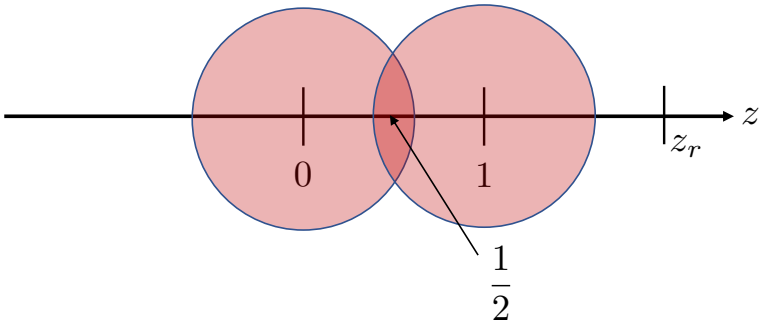

Figure 3.3: Diagram of the overlap of the convergence area. The solutions are regular near the singularities, and we assume that the midpoint of the two singularities ($z = 1/2$) is a suitable point to consider the Wronskian.

n	$\mathrm{Re}(\omega)$	$\mathrm{Im}(\omega)$
0	0.3383914276	-0.08175644548
1	0.3187586680	-0.2491966309
2	0.2827321809	-0.4294841197
3	0.2405415091	-0.6281919186

Table 3.1: First four quasi-normal modes. These values for $n = 0, 1$ agree with those derived in a previous study using the WKB approximation and approximation by the Pöshl-Teller potential [1].

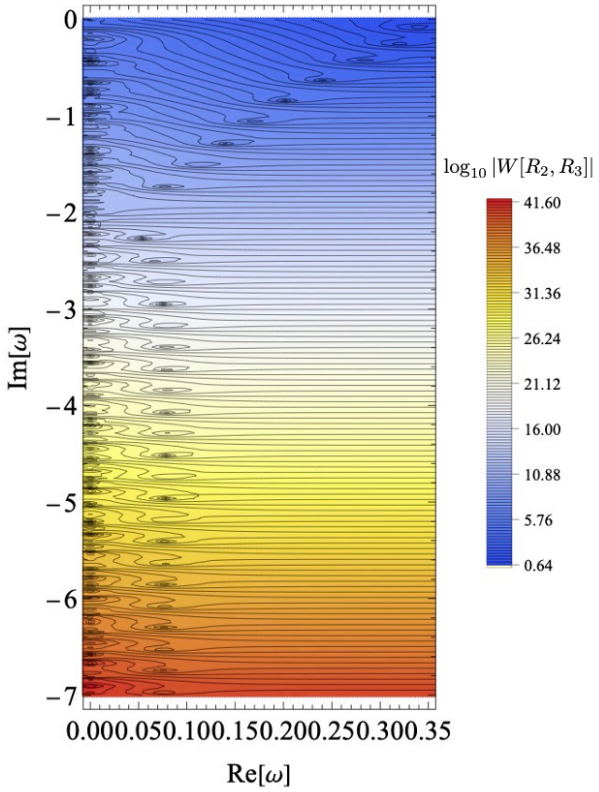

Figure 3.4: Contour plot of $\log_{10} W[R_2(z), R_3(z)]_{z=1/2}$. Solutions that satisfy the boundary conditions are given, (3.2.30), and we want the ω where the two solutions are linearly dependent. This condition corresponds to $W[R_2(z), R_3(z)] = 0$ at $z = 1/2$ (see Fig. 3.3). Thus, the singular points of this figure corresponds to the desired quasi-normal frequencies. Although this plot does not show the exact location of the singular points, the rough location is useful for using the function `FindRoot`.

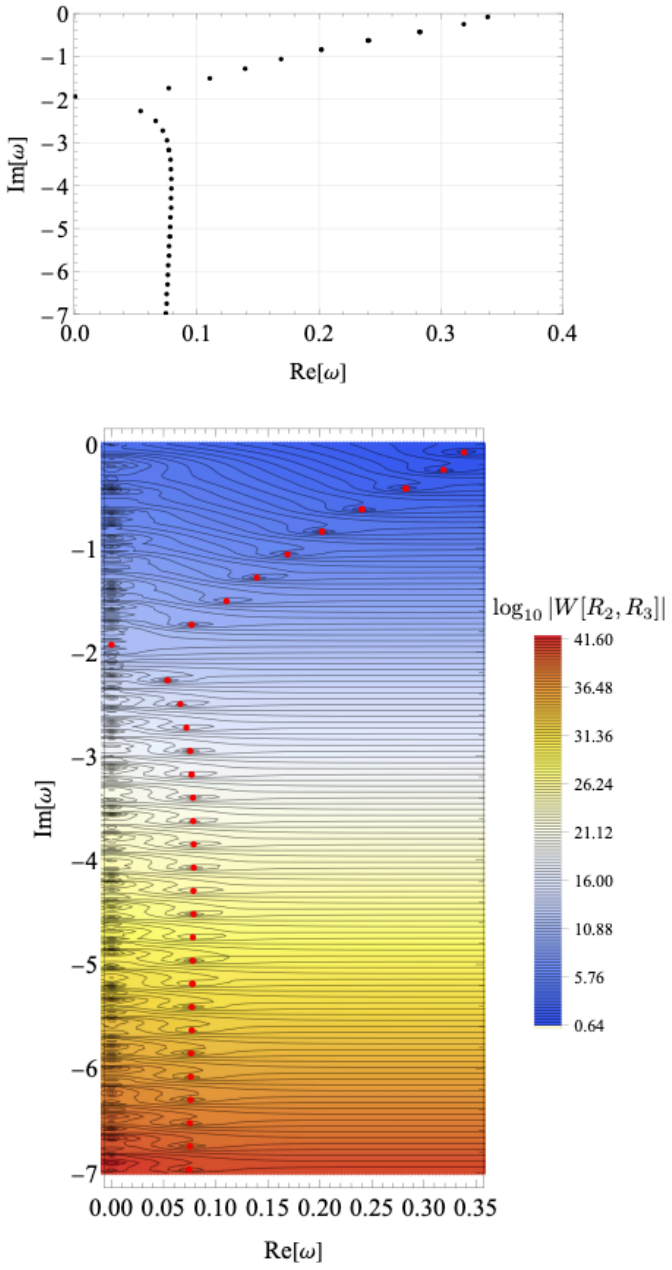

Figure 3.5: Plot of the identified quasi-normal frequencies using the function `FindRoot`. Overlaying this on the contour plot of Fig. 3.4 confirms that the poles of the contour plot match the numerically calculated quasi-normal frequencies.

Chapter 4

Catalytic Effect in Five Dimensions

In Sec. 2.6.1, we reviewed a bubble universe setup in which a bubble is nucleated in AdS_5 spacetime with a black hole and a cloud of strings, and the radiation and the matter energy densities were determined for the bubble spacetime. The study that proposed this setup [25] did not consider the catalytic effects of the black hole and the cloud of strings. In Sec. 2.5, we reviewed that the presence of a black hole enhances the decay rate of the vacuum decay. In this chapter we examine the catalytic effect in AdS_5.

4.1 Schwartzschild BH and Cloud of Strings

In this section, we will discuss the catalytic effect of a static black hole and a cloud of strings in AdS_5 [61]. The metric is (2.6.14), and the Euclidean bubble equation of motion for this condition is derived by substituting the metric into the following:

$$V_{\text{eff}}(\tilde{R}) = -\left(\frac{d\tilde{R}}{d\tilde{\lambda}}\right)^2 = -1 + \tilde{R}^2 + \frac{k_1 + 2k_2}{\tilde{R}^2} + \frac{k_2^2}{\tilde{R}^6} + \frac{k_3 + 2k_4}{\tilde{R}} + \frac{k_4^2}{\tilde{R}^4} + \frac{2k_2k_4}{\tilde{R}^5}, \tag{4.1.1}$$

where we have introduced the following parameters,

$$k_1 = \frac{8G_5}{3\pi}\left(\frac{\alpha}{\gamma}\right)^2\left(M_- + (1-\alpha)\frac{M_+ - M_-}{2\bar{\sigma}\gamma}\right), \quad k_2 = \frac{8G_5}{3\pi}\left(\frac{\alpha}{\gamma}\right)^3\frac{M_+ - M_-}{4\bar{\sigma}} \tag{4.1.2}$$

$$k_3 = \frac{2}{3}\left(\frac{\alpha}{\gamma}\right)\left(a_- + \frac{(a_+ - a_-)(1-\alpha)}{2\bar{\sigma}\gamma}\right), \quad k_4 = \frac{a_+ - a_-}{6\bar{\sigma}}\left(\frac{\alpha}{\gamma}\right)^2 \tag{4.1.3}$$

$$l^2 = \frac{6}{\Lambda_+ - \Lambda_-}, \quad \gamma = \frac{4\bar{\sigma}l^2}{1+4\bar{\sigma}^2l^2}, \quad \alpha^2 = 1 + \frac{3\Lambda_-\gamma^2}{3}. \tag{4.1.4}$$

Fig. 4.1 shows a plot of the effective potential, which can be used to derive the period of the bounce solution. The bounce action formula (2.4.38) is modified to consider five dimensions:

$$S_E = \frac{1}{16\pi G_5}\int_{\mathcal{W}} dx^4\sqrt{\gamma}\left(\left(\frac{2f_+}{R} - f_+'\right)\dot{\tau}_+ - \left(\frac{2f_-}{R} - f_-'\right)\dot{\tau}_-\right) - \sum_i \frac{\mathcal{A}_i}{4G_5}. \tag{4.1.5}$$

Remembering the bounce action formula, (2.4.41), and substituting the metric into (4.1.5), we obtain the bounce action:

$$B = \frac{\pi}{4G_5}\int_{\mathcal{W}} d\lambda\Big[\left(R^2 - 4G_5M_+ - a_+R\right)\dot{\tau}_+ - \left(R^2 - 4G_5M_- - a_-R\right)\dot{\tau}_-\Big] + \frac{\pi^2}{2G_5}\left(r_{h_+}^3 - r_{h-}^3\right). \tag{4.1.6}$$

Before evaluating the bounce action, we fix the difference between the true and false vacuum energy, $l_+/l_- = 0.6$. In this case, this combination is derived from (2.6.25):

$$\bar{\sigma}_{\text{crit}}l = \frac{1}{2}\sqrt{\frac{l_+ - l_-}{l_+ + l_-}} = 0.25. \tag{4.1.7}$$

Our universe is observationally de Sitter [14, 15] and has a very small cosmological constant. Thus, $\bar{\sigma}l$ is close to the critical value that corresponds to an observationally supported universe. In Figs. 4.2, 4.3, and 4.4, we numerically calculate the bounce action and show that a black hole and a cloud of strings also enhance the vacuum decay in AdS_5, where each plot has a minimum value when the bounce solution becomes stationary.

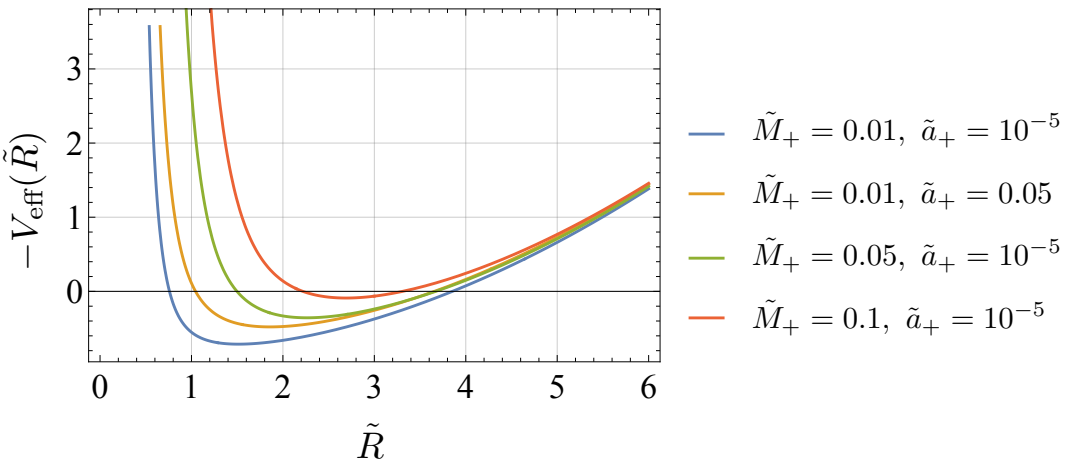

Figure 4.1: Plot of the effective potential for the various values of the two parameters: the black hole mass $\tilde{M}_+$ and the tension of the cloud of strings $\tilde{a}_+$. The other parameters are set to $4\pi G_5 \sigma l/3 = 0.2, l_-/l_+ = 0.6$. We can construct an oscillating bounce solution based on the potential shape.

4.2 Catalysis of Quintessence in Five Dimensions

The quintessence is the time varying scalar field that was first considered as a candidate for dark energy in a 4D universe. Here, we quickly review the 4D case and then consider a 5D case. With a scalar field ϕ in a 4D FLRW spacetime, whose potential is given by $V(\phi)$, the equation of state is derived as follows:

$$w = \frac{\dot{\phi}^2/2 - V(\phi)}{\dot{\phi}^2/2 + V(\phi)}. \tag{4.2.1}$$

Equation of state parameter w can vary with the time evolution, and the potential determines how it will change. Models for quintessence can be divided into two major categories: freezing and thawing models. In a freezing model, the field first moves quickly and then slows down. In such a case, w changes from 0 to -1. On the other hand, in a thawing model, the field stays calm at first and then at some time it starts to move quickly. In this case, w starts at -1 and then changes to 0. If the quintessence contributes to the dark energy, w must be very close to -1, which is realized for the late

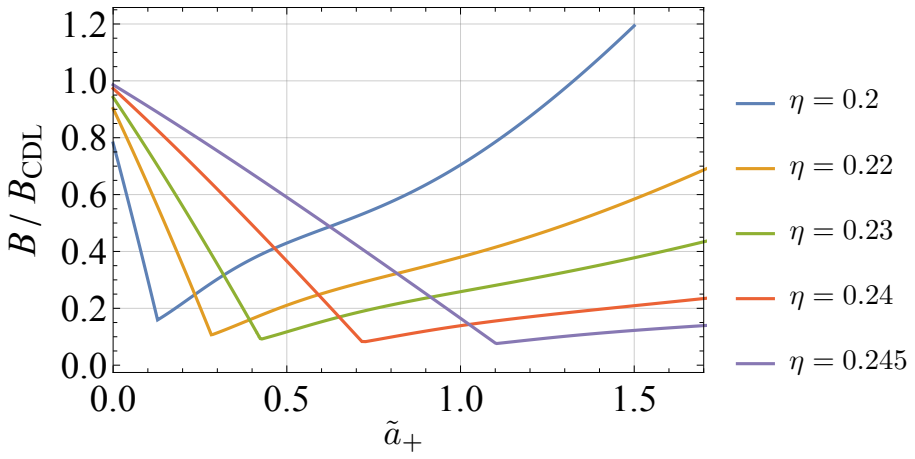

Figure 4.2: Plot of bounce action in the presence of a black hole and a cloud of strings for $\eta = 0.2 \sim 0.245$ with the black hole mass fixed $\tilde{M}_+ = 8G_5M_+/3\pi l^2 = 0.04$. The smallest action is derived as η approaches $\eta_{\rm crit} = 0.25$.

time of the freezing model and the first time of thawing model. We do not explain the details of the quintessence because the various applications and derivations are provided by review papers [92, 93]. Instead, we extend this quintessence to five dimensions.

The solution for the quintessence with a black hole was first studied by Kiselev [94] and extended to five dimensions by [95, 96]. The solution for the quintessence and cosmological constant in five dimensions is given by:

$$ds^2 = -f(r)^2dt^2 + \frac{dr^2}{f(r)^2} + r^2d\Omega_3^2, \tag{4.2.2}$$

$$f(r) = 1 - \frac{\Lambda r^2}{6} - \frac{\alpha}{r^{4w+2}}, \tag{4.2.3}$$

where α is a normalization parameter related to the energy density of quintessence,

$$\rho = -\frac{3\alpha w}{r^4(w+1)}. \tag{4.2.4}$$

We consider the decay from Minkowski to AdS_5 spacetime. For this case, the

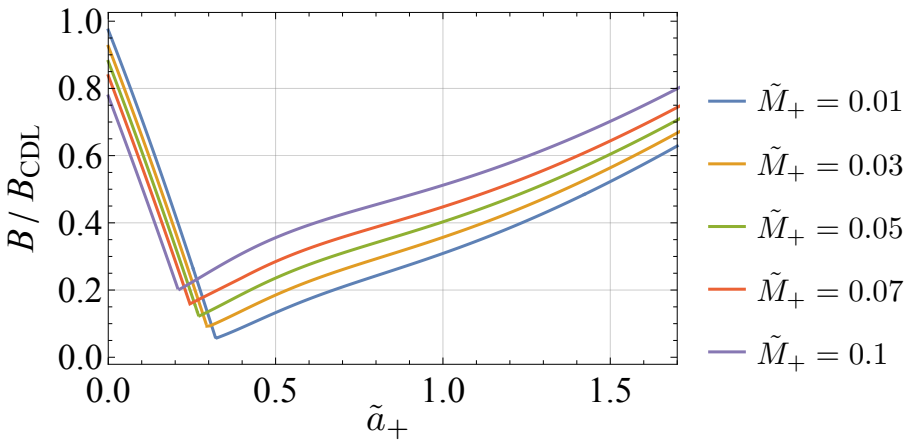

Figure 4.3: Plot of bounce the action in the presence of a black hole and cloud of strings. We fixed $\eta = 0.22$ and varied the black hole mass, $\tilde{M}_+ = 0.01 \sim 0.1$. The minimum value of each bounce action decreases with the black hole mass.

metric is as follows:

$$f_+(\tilde{r}) = 1 - \frac{q_+}{\tilde{r}^{4w+2}}, \qquad f_-(\tilde{r}) = 1 - \left(\frac{\gamma}{l_-\alpha}\right)^2 - \frac{q_-}{\tilde{r}^{4w+2}}, \tag{4.2.5}$$

where the parameters are defined in (4.1.4). In addition to these, we also define the following quintessence parameter:

$$Q_\pm^{(w)} = q_\pm \left(\frac{\alpha}{\gamma}\right)^{(4w+2)}. \tag{4.2.6}$$

Then, the equation of motion of the bubble is derived:

$$\dot{\tilde{R}}^2 = 1 - \tilde{R}^2 - \left(\bar{q} + \frac{\Delta q}{8\eta^2}\right)\frac{1}{\tilde{R}^{4w+2}} - \left(\frac{(1+\eta^2)\alpha\Delta q}{16\eta^2}\right)^2 \frac{1}{\tilde{R}^{8w+6}}, \tag{4.2.7}$$

and we numerically calculate the bounce action for some values of the equation of state parameter w. Fig. 4.5 and Fig. 4.6 show plots of the bounce action, and it can be seen that the quintessence also produces catalysis. in this thesis we do not focus on the relation with the bubble universe, although in [62] we discussed the realization of the inflation and cosmological constant in the quintessence scenario in five dimensions.

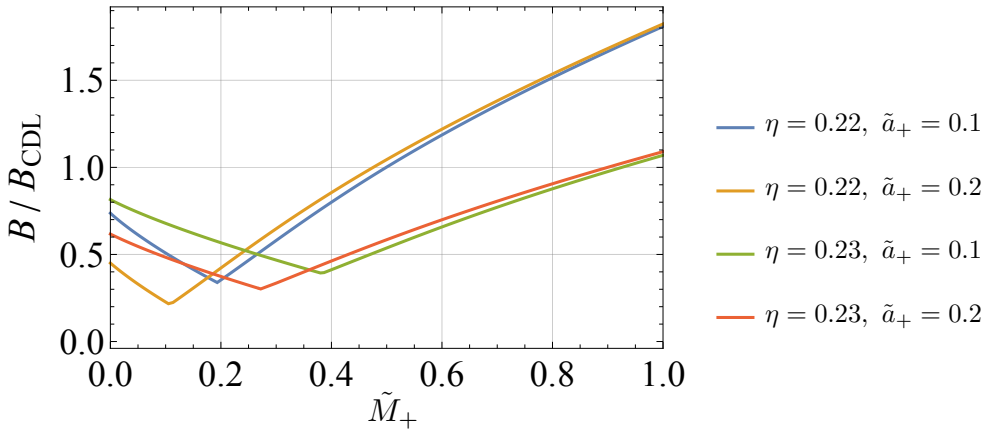

Figure 4.4: Plot of the bounce action in the presence of a black hole and a cloud of strings as afunction of the black hole mass M_+, where $\eta = 0.22, 0.23$, $\tilde{a}_+ = 0.1, 0.2$.

4.3 Catalysis Effect of Kerr-AdS$_5$

A black hole can have angular momentum and generally be rotating. The catalysis effects of rotating black holes in four and three dimensions were discussed in [55, 57, 56], but the rotating effect in AdS$_5$ is unknown. There are two orthogonal axes of rotation for a rotating black hole in five dimensions. Because it is difficult to construct a junction surface for the two-axis case, we assume that the values of angular momentum are the same for both axes and consider the so called "Myers-Perry black hole" [97]. This black hole was extended to the case with the cosmological constant [98, 99], and the rotating junction surface was introduced in [100, 101]. This thesis uses this construction and discusses the catalytic effect of a rotating black hole in five dimensions [63]. In particular, this section sets 5D Newton constant $G_5 = 1$.

4.3.1 Formalism

The line element of Kerr-AdS$_5$ spacetime with the cosmological constant $\Lambda = -6l^2$ is expressed by the coordinates of $x^\mu = (t, r, \theta, \psi, \phi)$ [99]:

$$ds^2 = -f(r)^2 dt^2 + g(r)^2 dr^2 + r^2 \hat{g}_{ab} dx^a dx^b + h(r)^2 \left[d\psi + A_a dx^a - \Omega(r) dt \right]^2, \qquad (4.3.1)$$

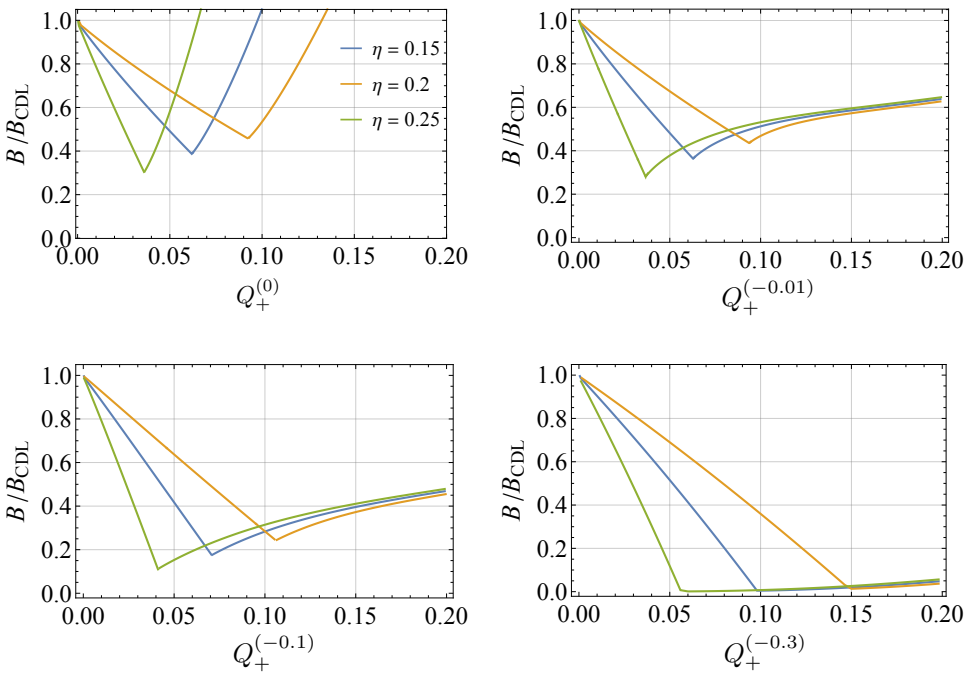

Figure 4.5: Plot of the bounce action in the presence of quintessence of the freezing model. The plot shows $w = 0, -0.01, 0.1, 0.3$ and $\eta = 0.15, 0.2, 0.25$, where the horizontal axis corresponds to quintessence parameter $Q_+^{(w)}$.

where

$$A_a dx^a \equiv \frac{1}{2}\cos\theta d\phi, \quad g(r)^2 \equiv \left(1 + \frac{r^2}{l^2} - \frac{2M\Xi}{r^2} + \frac{2Ma^2}{r^4}\right)^{-1}, \tag{4.3.2}$$

$$h(r)^2 \equiv r^2\left(1 + \frac{2Ma^2}{r^4}\right), \quad \Omega(r) \equiv \frac{2Ma}{r^2 h(r)^2}, \quad f(r) \equiv \frac{r}{g(r)h(r)} \tag{4.3.3}$$

$$\Xi \equiv 1 - \frac{a^2}{l^2}, \quad \hat{g}_{ab}dx^a dx^b \equiv \frac{1}{4}(d\theta^2 + \sin^2\theta d\phi^2). \tag{4.3.4}$$

We then use the similar manner as in Sec.2.4.1, and set a junction surface Σ as:

$$\Sigma = \{x^\mu : t = T(\lambda),\ r = R(\lambda)\}, \tag{4.3.5}$$

where this surface separates two different AdS vacua, the false ($\Lambda_+ = -6l_+^2$) and true ($\Lambda_- = -6l_-^2$) vacua. Then, we transform the coordinates to a

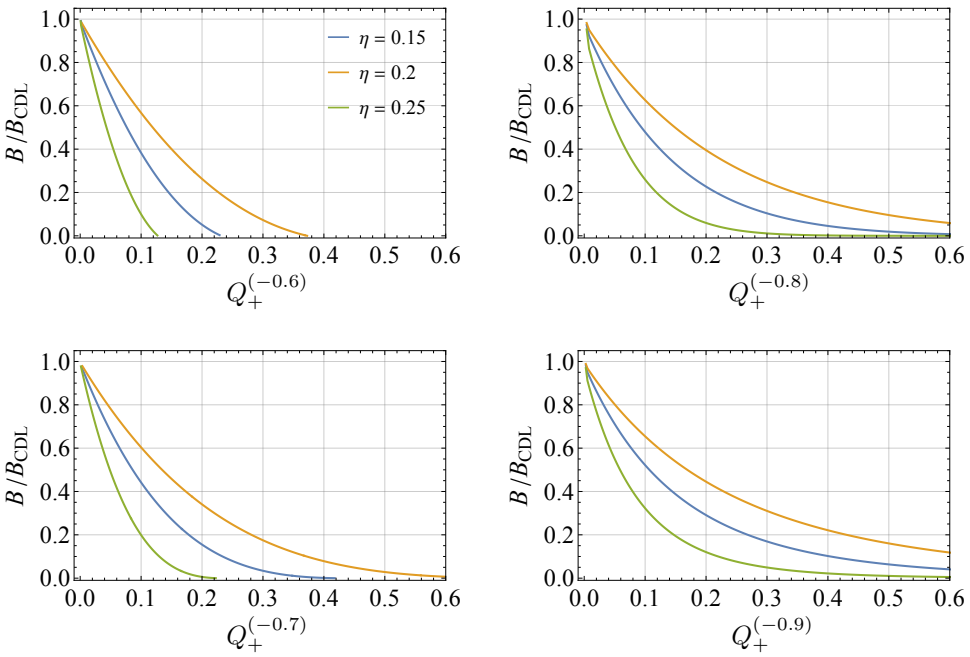

Figure 4.6: Plot of the bounce action in the presence of quintessence of thawing model. The plot shows $w = -0.6, -0.7, -0.8, -0.9$ and $\eta = 0.15, 0.2, 0.25$, where the horizontal axis corresponds to quintessence parameter $Q_+^{(w)}$.

co-moving frame:

$$d\psi \to d\psi' + \Omega_\pm(R(t))dt, \tag{4.3.6}$$

$$dt \to \frac{dT}{d\tau}d\tau, \tag{4.3.7}$$

$$dr \to \frac{dR}{d\tau}d\tau, \tag{4.3.8}$$

then the metric (4.3.1) also changes:

$$\begin{aligned} ds_\pm^2 = &- f_\pm(r)^2 dt^2 + g_\pm(r)^2 dr^2 + r^2 \hat{g}_{ab} dx^a dx^b \\ &+ h_\pm(r)^2 \left[d\psi + A_a dx^a + (\Omega_\pm(R) - \Omega_\pm(r))\, dt \right]^2. \end{aligned} \tag{4.3.9}$$

The induced metric for this metric on the junction surface is:

$$ds_\pm^2 = \gamma_{\pm ij}dy^i dy^j = -\left[f_\pm^2\left(\frac{dT}{d\lambda}\right)^2 - g_\pm^2\left(\frac{dR}{d\lambda}\right)^2\right]d\lambda^2 + r^2\hat{g}_{ab}dx^a dx^b + h_\pm^2\left[d\psi + A_a dx^a\right]^2. \tag{4.3.10}$$

Then, the first Israel junction condition (2.4.7) is used to derive the following conditions:

$$f_\pm^2 \dot{T_\pm}^2 - g_\pm^2 \dot{R}^2 = 1, \tag{4.3.11}$$

$$M_+ a_+^2 = M_- a_-^2 \equiv Ma^2, \tag{4.3.12}$$

where the dot denotes the derivative with respect to the proper time on the junction surface, λ. Formula (4.3.12) implies that the black hole must not vanish after the vacuum decay (false vacuum). This is different from the Schwartzschild black hole case. The extrinsic curvature is given as:

$$K_{\mu\nu} = \left(g_{\mu\nu} - n_\mu n_\sigma\right)\Delta^\sigma n_\nu, \tag{4.3.13}$$

where n_μ is the unit normal vector to Σ,

$$n_\pm = f_\pm(r)g_\pm(r)\left(-\dot{R}dt_\pm + \dot{T}_\pm dr_\pm\right). \tag{4.3.14}$$

The induced extrinsic curvature is obtained using a tangent vector to Σ ($e_i^\mu = dx^\mu/dy^i$):

$$K_{ij} = e_i^\mu e_j^\nu K_{\mu\nu}. \tag{4.3.15}$$

For the spherically symmetric 4D and 5D cases, we assumed that the reduced energy momentum tensor S_{ij} was uniform, but now we consider a junction surface that is deformed from a spherical shape. Hence, the surface should be expressed as an imperfect fluid with anisotropic and intrinsic momentum:

$$\mathcal{S}_{ij} = (\sigma + P)u_i u_j + Pq_{ij} + 2\varphi u_{(i}\xi_{j)} + \Delta P R^2 \hat{g}_{ij}, \tag{4.3.16}$$

where $\xi = h^{-1}(R)\partial_\psi$, and u^i is the unit tangent vector on Σ:

$$u^\mu = \dot{t}\frac{\partial x^\mu}{\partial t} + \dot{r}\frac{\partial x^\mu}{\partial r}, \quad u^\mu u_\mu = -1. \tag{4.3.17}$$

Then, the second junction condition for this imperfect fluid is derived [100, 101, 102]:

$$\sigma = -\frac{(\beta_+ - \beta_-)(R^2 h)'}{8\pi R^3}, \tag{4.3.18}$$

$$P = \frac{h}{8\pi R^3}[R^2(\beta_+ - \beta_-)]', \tag{4.3.19}$$

$$\varphi = \frac{(\Omega'_+ - \Omega'_-)h^2}{16\pi R}, \tag{4.3.20}$$

$$\Delta P = \frac{(\beta_+ - \beta_-)}{8\pi}\left[\frac{h}{R}\right]', \tag{4.3.21}$$

where the prime denotes the derivative with R and

$$\beta_\pm \equiv f_\pm^2 \dot{T}_\pm = \epsilon_\pm f_\pm(R)\sqrt{1 + g_\pm^2 \dot{R}^2}. \tag{4.3.22}$$

Here, $\epsilon_\pm$ represent a sign ambiguity of $\dot{T}_\pm$, which corresponds to the bubble wall orientation, and from (4.3.22) the sign of β tells us the orientation. We expect the bubble to expand both inside and outside after the nucleation, and this situation corresponds to the sign of $\dot{T}_\pm$ being positive ($\epsilon_\pm = +1$) at both sides, so we impose this sign. We assume the following equation of state:

$$P = w\sigma, \tag{4.3.23}$$

then we combine (4.3.18) and (4.3.19) to obtain the following formula:

$$\frac{[R^2(\beta_+ - \beta_-)]'}{R^2(\beta_+ - \beta_-)} = -w\frac{[R^2 h]'}{R^2 h}. \tag{4.3.24}$$

Integrating this gives an equation that describes the bubble dynamics:

$$\beta_+ - \beta_- = -\frac{m_0^{1+3w/2}}{R^{2(1+w)}h^w(R)} \equiv -A(R), \tag{4.3.25}$$

where m_0 is an integration constant with the dimension of the mass. Then, we obtain the equation of motion of the bubble:

$$\dot{R}^2 + V_{\text{eff}} = 0, \tag{4.3.26}$$

$$V_{\text{eff}} = \frac{1}{g_-^2}\left[1 - \left(\frac{-f_+^2 + f_-^2 + A^2}{2Af_-}\right)^2\right]. \tag{4.3.27}$$

From here, we assume that $w = -1$, in this assumption the equation of state (4.3.23) satisfies the relation $P = -\sigma$. Then, we substitute the metrics and equation (4.3.25) into the effective potential, and organizing the terms, we obtain a Friedmann-like equation, (2.6.22), for the rotating junction surface:

$$\begin{aligned}\left(\frac{\dot{R}}{R}\right)^2 + R^{-2} = &-\frac{1}{4}\left(-\frac{(l_+^2 - m_0)^2}{l_+^4 m_0} - \frac{m_0}{l_-^4} + \frac{2}{l_-^2} + \frac{2m_0}{l_-^2 l_+^2}\right) \\ &- M_- a_-^2\left(-\frac{1}{a_-^2} - \frac{1}{a_+^2} + \frac{1}{l_-^2} + \frac{1}{l_+^2} - \frac{1}{m_0}\right)R^{-4} \\ &- 2Ma^2 R^{-6} + \frac{(Ma^2)^2}{m_0}R^{-8} + \frac{(a_-^2 - a_+^2)^2 M_-^2 m_0}{a_+^2(2Ma^2 + R^4)^2} \\ &- \frac{(a_- - a_+)(a_- + a_+)(l_- - l_+)(l_- + l_+)M_- m_0}{a_+^2 l_-^2 l_+^2 (2Ma^2 + R^4)}. \end{aligned} \tag{4.3.28}$$

Note that this equation is an exact expression, unlike (2.6.22), which is an expression of the large R approximation. As an example, Fig. 4.7 shows a plot of the effective potential.

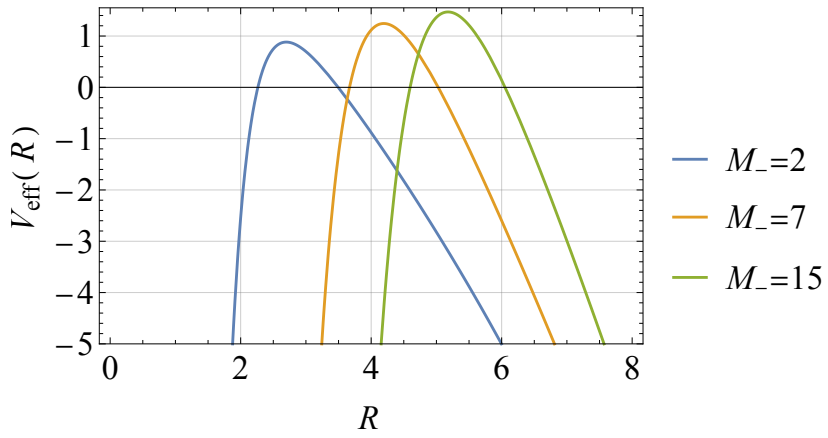

Figure 4.7: Plot of the effective potential, (4.3.28), for several values of parameters. The parameters are set to $M_+ = 1$, $a_+ = 0.6$, $l_+ = 7$, $l_= = 4$, $m_0 = 500$, and $w = -1$. Because of the junction condition (4.3.12), there is always a remnant black hole, and we changed this remnant black hole mass $M_- = 2, 7, 15$

4.3.2 Euclidean Action

We evaluate the Euclidean formalism and show the results. From (2.3.2), the catalysis of the vacuum decay is estimated by the bounce action:

$$\Gamma = Ae^{-B}, \qquad B = S_E(\phi) - S_E(\phi_{fv}), \tag{4.3.29}$$

where the bounce action is derived from the Euclidean on-shell action. We here perform the coordinate change:

$$t \to -it_E, \qquad \lambda \to -i\lambda_E, \tag{4.3.30}$$

which changes the sign of the potential, (4.3.26),

$$\dot{R}^2 - V_{\text{eff}} = 0. \tag{4.3.31}$$

Then, we calculate the bounce action similar way of Sec.2.4.2. The Euclidean action can be divided into four parts: those around the BH horizon ($S_{\mathcal{H}}$), inside the bubble ($S_{\mathcal{M}_-}$), outside the bubble ($S_{\mathcal{M}_+}$), and the wall itself ($S_{\mathcal{W}}$).

$$S_E = S_{\mathcal{H}} + S_{\mathcal{M}_-} + S_{\mathcal{M}_+} + S_{\mathcal{W}} \tag{4.3.32}$$

$$S_{\mathcal{H}} = -\frac{1}{16\pi G}\int_{\mathcal{M}} dx^5\sqrt{g_E}R + \frac{1}{8\pi G}\int_{\partial\mathcal{H}} d^4x\sqrt{g_E}K_E \tag{4.3.33}$$

$$S_{\mathcal{M}_\pm} = -\frac{1}{16\pi G}\int_{\mathcal{M}} dx^5\sqrt{g_E}R + \frac{1}{8\pi G}\int_{\partial\mathcal{H}} d^4x\sqrt{q_E}K_{E\pm} - \int_{\mathcal{M}_\pm} dx^5\sqrt{g_E}\mathcal{L}_m \tag{4.3.34}$$

$$S_{\mathcal{W}} = -\int_{\mathcal{W}} dx^5\sqrt{g_E}\mathcal{L}_m \approx \int_{\mathcal{W}} dx^4\sqrt{g_E}\sigma \tag{4.3.35}$$

where we asuumed the action of the wall Lagrangian is expressed as one parameter σ. The action around the horizon can be expressed as the area of the horizon [103]:

$$S_{\mathcal{H}} = -\frac{\mathcal{A}}{4G} = -\frac{\pi^2 r_+(r_+^2 + a^2)}{2G(1 - a^2/l^2)}. \tag{4.3.36}$$

This formula also matches the entropy of the black hole [98]. Here, we define n and u as the normal vectors on the wall and a constant t_E surface,

respectively:

$$n_{\pm\mu} = \pm f(r)g(r)\left(-\frac{d\mathcal{R}_E}{d\tau_E}, \frac{d\mathcal{T}_E}{d\tau_E}, 0, 0, 0\right) \tag{4.3.37}$$

$$u_{\pm\mu} = (f_\pm, 0, 0, 0, 0) \tag{4.3.38}$$

$$u^{\pm\mu} = g^{\mu\nu}u_{\pm\nu} = \left(\frac{1}{f_\pm}, 0, 0, -\frac{i\Omega}{f_\pm}, 0\right). \tag{4.3.39}$$

Note that $u^\mu u_\mu = 1$ for Euclidean spacetime. Then, using the ADM formalism, we decompose the action and organize the terms. The action of the bulk part is obtained as follows:

$$S_{\mathcal{M}_\pm} = \frac{1}{8\pi G}\int_{\partial\mathcal{H}} d^4x\sqrt{q_E}\tilde{K}_{E\pm} + \frac{1}{8\pi G}\int_{\partial\mathcal{H}} d^4x\sqrt{q_E}\kappa_\pm, \tag{4.3.40}$$

$$\kappa_\pm = n_{\pm\mu}u^\nu_\pm u^\mu_{\pm;\nu}. \tag{4.3.41}$$

Here, κ is the surface term, which is given as:

$$\kappa_\pm = n_{\pm1}u^0_\pm\left(u^0_\pm\Gamma^1_{\pm00} + u^3_\pm\Gamma^1_{\pm30}\right) + n_{\pm1}u^3_\pm\left(u^0_\pm\Gamma^1_{\pm30} + u^3_\pm\Gamma^1_{\pm33}\right) \tag{4.3.42}$$

$$= \mp\frac{\dot{T}_E f'_\pm}{g_\pm} = \mp\frac{f'_\pm}{f_\pm g_\pm}\sqrt{1 + g^2_\pm V_{\text{eff}}}. \tag{4.3.43}$$

The Christoffel symbols are given:

$$\Gamma^1_{\pm00} = \frac{f^3_\pm}{g^2_\pm r}\left(\frac{-4a^2_\pm M^2_\pm g^3_\pm}{r^7}(rh' + 2h) + hg'_\pm + \frac{g_\pm}{r}(rh' - h)\right) \tag{4.3.44}$$

$$\Gamma^1_{\pm30} = \frac{2ia_\pm M_\pm}{r^3 g^2_\pm}, \qquad \Gamma^1_{\pm33} = -\frac{hh'}{g^2_\pm}. \tag{4.3.45}$$

Next, we take the trace of S_{ij}:

$$S = S_{ij}q^{ij} = -4\sigma + 2\Delta P = \frac{3(\beta_+ - \beta_-)}{4\pi G}\left(\frac{h}{\mathcal{R}^2} + \frac{h'}{\mathcal{R}}\right) \tag{4.3.46}$$

where we use the relations (4.3.18) and (4.3.21). Combining these formulas, finaly we obtain the Euclidean action as:

$$S_{\rm E}^{(\rm f)} = -\frac{\mathcal{A}_-}{4} + \frac{1}{8\pi}\int_{\mathcal{W}} dx^4\sqrt{q_{\rm E}}(K_{\rm E+} - K_{\rm E-}) + \int_{\mathcal{W}} dx^4\sqrt{q_{\rm E}}\sigma + \frac{1}{8\pi}\int_{\mathcal{W}} dx^4\sqrt{q_{\rm E}}(\kappa_+ + \kappa_-), \tag{4.3.47}$$

$$= -\frac{\mathcal{A}_-}{4} + \int_{\mathcal{W}} dx^4\sqrt{q_{\rm E}}\left(-\frac{1}{3}\sigma + \frac{2}{3}\Delta P\right) + \frac{1}{8\pi}\int_{\mathcal{W}} dx^4\sqrt{q_{\rm E}}(\kappa_+ + \kappa_-), \tag{4.3.48}$$

$$= \int d\lambda_{\rm E}\int d^3x\frac{\sqrt{q_{\rm E}}}{8\pi}\left\{\left(\frac{h'f_+}{R} - \frac{f'}{f_\pm g_\pm}\right)\sqrt{1+V_{\rm eff}g_+^2} - (+\leftrightarrow -)\right\} - \frac{\mathcal{A}_-}{4} \tag{4.3.49}$$

$$= \int d\lambda_{\rm E}\int d^3x\frac{\sqrt{q_{\rm E}}}{8\pi}\left\{\frac{h'f_+ - hf'}{R}\sqrt{1+V_{\rm eff}g_+^2} - (+\leftrightarrow -)\right\} - \frac{\mathcal{A}_-}{4}. \tag{4.3.50}$$

The bounce action is derived:

$$B = S_E(\phi) - S_E(\phi_{\rm fv}) \tag{4.3.51}$$

$$= \frac{\mathcal{A}_+ - \mathcal{A}_-}{4} + \int d\lambda_{\rm E}\int d^3x\frac{\sqrt{q_{\rm E}}}{8\pi}\left\{\frac{h'f_+ - hf'}{R}\sqrt{1+V_{\rm eff}g_+^2} - (+\leftrightarrow -)\right\}, \tag{4.3.52}$$

where $S_E(\phi_{\rm fv}) = -\mathcal{A}_+/4$.

4.3.3 Numerical Estimation of Bounce Action

In this section, we numerically evaluate the bounce action derived in the previous section. In the catalysis of Kerr-AdS$_5$, there are some parameters we need to fix: m_0, $M_\pm$, $a_\pm$, and $l_\pm$. As for several values of parameters, we here set $m_0 = 500$, $l_+ = 7$, $l_- = 4$. Fig. 4.8 shows a plot of the effective potential, where the same type of bounce solution as shown in Fig. 2.9 is obtained. In addition, we studied the allowed parameter range for stationary solutions and show this range in Fig. 4.9. This parameter restriction is based on the condition that the black hole before and after the decay must be regular. From this figure, the constraints from before and after the decay

are close to each other as the seed black hole mass becomes large, and the constraint from the remnant black hole (before the decay) is always strong.

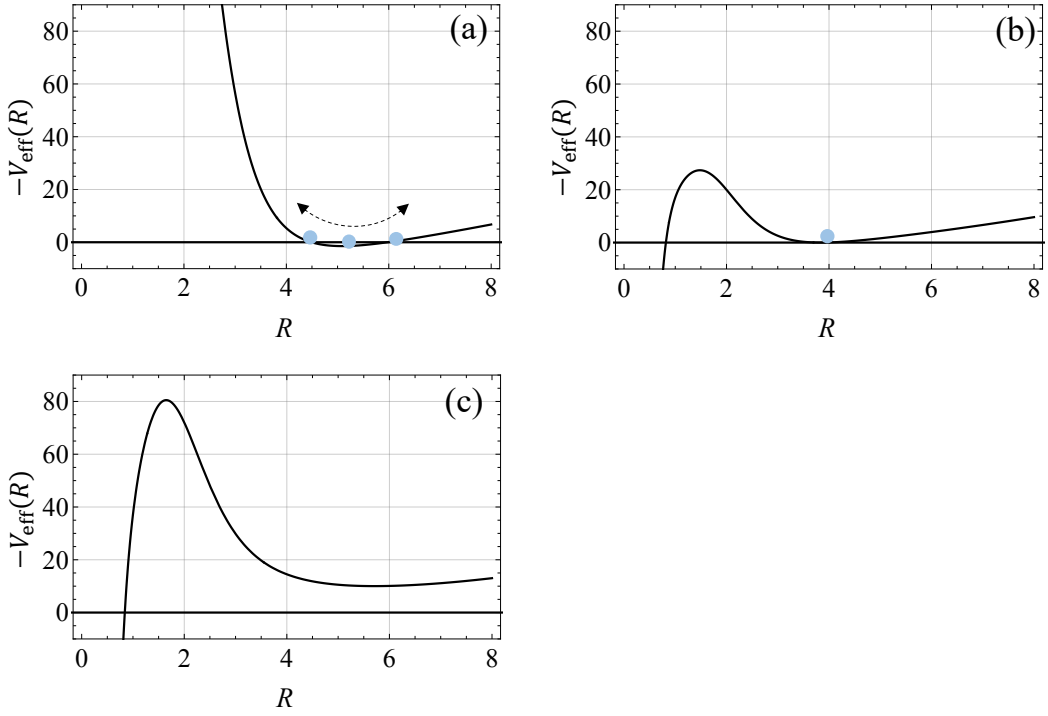

Figure 4.8: Plot of effective Euclidean potential, (4.3.31), for example parameters. The parameters are set to $M_- = 14.04,\ a_+ = 1,\ l_+ = 7,\ l_= = 4,\ m_0 = 500$, where (a) shows an oscillating solution, (b) shows a stationary solution, and (c) does not show a bounce solution. The mass parameter of the false vacuum differs and is set to (a)$M_+ = 1$ (b)$M_+ = 10$, and (c)$M_+ = 19.5$.

Then, we numerically evaluate the bounce action for the allowed parameters. In Fig. 4.10, we compare the non-stationary and stationary cases. The marker at each plot corresponds to the stationary solutions, and dashed line is the non-stationary bounce action. We found that when we fixed the seed black hole mass the stationary solution gave the minimum bounce action, and this means that the stationary bounce solution has the largest decay rate. Fig. 4.11 show the ratio of bounce action with the non-rotating black hole. From this figure, the bounce action is slightly decrease by the rotation, though the action increase for the large spin parameters. Small rotation do not change the decay rate so much, but the large rotation surpress the decay.

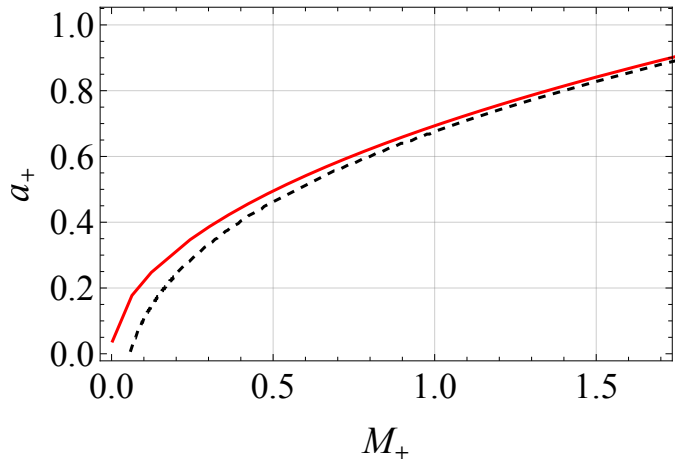

Figure 4.9: Plot of allowed range of the parameters (M_+, a_+) from the constraint that there is no naked singularity. The area below the red solid line indicates the constraint of the false vacuum (seed) black hole, while that below the black dashed line indicates the constraint of the true vacuum (remnant) black hole.

Let us consider the stationary bounce action, and the stationary bounce action is derived as follows:

$$e^{-B} = e^{\mathcal{A}_+ - \mathcal{A}_-/4} = e^{-\Delta S_{\rm BH}}, \tag{4.3.53}$$

where $\Delta S_{\rm BH} = (\mathcal{A}_+ - \mathcal{A}_-)/4$ is the entropy difference for the black hole before and after the decay. In the general vacuum decay case, the entropy difference $\Delta S_{\rm BH}$ is always positive, and the Bekenstein-Hawking entropy decreases after the vacuum decay (see the results in Sec.2.5 and Sec.4.1). However, we found that the entropy difference for the decay induced by a black hole with a large spin could be positive (Fig. 4.12). Naively, this case corresponds to $e^{-B} \gg 1$, and our Euclidean method seems invalid because of the breakdown of the semi-classical approximation. Contrary to this, there is another understanding of these results from the viewpoint of thermodynamics. The positive entropy difference, $0 < \Delta S_{\rm BH} = (\mathcal{A}_+ - \mathcal{A}_-)/4$, suggests that the entropy increases after the decay, and from the second law of thermodynamics, this entropy increase process is seen just a thermal phase transition and can be regard as a physical process.

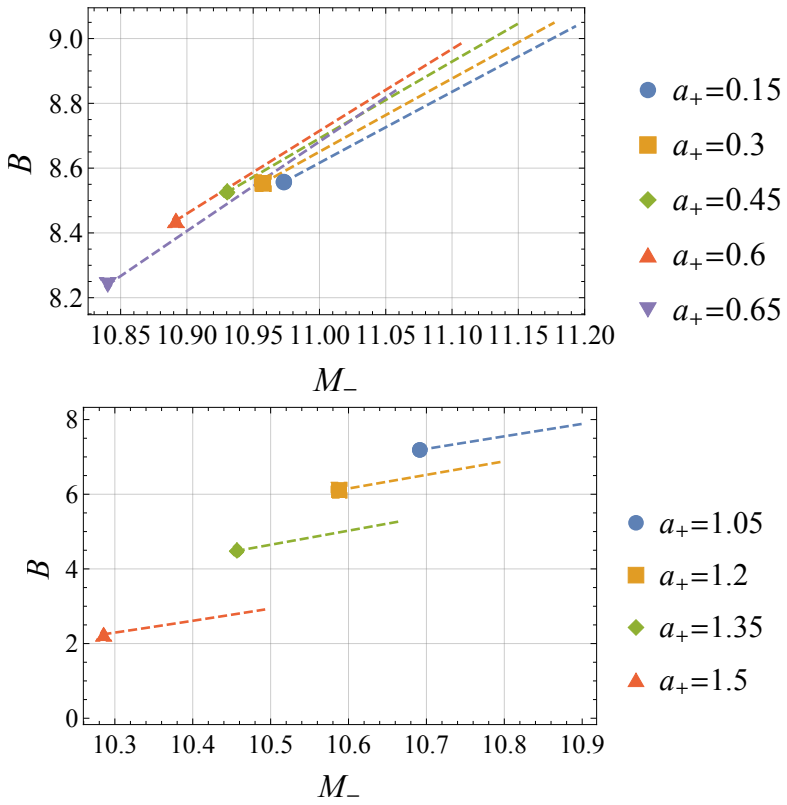

Figure 4.10: Plot of the bounce action for stationary (markers) and non-stationary (dashed lines) solutions. We varied spin parameter a_+ from $a_+ = 0.15$ to $a_+ = 1.5$. The non-stationary solution was constructed by shifting remnant mass M_- from a critical value using parameter $\delta \equiv M_-/M_-^{\rm crit}$. We evaluate for $10^{-13} \leq \delta \leq 0.02$, where $\delta = 0.02$ is the maximum difference because $0.02 \lesssim \delta$ alters the orientation of the bubble wall and breaks our scenario.

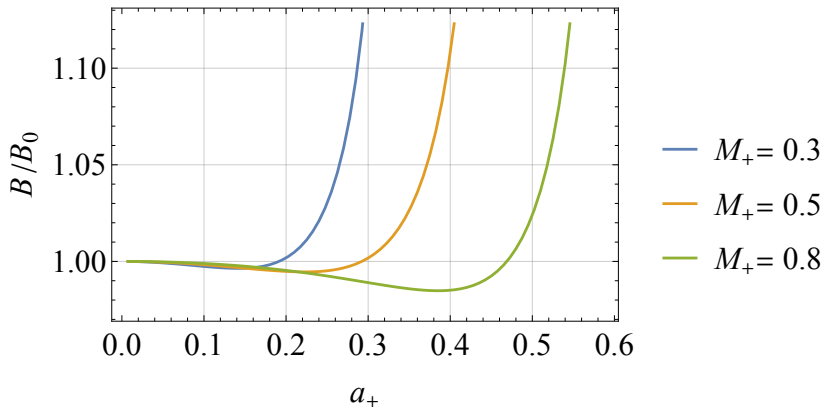

Figure 4.11: Plot of the ratio of bounce action with the non-rotationg case. The parameters are set to $m_0 = 500, l_+ = 7, l_- = 4$ and varied $M_+ = 0.3, 0.5, 0.8$.

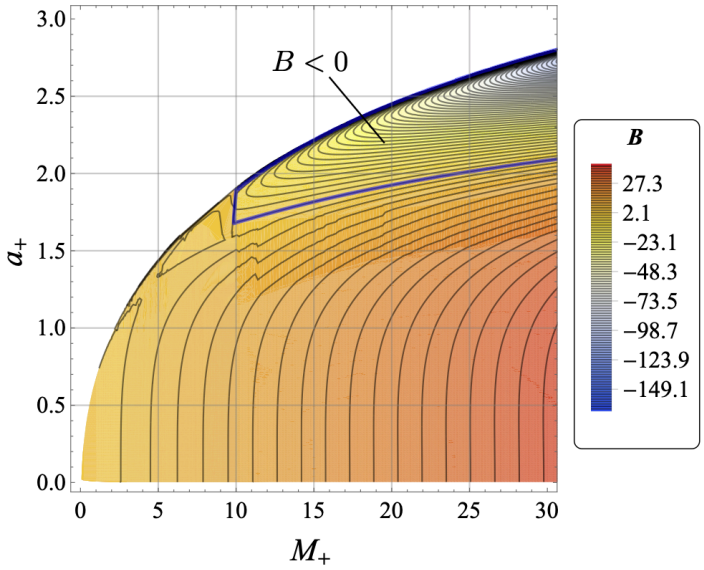

Figure 4.12: Contour plot of the bounce action for stationary solutions using the parameters allowed by the regularity conditions. The area surrounded by the blue solid line indicates that the bounce action is negative.

Chapter 5

Quasi-normal Modes of Kerr-AdS$_5$

This chapter first briefly reviews the superradiant instability, which cause the classical instability of rotating black holes. Then, the subsequent sections focus on the quasi-normal modes of a Kerr-AdS$_5$ black hole. We adopt Heun's equation method to identify the quasi-normal modes and show that there are two types of quasi-normal modes [39]. Then, we discuss the spacetime instability due to the superradiance and thermal properties of the quasi-normal modes. Finally, we discuss the competition between the unstable quasi-normal modes and catalytic effect of the vacuum decay.

5.1 Superradiant Instability

The waves scattered by a Kerr black hole extract the energy from the black hole, and the energy increases after the scattering. This phenomenon is known as superradiant scattering [29, 30, 31, 32]. This amplified scattering occurs when the incident wave $e^{-\omega t+im\phi}$, and angular velocity of the Kerr black hole Ω satisfy the following relation:

$$\omega < m\Omega. \tag{5.1.1}$$

Press and Tuekolsky suggested that if the Kerr black hole was surrounded by mirrors that reflected the wave, the incident wave would be amplified by the black hole, reflected by the mirrors, return to the black hole, be amplified again, reflected again, and so on. This repetition would continue until the

mirror was destroyed by the radiation pressure of the amplified wave [104]. This phenomena is so-called "black hole bomb" and was studied in detail by [105]. In the first suggestion, the mirrors was put by hands. However, Damour et al. showed that this situation could be realized using a charged massive scalar field for the charged and rotating Kerr-Newman black hole case [106]. In this case, there is a local minimum in the effective potential, and the scalar field is trapped in this minimum and can be regard as a mirror. The relations among the instability, the scalar field mass and charge have been studied [107, 108, 109]. On the other hand, AdS spacetime itself can be regarded as a box, whose boundary can be seen as a mirror. This is explained by considering the Regge-Wheeler potential (3.1.6) for AdS spacetime. The metric for Schwarzschild-AdS spacetime is given by:

$$ds^2 = f(r)dt^2 - \frac{dr^2}{f(r)} - r^2(d\theta^2 + \sin^2\theta d\phi^2), \tag{5.1.2}$$

$$f(r) = 1 - \frac{2M}{r} - r^2, \tag{5.1.3}$$

where we set the AdS radius equals to one. Then, the Regge-Wheeler equation and its potential for the scaler perturbation are obtained: [110, 111],

$$\left(-\frac{d^2}{dr_*^2} + V(r)\right) R(r,\omega) = \omega^2 R(r,\omega), \tag{5.1.4}$$

$$V(r) = \left(1 - \frac{2M}{r} + r^2\right)\left(\frac{l(l+1)}{r^2} - \frac{2M}{r^3} + 2\right), \tag{5.1.5}$$

where r_* is the tortoise coordinate, which is defined as:

$$\frac{\partial r}{\partial r_*} = f(r). \tag{5.1.6}$$

Fig. 5.1 shows a plot of the potential $V(r_*)$. This figure shows the potential barrier around the horizon and at infinity. This is the difference when we plot the potential for the gravitational perturbation for Schwartzschild black hole case, Fig. 3.1. Thus, the AdS spacetime is thought to be a box, and the region between two potential barriers acts as a kind of cavity, in which the situation of surrounding a black hole by reflectiong mirrors can be realized by placing the black hole there. Naively, AdS spacetime with a Kerr black hole is unstable as a result of the superradiance. The instability of a small

Kerr-AdS$_4$ was confirmed by [33]. However, the black hole also acts like an absorber because only ingoing modes at the event horizon, and it is proposed that spacetime is stable for a large black hole[112, 113, 114, 115]. In the following sections, we discuss the quasi-normal modes of a Kerr-AdS$_5$ black hole, along with the instability caused by superradiance. The instability was investigated using Painlevé transcendents, but the parameters were restricted to special cases such as those with nearly equal spins, a near extremal or small black hole [34, 35, 36, 37, 38].

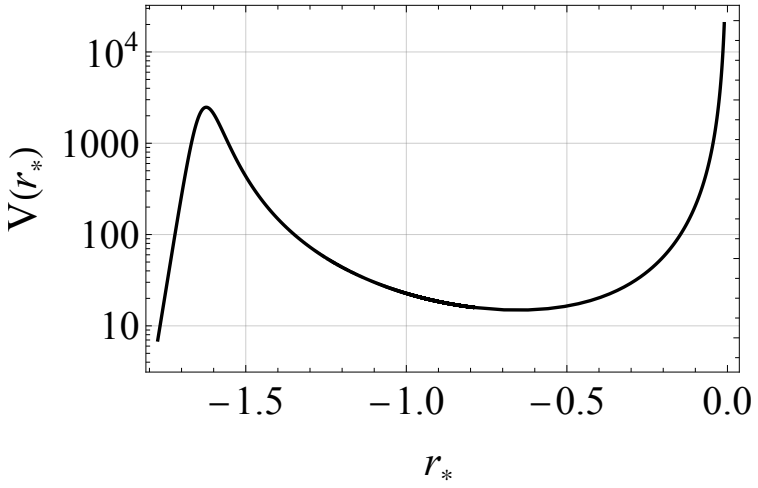

Figure 5.1: Plot of the Regge-Wheeler potential of scalar perturbation for the Schwarzschild-AdS black hole. The parameters are set to $M = 10^{-2}$and$l = 0$. There are the potential barriers near the horizon and the infinity can be seen, and this structure is considered to be a black hole in a box.

5.2 Setups

In this section, we consider the perturbations of a scalar field, and apply the Heun's equation method we reviewed in Sec. 3.2. Let us start with the

Kerr-AdS$_5$ metric:

$$\begin{aligned} ds^2 = &-\frac{\Delta_r}{\rho^2}\left(dt - \frac{a_1 \sin^2\theta}{1-a_1^2}d\phi - \frac{a_2\cos^2\theta}{1-a_2^2}d\psi\right)^2 \\ &+ \frac{\Delta_\theta \sin^2\theta}{\rho^2}\left(a_1 dt - \frac{r^2+a_1^2}{1-a_1^2}d\phi\right)^2 \\ &+ \frac{1+r^2}{r^2\rho^2}\left(a_1 a_2 dt - \frac{a_2(r^2+a_1^2)\sin^2\theta}{1-a_1^2}d\phi - \frac{a_1(r^2+a_2^2)\cos^2\theta}{1-a_2^2}d\psi\right)^2 \\ &+ \frac{\Delta_\theta \cos^2\theta}{\rho^2}\left(a_2 dt - \frac{r^2+a_2^2}{1-a_2^2}d\psi\right)^2 + \frac{\rho^2}{\Delta_r}dr^2 + \frac{\rho^2}{\Delta_\theta}d\theta^2, \end{aligned} \tag{5.2.1}$$

where the AdS curvature radius is set to one, and M is the mass parameter of the Kerr-AdS$_5$ black hole. Because the 5D rotating black hole has two independent rotation axes, a_1 and a_2 are the spin parameters for the two rotations of the Kerr-AdS$_5$ black hole. In addition, the following parameters are defined:

$$\Delta_r \equiv \frac{1}{r^2}(r^2+a_1^2)(r^2+a_2^2)(1+r^2) - 2M \tag{5.2.2}$$

$$= \frac{1}{r^2}(r^2-r_0^2)(r^2-r_+^2)(r^2-r_+^2), \tag{5.2.3}$$

$$\Delta_\theta \equiv 1 - a_1^2\cos^2\theta - a_2^2\sin^2\theta, \tag{5.2.4}$$

$$\rho^2 \equiv r^2 + a_1^2\cos^2\theta + a_2^2\sin^2\theta. \tag{5.2.5}$$

Here, $r_+,\ r_-,\ r_0$ are the roots of the equation $\Delta_r = 0$; r_+ and r_- are the real roots and correspond to the outer and inner horizon radii, respectively; and r_0 is the imaginary root. Based on the thermodynamics of Kerr-AdS$_5$ spacetime, the Arnowitt-Deser-Misner (ADM) mass and angular momentum are given by: [116, 117, 118]

$$\mathcal{M} \equiv \frac{\pi M(2\Xi_1 + 2\Xi_2 - \Xi_1\Xi_2)}{4\Xi_1^2\Xi_2^2},\ \mathcal{J}_\phi \equiv \frac{\pi M a_1}{2\Xi_1^2\Xi_2},\ \mathcal{J}_\psi \equiv \frac{\pi M a_2}{2\Xi_1\Xi_2^2}, \tag{5.2.6}$$

where $\Xi_i \equiv 1 - a_i^2$ $(i = 1, 2)$. From these formulas, the spin parameters, $a_1,\ a_2$, are restricted to $a_1, a_2 \leq 1$, in order for all the physical quantities in (5.2.6) to be well defined. Then, we consider the instability of a scalar field with mass μ and compute the quasi-normal modes of the Kerr-AdS$_5$ black

hole. In this case, the Klein-Gordon equation with scalar field $\Phi(t, r, \theta, \phi, \psi)$ is:

$$\left[\nabla_\mu \nabla^\mu - \mu^2\right] \Phi = 0. \tag{5.2.7}$$

Assuming the ansatz, $\Psi = e^{-i\omega t + im_1\phi + im_2\psi} S(\theta) R(r)$, the equation is decomposed into the following radial and angular equations:

$$\begin{aligned}
&\frac{1}{r}\frac{d}{dr}\left(r\Delta_r \frac{dR(r)}{dr}\right) \\
&- \left[\lambda + \mu^2 r^2 + \frac{1}{r^2}\left(a_1 a_2 \omega - a_2(1-a_1^2)m_1 - a_1(1-a_2^2)m_2\right)^2\right] R(r) \\
&+ \frac{(r^2+a_1^2)^2(r^2+a_2^2)^2}{r^4\Delta_r}\left(\omega - \frac{m_1 a_1(1-a_1^2)}{r^2+a_1^2} - \frac{m_2 a_2(1-a_2^2)}{r^2+a_2^2}\right)^2 R(r) = 0,
\end{aligned} \tag{5.2.8}$$

$$\begin{aligned}
&\frac{1}{\sin\theta\cos\theta}\frac{d}{d\theta}\left(\sin\theta\cos\theta\,\Delta_\theta \frac{dS(\theta)}{d\theta}\right) \\
&- \left[-\lambda + \omega^2 + \frac{(1-a_1^2)m_1^2}{\sin^2\theta} + \frac{(1-a_2^2)m_2^2}{\cos^2\theta}\right. \\
&\left. - \frac{(1-a_1^2)(1-a_2^2)}{\Delta_\theta}(\omega + m_1 a_1 + m_2 a_2)^2 + \mu^2(a_1^2\cos^2\theta + a_2^2\sin^2\theta)\right] S(\theta) = 0,
\end{aligned} \tag{5.2.9}$$

where λ is the separation constant, which is determined by the regularity condition, $S(\theta)$, at $\theta = 0$ and $\theta = \pi/2$ [119]. Then we perform the following transformations like we did at (3.2.8)-(3.2.11):

$$r \to z \equiv \frac{r^2 - r_-^2}{r^2 - r_0^2}, \tag{5.2.10}$$

$$R(r) \to R(z) \equiv z^{-\theta_-/2}(z - z_0)^{-\theta_+/2}(z-1)^{\Delta/2}\Pi(z), \tag{5.2.11}$$

$$\sin^2\theta \to u \equiv \frac{\sin^2\theta}{\sin^2\theta - \chi_0}, \text{ with } \chi_0 \equiv \frac{1-a_1^2}{a_2^2 - a_1^2}, \tag{5.2.12}$$

$$S(\theta) \to S(u) \equiv u^{m_1/2}(u-1)^{\Delta/2}(u-u_0)^{m_2/2}\Theta(u), \tag{5.2.13}$$

where

$$z_0 \equiv \frac{r_+^2 - r_-^2}{r_+^2 - r_0^2}, \quad u_0 \equiv \frac{a_2^2 - a_1^2}{a_2^2 - 1}, \quad \Delta \equiv 2 + \sqrt{4 + \mu^2}. \tag{5.2.14}$$

Under these transformations, the boundaries are mapped to:

$$r : (r_+, \infty) \to z : (z_0, 1), \tag{5.2.15}$$

$$\theta : (0, \frac{\pi}{2}) \to u : (0, 1). \tag{5.2.16}$$

Note that for these transformations, black hole horizon r_+ is mapped to z_0, which is different from the mapping at (3.2.21). Then, the radial and angular equations are reduced to the Heun's differential equations [34]:

$$\frac{d^2\Pi}{dz^2} + \left[\frac{1-\theta_-}{z} + \frac{-1+\Delta}{z-1} + \frac{1-\theta_+}{z-z_0}\right]\frac{d\Pi}{dz} + \left(\frac{\kappa_1\kappa_2}{z(z-1)} - \frac{K}{z(z-1)(z-z_0)}\right)\Pi = 0, \tag{5.2.17}$$

$$\frac{d^2\Theta}{du^2} + \left[\frac{1+m_1}{u} + \frac{-1+\Delta}{u-1} + \frac{1+m_2}{u-u_0}\right]\frac{d\Theta}{du} + \left(\frac{q_1 q_2}{u(u-1)} - \frac{Q}{u(u-1)(u-u_0)}\right)\Theta = 0, \tag{5.2.18}$$

where

$$T_i \equiv \frac{r_i^2 \Delta_r'(r_i)}{4\pi(r_i^2+a_1^2)(r_i^2+a_2^2)} = \frac{r_i(r_i^2-r_j^2)(r_i^2-r_k^2)}{2\pi(r_i^2+a_1^2)(r_i^2+a_2^2)}, i \neq j, k, \tag{5.2.19}$$

$$\theta_i \equiv \frac{i}{2\pi}\frac{\omega - m_1\Omega_{i,1} - m_2\Omega_{i,2}}{T_i},\ \Omega_{i,1} \equiv \frac{a_1\Xi_1}{r_i^2+a_1^2},\ \Omega_{i,2} \equiv \frac{a_2\Xi_2}{r_i^2+a_2^2}, \tag{5.2.20}$$

$$\kappa_1 \equiv -\frac{1}{2}\left(\theta_- + \theta_+ - \Delta - \theta_0\right),\ \kappa_2 \equiv -\frac{1}{2}\left(\theta_- + \theta_+ - \Delta + \theta_0\right), \tag{5.2.21}$$

$$q_1 \equiv \frac{1}{2}\left(m_1 + m_2 + \Delta - \zeta\right),\ q_2 \equiv \frac{1}{2}\left(m_1 + m_2 + \Delta + \zeta\right), \tag{5.2.22}$$

$$\zeta \equiv \omega + a_1 m_1 + a_2 m_2, \tag{5.2.23}$$

$$K \equiv -\frac{1}{4}\left\{\frac{\lambda + \mu^2 r_-^2 - \omega^2}{r_+^2 - r_0^2} + (z_0-1)[(\theta_+ + \theta_- - 1)^2 - \theta_0^2 - 1] + z_0\left[2(\theta_+ - 1)(1-\Delta) + (2-\Delta)^2 - 2\right]\right\}, \tag{5.2.24}$$

$$Q \equiv -\frac{1}{4}\left\{\frac{\omega^2 + a_1^2\mu^2 - \lambda}{a_2^2 - 1} + u_0\left[(m_2 + \Delta - 1)^2 - m_2^2 - 1\right] + (u_0 - 1)\left[(m_1 + m_2 + 1)^2 - \zeta^2 - 1\right]\right\}. \tag{5.2.25}$$

For the radial part, we are interested in the solution near $z = z_0, 1$ because the boundaries are mapped to these points, and the general solutions of Heun's differential equation for the radial part at each point can be found as follows (5.2.17) [1], for $z \sim z_0$ ($r \sim r_+$):

$$\begin{aligned}\Pi(z) = a_1 H\ell\left(\frac{z_0}{z_0-1}, \frac{-K}{z_0-1}; \kappa_1, \kappa_2, 1-\theta_+, \Delta-1; \frac{z_0-z}{z_0-1}\right) \\ + a_2\left(\frac{z_0-z}{z_0-1}\right)^{\theta_+} H\ell\left(\frac{z_0}{z_0-1}, \frac{\theta_+[z_0(\Delta-\theta_-)-1+\theta_-]}{z_0-1} - \frac{K}{z_0-1}; \right. \\ \left. \kappa_1+\theta_+, \kappa_2+\theta_+, 1+\theta_+, \Delta-1; \frac{z_0-z}{z_0-1}\right),\end{aligned} \tag{5.2.26}$$

and for $z \sim 1$ ($r \sim \infty$):

$$\begin{aligned}\Pi(z) = a_3 H\ell\left(1-z_0, \kappa_1\kappa_2 - \tilde{K}; \kappa_1, \kappa_2, \delta-1, 1-\theta_-; 1-z\right) \\ + a_4(1-z)^{2-\Delta} H\ell\left(1-z_0, [(1-z_0)(1-\theta_-)+1-\theta_+](2-\Delta)\right. \\ \left. + \kappa_1\kappa_2 - \tilde{K}; \kappa_1+2-\Delta, \kappa_2+2-\Delta, 3-\Delta, 1-\theta_-; 1-z\right),\end{aligned} \tag{5.2.27}$$

where a_1, a_2, a_3, a_4 are the arbitrary constants, and we define $\tilde{K} \equiv K + \kappa_1\kappa_2 z_0$. For the angular equation (5.2.18), we are interested in the solution around $u = 0, 1$, and the general solutions at each point can be found as follows, for $u \sim 0$ ($\theta \sim 0$):

$$\begin{aligned}\Theta(u) = b_1 H\ell\left(u_0, \tilde{Q}; q_1, q_2, 1+m_1, \Delta-1; u\right) \\ + b_2 z^{m_1} H\ell\left(u_0, \tilde{Q} - m_1[u_0(\Delta-1)+m_2+1]; \right. \\ \left. q_1-m_1, q_2-m_1, 1-m_1, \Delta-1; u\right)\end{aligned} \tag{5.2.28}$$

[1] We also refer https://dlmf.nist.gov/31.

and for $u \sim u_0$ ($\theta \sim \pi/2$):

$$\Theta(u) = b_3 H\ell\left(\frac{u_0}{u_0-1}, \frac{-Q}{u_0-1}; q_1, q_2, 1+m_2, \Delta-1; \frac{u_0-u}{u_0-1}\right) + b_4\left(\frac{u_0-u}{u_0-1}\right)^{-m_2} H\ell\left(\frac{u_0}{u_0-1}, \frac{-Q-m_2[u_0(\Delta+m_1)-(1+m_1)]}{u_0-1}; q_1-m_2, q_2-m_2, 1-m_2, \Delta-1; \frac{u_0-u}{u_0-1}\right), \tag{5.2.29}$$

where b_1, b_2, b_3, b_4 are also arbitrary constants, and we define $\tilde{Q} \equiv Q + q_1 q_2 u_0$. The boundary conditions for the radial modes consist only of the ingoing mode at the horizon and Dirichlet boundary conditions at the infinity. These conditions are translated into the following formulas, for $\Pi(z)$:

$$R(z) \sim \begin{cases} (z-z_0)^{-\theta_+/2} \sim (r-r_+)^{-i\omega} & \text{for } z \to z_0 \ (r \to r_+), \\ (z-1)^{\Delta/2} \sim \text{finite value} & \text{for } z \to 1 \ (r \to \infty), \end{cases} \tag{5.2.30}$$

and for the angular modes, the regularity conditions of the separation of variables using separation constant λ at $u = 0$ ($\theta = 0$) and $u = u_0$ ($\theta = \pi/2$) are as follows:

$$S(u) \sim \begin{cases} u^{|m_1|/2} & \text{for } u \to 0 \ (\theta \to 0), \\ (u-u_0)^{|m_2|/2} & \text{for } u \to u_0 \ (\theta \to \pi/2). \end{cases} \tag{5.2.31}$$

To satisfy the boundary conditions (5.2.30), a_2 and a_4 should be zero ($a_2 = a_4 = 0$). Then, the solutions are derived as follows:

$$R(z) \sim \begin{cases} R_{\text{in}} & \equiv z^{-\theta_-/2}(z-z_0)^{-\theta_+/2}(z-1)^{\Delta/2} \\ & \quad \times H\ell\left(\frac{z_0}{z_0-1}, \frac{-K}{z_0-1}; \kappa_1, \kappa_2, 1-\theta_+, \Delta-1; \frac{z_0-z}{z_0-1}\right) \\ & \quad \text{for } z \to z_0 \ (r \to r_+) \\ R_{\text{AdS}} & \equiv z^{-\theta_-/2}(z-z_0)^{-\theta_+/2}(z-1)^{\Delta/2} \\ & \quad \times H\ell\left(1-z_0, \kappa_1\kappa_2 - \tilde{K}; \kappa_1, \kappa_2, \delta-1, 1-\theta_-; 1-z\right) \\ & \quad \text{for } z \to 1 \ (r \to \infty) \end{cases} \tag{5.2.32}$$

where we define $R_{\rm in}$ and $R_{\rm AdS}$ for later convenience. In addition, the regularity conditions are distinguished by the value of m_1 or m_2, for $u \sim u_0(\theta \sim 0)$:

$$\Theta(u) = \begin{cases} H\ell(u_0, \tilde{Q}; q_1, q_2, 1+m_1, \Delta-1; u) & \text{for } m_1 \geq 0, \\ z^{-m_1} H\ell\Big(u_0, -m_1[u_0(\Delta-1)+1+m_2] + \tilde{Q}; & \\ \qquad q_1 - m_1, q_2 - m_1, 1-m_1, \Delta-1; u\Big) & \text{for } m_1 \leq 0, \end{cases} \tag{5.2.33}$$

and for $u \sim u_0(\theta \sim \pi/2)$:

$$\Theta(u) = \begin{cases} H\ell\left(\dfrac{u_0}{u_0-1}, \dfrac{q_1 q_2 u_0 - \tilde{Q}}{u_0-1}; q_1, q_2, 1+m_2, \Delta-1; \dfrac{u_0-u}{u_0-1}\right) & \\ \qquad \text{for } m_2 \geq 0 & \\ \left(\dfrac{u_0-u}{u_0-1}\right)^{-m_2} H\ell\Big(\dfrac{u_0}{u_0-1}, \dfrac{-m_2[u_0(m_1+\Delta)-1-m_1]}{u_0-1} & \\ + \dfrac{q_1 q_2 u_0 - \tilde{Q}}{u_0-1}; q_1 - m_2, q_2 - m_2, 1-m_2, \Delta-1; \dfrac{u_0-u}{u_0-1}\Big) & \\ \qquad \text{for } m_2 \leq 0. & \end{cases} \tag{5.2.34}$$

We have derived the solutions for the Heun's equations (5.2.32)-(5.2.34) that satisfy the boundary conditions, and the next step is to evaluate the quasi-normal modes. As a similar manner in Sec.3.3 for equal spins ($a_1 = a_2$) because the separation constant is given analytically. However, in the case of a spin hierarchy case ($a_1 \neq a_2$), we need to simultaneously solve the separation constant, $\lambda_{lm_1m_2n}$, and quasi-normal frequency, $\omega_{lm_1m_2n}$.

5.2.1 Two Types of Quasi-normal Modes

In this section, we introduce the two types of quasi-normal modes. As a simple case, we consider the quasi-normal frequencies for the equal spin case, $a_1 = a_2 \equiv a$. In this case, the angular equation is reduced to a hypergeometric differential equation, and the separation constant is obtained analytically [119]:

$$\begin{aligned} \lambda =& (1-a^2)\left[l(l+2) - 2\omega a(m_1+m_2) - a^2(m_1+m_2)^2\right] \\ & + a^2\omega^2 + a^2\Delta(\Delta-4). \end{aligned} \tag{5.2.35}$$

n	Re(ω)	Im(ω)
0	5.823324048	$2.617598939 \times 10^{-6}$
1	7.748178566	$1.094235728 \times 10^{-5}$
2	9.629738537	$2.394806362 \times 10^{-5}$
3	11.45780837	$3.290281046 \times 10^{-5}$
4	13.20764082	$-3.386089822 \times 10^{-4}$

Table 5.1: First five type-I quasi-normal modes of Fig. 5.2, and first four modes show the unstable modes (positive sign of Im(ω)). The threshold between unstable and stable is $\Omega = 12.53888341$ for this parameter choice, and the result satisfies this condition. In addition, the value of the imaginary part is small compared to the real part, so the type-I modes are located along the real axis.

Using this formula, the problem is reduced to only the radial equation. Then, we plot the Wronskian[2] of the radial solutions, $W\left[R_{\rm in}(z), R_{\rm AdS}(z)\right]$, and find that there are two types of quasi-normal frequencies, as seen in Fig. 5.2: the type-I modes are localized at the real axis ($|{\rm Re}(\omega)| \gg |{\rm Im}(\omega)|$), and type-II modes are localized near the superradiant frequency Ω. This superradiant frequency is obtained for the Kerr-AdS$_5$ black hole case as:

$$ {\rm Re}(\omega_{lm_1m_2n}) < m_1\Omega_{+1} + m_2\Omega_{+2} \equiv \Omega, \tag{5.2.36} $$

where $\Omega_{1,2}$ are defined by (5.2.20).

These two types of quasi-normal modes have their own characteristics. Type-I modes correspond to the instability due to the superradiance because the first four type-I modes satisfy the superradiant condition (5.2.36), and the sign of their imaginary part is positive (Table 5.1), so their amplitudes are diverge as time evolution. On the other hand, the type-II modes are not related to the instability, but reflect the thermal properties of the Kerr-AdS$_5$ black hole. These properties are discussed in the following sections.

[2]For the Kerr-AdS$_5$ black hole case, because the radial boundaries are mapped to $r : (r_+, \infty) \to z : (z_0, 1)$ (5.2.15), the Wronskian is evaluated at $z = (z_0 + 1)/2$.

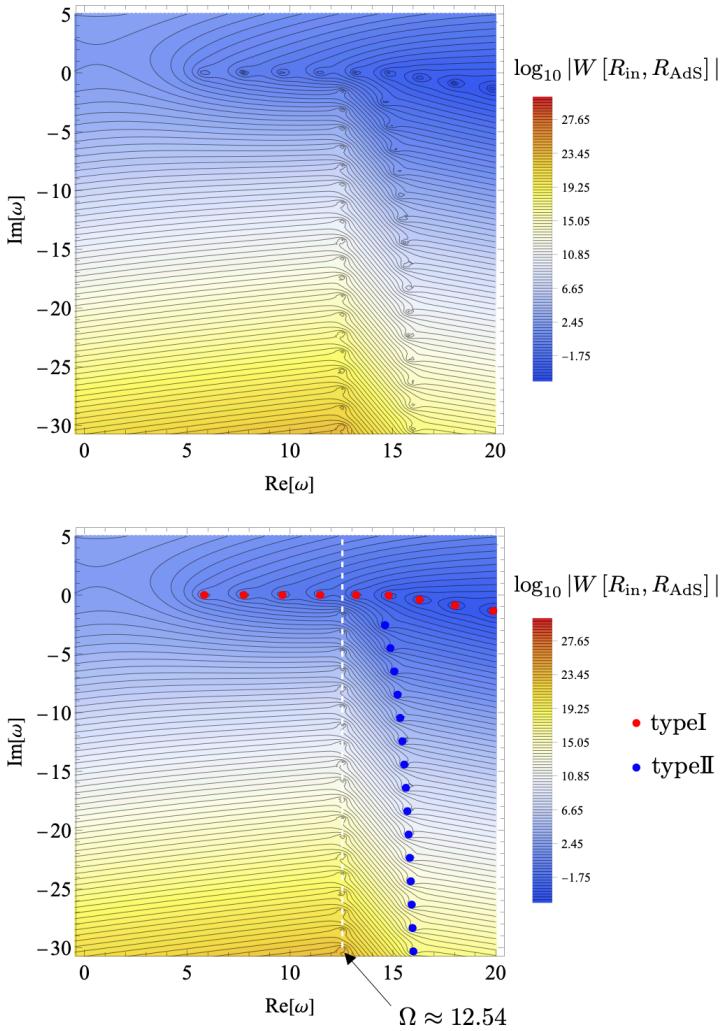

Figure 5.2: Contour plot of Wronskian $W\left[R_{\text{in}}(z), R_{\text{AdS}}(z)\right]$ evaluated at $z = (z_0 + 1)/2$. The parameters are set to $M = 10^{-2}, \mu = 10^{-3}, a_+ = 0.07, l = 2, m_1 = m_2 = 1$. For these parameters, the superradiant frequency $\Omega = 12.53888341$. The top figure shows the original contour plot, and in the lower figure, we identify the poles as the type-I modes, type-II modes, and singular points that are not quasi-normal modes $\text{Re}(\omega) = \Omega$.

5.3 Instability

5.3.1 Small black hole

We begin with an equal spin and small black hole ($\mathcal{M} \ll 1$). We plotted the type-I modes for $l = 1, 2, 3, 4$ up to $\mathrm{Re}(\omega_{lm_1m_2n}) < \Omega$ in Fig. 5.3, and it can be seen that the sign of the real part is positive in every case. This means that for a small black hole, unstable modes exist, and this instability is related to the superradiance. The figure also shows that the $l = 1$ modes have the largest instability, and each plot shows a slight peak before the superradiant frequency. These instabilities are thought to arise as a result of the resonance between the ergo region and AdS boundary, like in the 4D case. In addition, in Fig. 5.4, we vary the spin, $10^{-4} \leq a \leq 10^{-3}$, and find that a large spin enhances the instability because the value of $\mathrm{Im}(\omega)$ increases.

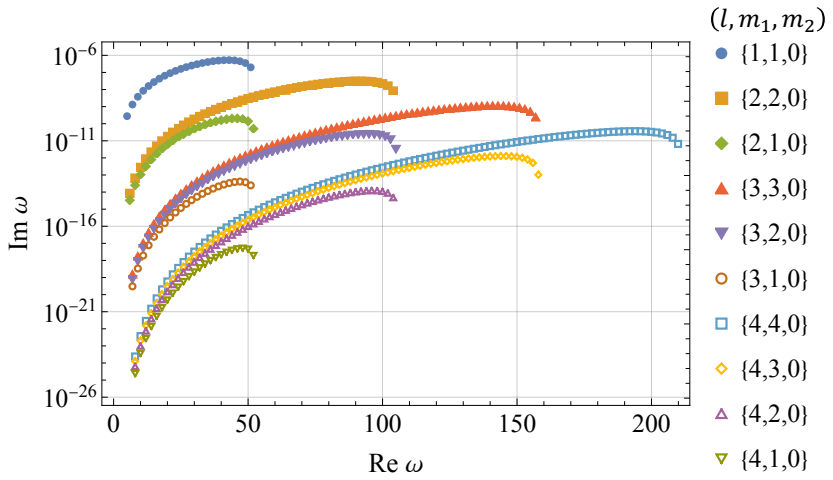

Figure 5.3: Plot of type-I modes that satisfy the superradiant condition for several values of angular modes (l, m_1, m_2). The parameters are set to $\mathcal{M} = 10^{-5}, a = 4 \times 10^{-4}, \upsilon = 10^{-2}$. The angular modes for $l = 1$ show the largest instability.

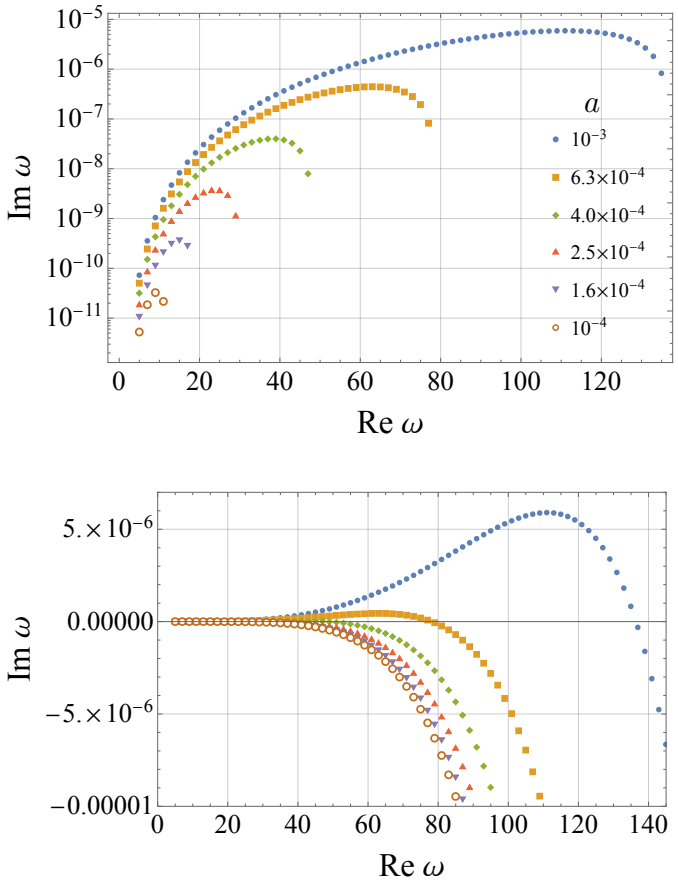

Figure 5.4: Plot of type-I modes for various spin parameters, a_+: $10^{-4} \leq a \leq 10^{-3}$. Other parameters are set to $\mathcal{M} = 10^{-5}, \mu = 10^{-2}$, and the angular modes are fixed to $(l, m_1, m_2) = (1, 1, 0)$. The upper and lower figures show log and linear scale plots. Larger spin indicates the larger value of Im(ω), so the instability increase with the spin.

The next step is to create a spin difference ($a_1 \neq a_2$) and investigate how the instability changes. The symmetry of the spacetime is reduced from $U(2)$ to $U(1) \times U(1)$ as a result of the spin difference. We express the spin difference as the ratio of the spin parameters, $a_2/a_1 \leq 1$, where a ratio equal to one corresponds to the equal spin case, and we assume that a_1 is larger. Then, in Fig. 5.5, we fix the superradiant frequency $\Omega = 116$ and vary spin ratio $a_2/a_1 = 1, 0.5, 0.9$. We find that the instability is enhanced when the spin ratio is large. From this result, the symmetry reduction of the Kerr-AdS$_5$ black hole enhances the superradiant instability when the parameters $\mathcal{M}, \mu, \Omega$ are fixed.

5.3.2 Large black hole

Next, we consider the instability of a large black hole ($1 \ll \mathcal{M}$). Just as with the small case, we first plot the contour plot of the Wronskian in Fig. 5.6 and find that there are also two types of quasi-normal modes. However, there are no unstable modes for a large black hole. This can be understood that the superradiant frequency for the large black hole is very small (e.g., the parameters in Fig. 5.6 are $M = 5, a = 0.5$, and $\Omega = 0.2821488469$). On the other hand, based on the physical understanding, the large black hole acts as a kind of absorber, so the resonance between the ergo region and AdS boundary disappears.

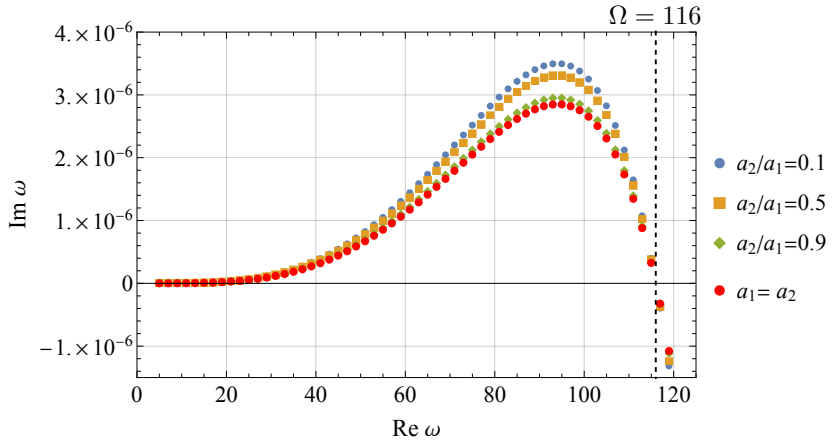

Figure 5.5: Plot of quasi-normal frequencies for several values of spin ratios a_2/a_1. We fixed parameters $\mathcal{M} = 10^{-5}, \mu = 10^{-2}$ and also fixed the superradiant frequency $\Omega = 116$ and angular modes $(l, m_1, m_2) = (1, 1, 0)$. We took the spin ratio $a_2/a_1 = 1, .0.9, 0.5, 0.1$. The black dashed line shows the superradiant frequency Ω. The instability increase as the spin difference becomes large.

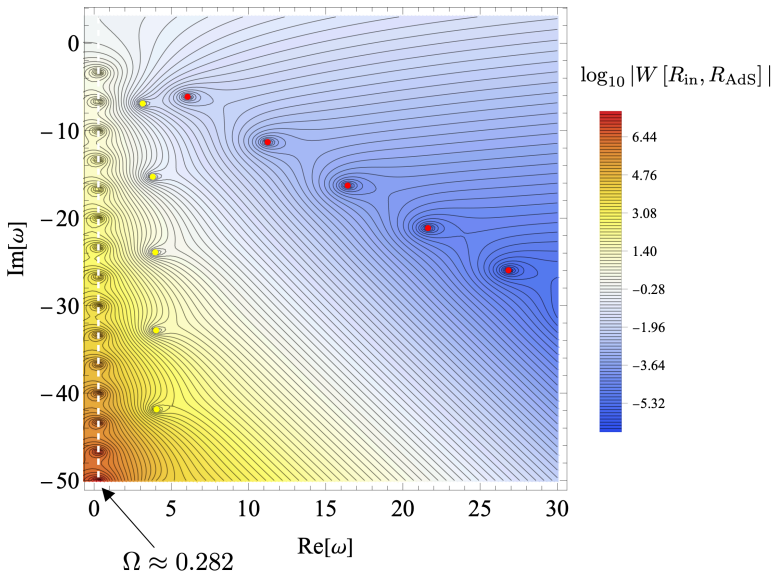

Figure 5.6: Contour plot of Wronskian, $W\left[R_{\rm in}(z), R_{\rm AdS}(z)\right]$, evaluated at $z = (z_0 + 1)/2$, especially for the large black hole. The parameters are set to $M = 5, \mu = 10^{-2}, a_+ = 0.5, l = 2, m_1 = m_2 = 1$. For these parameters, the superradiant frequency $\Omega = 0.2821488469$. The identified modes are overplotted, where the red dots correspond to type-I modes and yellow dots correspond to type-II modes. The white dashed line represents the superradiant frequency. Because Ω becomes small for the large black hole, there is no unstable modes for the type-I modes.

5.4 Thermality and Other Properties

This section focuses on the type-Ⅱ modes, and the signs of these modes are all negative. Thus, they are not related to the instability. On the other hand, the imaginary part of a type-Ⅱ mode shows an interesting feature. Fig. 5.9 shows a plot of the separation of the imaginary part of the quasi-normal frequencies $\Delta\mathrm{Im}(\omega_{lm_1m_2n})$ for a small black hole. Here, $\Delta\mathrm{Im}(\omega_{lm_1m_2n})$ is defined as:

$$\Delta\mathrm{Im}(\omega_{lm_1m_2n}) \equiv \mathrm{Im}(\omega_{lm_1m_2n}) - \mathrm{Im}(\omega_{lm_1m_2(n+1)}), \tag{5.4.1}$$

and the separation, $\Delta\mathrm{Im}(\omega_{lm_1m_2n})$, is seemed to approach $2\pi T_H$ at the zero temperature limit ($a \to a_{max}$). Then, we investigate the large black hole in Fig. 5.8. This figure confirms that even for a low temperature limit ($a \to 1$), the separation effectively and asymptotically approaches $2\pi T_H$, except for the fundamental mode ($n = 0$). Note that for the large black hole case, because the condition of $a_1, a_2 \leq 1$ is stronger, we cannot take the zero temperature limit. From these results, we conclude that type-Ⅱ modes reflect the thermal property of a Kerr-AdS$_5$ black hole.

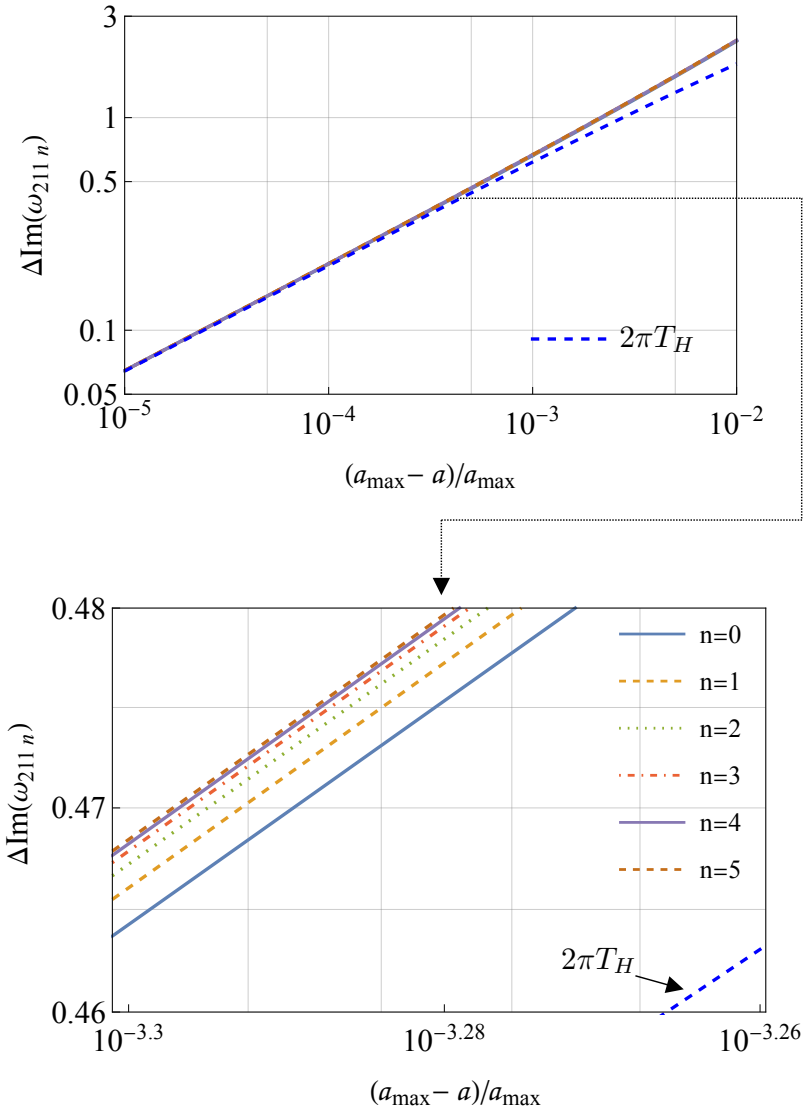

Figure 5.7: Plot of imaginary part spacing $\Delta\mathrm{Im}(\omega_{lm_1m_2n})$ of the small black hole case. The parameters are set to $M = 10^{-2}, \mu - 10^{-2}$, and angular modes are $(l, m_1, m_2) = (2, 1, 1)$. In this case, there is a maximum spin parameter $a_{\max}$, and the vertical axis is scaled for $a_{\max}$. The spacings are plotted for $n = 0 \sim 5$. The blue dashed line shows $2\pi T_H$, and the Hawking temperature is zero at the limit of $a \to a_{\max}$. The lower panel shows an enlarged view of the region for $10^{-3.3} \leq (a_{\max} - a)/a_{\max} \leq 10^{-3.26}$.

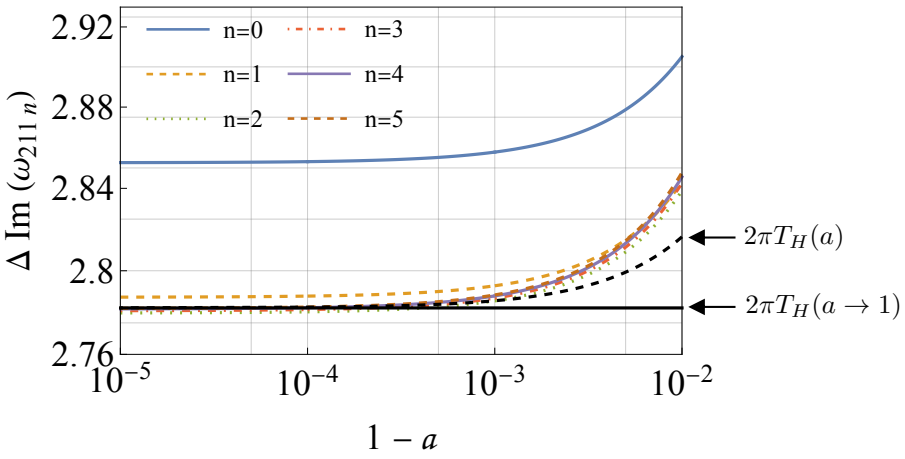

Figure 5.8: Plot of imaginary part spacing $\Delta\mathrm{Im}(\omega_{lm_1m_2n})$ of large black hole case. The parameters include $M = 10, \mu - 10^{-2}$, and angular modes are $(l, m_1, m_2) = (2, 1, 1)$. In this case, the maximum spin is one, and we take this limit. The spacings are plotted for $n = 0 \sim 5$. The black dashed line shows $2\pi T_H(a)$, and black solid line shows the asymptotic value of the Hawking temperature $(a \to 1)$.

Finally, we consider the asymptotic behavior of $\mathrm{Re}(\omega_{lm_1m_2n})$. Figs. 5.9 and 5.8 show plots of the asymptotic behaviors of $\mathrm{Re}(\omega_{lm_1m_2n})$ for small and large black holes, respectively. As seen in these figures, the real part approaches Ω for the zero or low temperature limit:

$$\mathrm{Re}(\omega) \to \Omega = m_1\Omega_1 + m_2\Omega_2. \tag{5.4.2}$$

We discuss the interpretation of this aymptotic value at Appendix A.1.

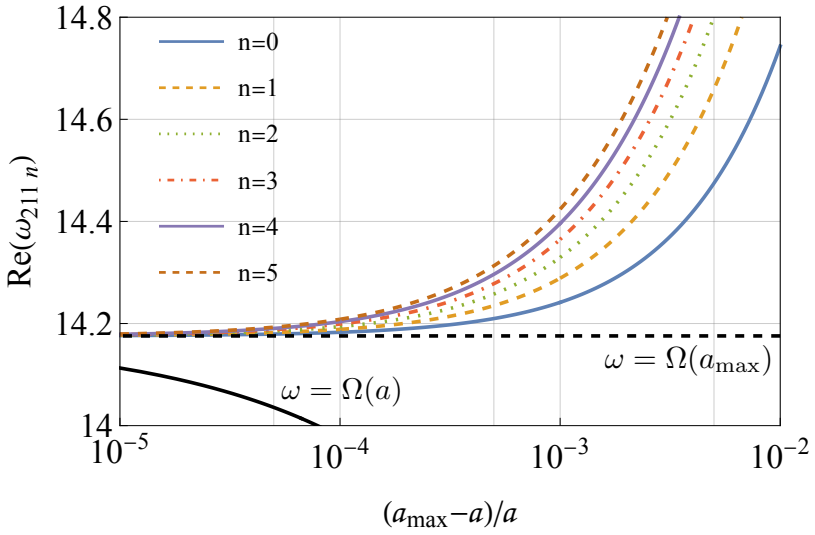

Figure 5.9: Plot of asymptotic value of real part for small black hole case. The parameters are $M = 10^{-2}, \mu - 10^{-2}$ and angular modes are $(l, m_1, m_2) = (2, 1, 1)$. In this plot, the vertical axis is scaled to $a_{\max}$. The black solid line shows the superradiant frequency as a function of a, and black dashed line represents Ω for the limit of $a \to a_{\max}$.

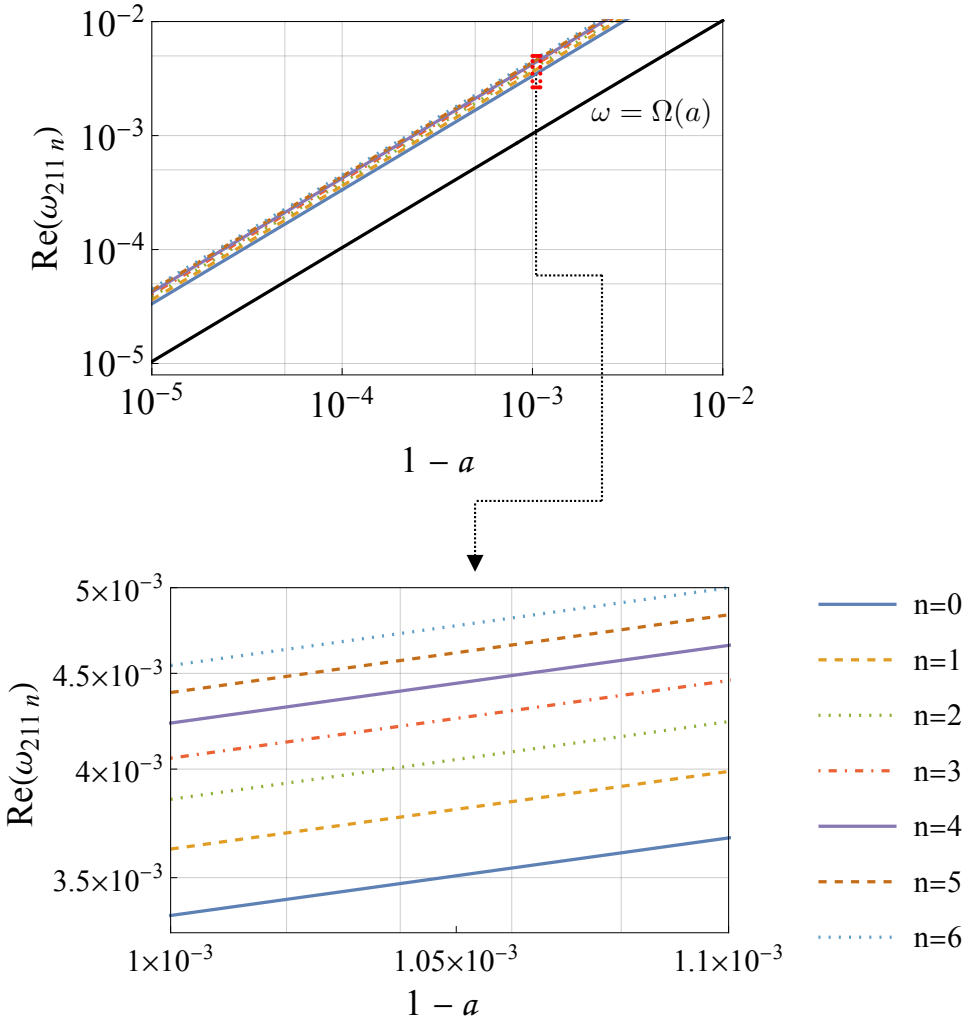

Figure 5.10: Plot of asymptotic value of real part for large black hole case. The parameters are $M = 10, \mu - 10^{-2}$ and angular modes are $(l, m_1, m_2) = (2, 1, 1)$. The lower figure shows an enlarged view of the region at $1 \times 10^{-3} \leq 1 - a \leq 1.1 \times 10^{-3}$.

5.5 Quasi-normal Modes vs. Catalytic effect

Finally, we compare the time scales, including the lifetime of the vacuum due to catalysis and the time scale of the superradiant instability. The lifetime of the vacuum can be obtained using the bounce action we investigated in Sec. 4.3. The lifetime and bounce action are related:

$$\tau_{\rm vacuum} = \frac{1}{\Gamma}, \qquad \Gamma = Ae^{-B}, \tag{5.5.1}$$

where B is the bounce action, and A is the pre-factor that comes from the zero modes of the instanton and the loop corrections, and is usually determined by a dimensional analysis. Here, we assume that $A = 1/r_+$ as the pre-factor because this determines the typical size of the nucleated bubble, and this assumption has been adopted in the previous studies [53, 58, 54].

The other timescale is the classical instability due to superradiance. This instability is studied using the quasi-normal modes and is related to the sign of the imaginary part. If the imaginary parts of the quasi-normal modes are positive, the amplitudes of the perturbation diverges exponentially with the time evolution $e^{{\rm Im}(\omega){\rm t}}$. Then, the time scale of this instability is given as follows:

$$\tau_{\rm SR} = \frac{1}{\max\left[{\rm Im}(\omega)\right]}, \tag{5.5.2}$$

where $\max\left[{\rm Im}(\omega)\right]$ is the value of the maximum positive imaginary part. This is because the quasi-normal modes arise when the frequency satisfies the superradiant frequency, and in general we do not know which mode expresses the largest instability. Thus, we here denote this most unstable mode as $\max\left[{\rm Im}(\omega)\right]$.

We derived the formulas of the two timescales and plotted for several values of parameters, comparing these in Fig. 5.11. From this figure the timescale of the classical instability is always longer. This means that even though Kerr-AdS$_5$ spacetime has a classical instability, the "bubble universe" scenario is realizable.

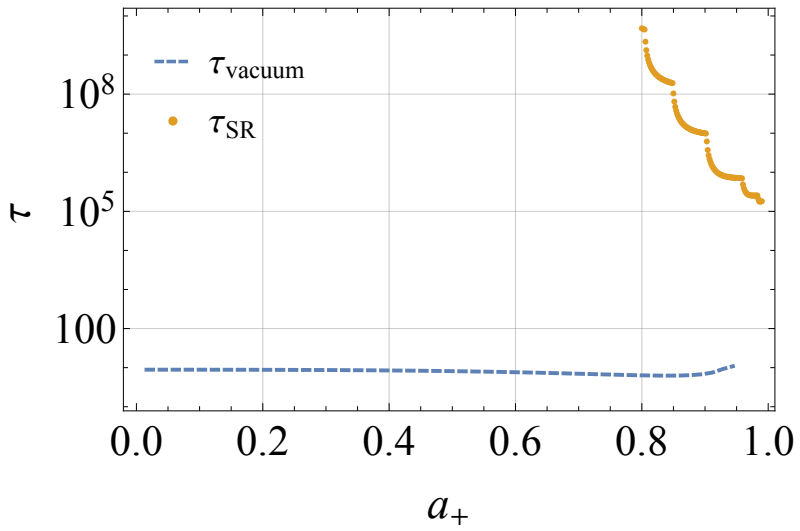

Figure 5.11: Plot of τ_{SR} and τ_{vacuum} as a function of the spinparameter a_+ for the parameters $\mu = 10^{-2}, M_+ = 2, l_+ = 7, l_- = 4$, where τ_{vacuum} is evaluated as a stationary solution, and τ_{SR} is evaluated as the mode that indicates the largest instability. Note that τ_{SR} is evaluated for the black hole in a false vacuum.

Chapter 6

Conclusion

In this thesis, we considered Kerr-AdS$_5$ spacetime in relation to the catalytic effects of the vacuum decay and quasi-normal modes having the motivation to apply to the "bubble universe" scenario, including the catalytic effects of other objects in five dimensions, such as a Schwarzschild black hole, a cloud of strings, and quintessence. We showed that objects in five dimensions also have a catalytic effect. Here, we briefly summarize the contents of this thesis.

In Chap. 4, we investigated the catalysis effect in five dimensions. In the bubble universe setup, the catalysis of a black hole and a cloud of strings were not considered, but we revealed that they play a role in the catalysis of the vacuum decay. This result could be extended to discuss the more realistic bubble nucleation.

The same chapter evaluated the catalysis of a rotating black hole in 5D AdS spacetime (Kerr-AdS$_5$). Because of the rotation, the spacetime is no longer spherically symmetric, and we used the rotating shell as a junction surface. The junction conditions were derived for this setup, and we calculated the Euclidean action. We numerically estimated the action and found that the rotation can enhance the vacuum decay slightly, and the stationary bounce solution gives the most probable process, which is the same as the results for the 4D and 5D spherical symmetric cases. We also found the parameter where the bounce action could have a negative value, and that this process naively violates the semi-classical approximation. On the other hand, based on the second law of thermodynamics, this process can be regarded as a thermal transition with an increase of entropy. Thus, we may accept that in this parameter region, the vacuum decay is nucleated by the thermal effect of the black hole.

In Chap. 5, we investigated the quasi-normal modes of Kerr-AdS$_5$ spacetime, and discussed the instability, thermal properties. First, we found that there are two types of quasi-normal modes for Kerr-AdS$_5$ spacetime. Type-I is a mode that corresponds to the resonance between the black hole ergo region and AdS boundary, which causes a spacetime instability. Type-II is a mode that reflects the thermal property of the black hole because the spacing of the imaginary part ($\Delta \mathrm{Im}(\omega_{lm_1m_2n})$) approaches $2\pi T_H$. We further investigated the spin effect on the instability, increment of the spin, and hierarchy of spins. We showed that the spin enhances the instability and hierarchy, which results in a symmetry reduction also enhances the instability. The instabilities of the quasi-normal modes are related with the superradiant instability of the black hole, and this phenomenon has the threshold to occur. We confirmed that the unstable modes arise if the quasi-normal frequencies satisfy this condition.

Finally, we compare two time scales, the lifetime due to the catalysis of the vacuum decay and the classical instability studied based on the quasi-normal modes. We found that at values of parameters the time scale of the classical instability is always longer. We showed that a bubble universe can be realized by the nucleation around a rotating black hole even though the rotating black hole is unstable due to the superradiant instability.

In conclusion, we have some comments about the contents as a whole. We studied Kerr-AdS$_5$ spacetime in relation to the quasi-normal modes and catalytic effect of the vacuum decay based on a strong motivation to resolve the open question about the very beginning of the universe, and our study was based on the bubble universe setup. We extended this model to a rotating black hole and showed that this scenario can be realized for a large framework, without considering the localization of matter, inflation, big-bang, and other conditions that the universe must have. A consideration of these properties still remains as future work, although we hope that our study will provide some insight or make a contribution to other studies attempting to answer the open questions of modern physics, especially those in cosmology, from a higher dimensional point of view.

Appendix A

Hod's Conjecture -Black Hole Area Quantization-

In this appendix we introduce Hod's conjecture [42], which addresses the black hole quantization using the asymptotic value quasi-normal modes. We start with Schwartzschild black hole with mass M. The horizon area of the black hole is:

$$\mathcal{A}_h = 4\pi r_h^2 = 16\pi M^2. \tag{A.0.1}$$

Then, we drop the object with mass m to the black hole, and the area of the horizon changes according to the mass gained from the black hole:

$$\Delta\mathcal{A}_h = 16\pi(M+m)^2 - 16\pi M^2 = 32\pi M\Delta M, \tag{A.0.2}$$

where we assume that $m \ll M$ and $m = \Delta M$. On the other hand, giving the perturbation to the black hole corresponds to exchanging the energy and may change its mass. Then we assume the quasi-normal frequency is related to the energy:

$$E = \Delta M = \hbar\omega. \tag{A.0.3}$$

Combining (A.0.2) and (A.0.3), we get:

$$\Delta\mathcal{A}_h = 32\pi M\hbar\omega. \tag{A.0.4}$$

This formula suggests that the quasi-normal frequency is related to the area of the black hole. Hod discussed this relation based on the Bohr's correspondence principle: "the classical limit of quantum theory (large quantum

numbers) should be equal to the classical one." The quasi-normal modes that were showed at (3.1.24), indicates the asymptotic behavior of a large n. Because a large n quasi-normal frequency has a large negative imaginary part, which corresponds to the damping of the frequency, the relaxation times, $\tau = 1/\mathrm{Im}(\omega)$, of these modes are very small. If we take $n \to \infty$, the relaxation time becomes $\tau \to 0$. In this limit, we assume that the energy exchange occurs as a quantum transition, which is the Bohr's correspondence principle. Then, (3.1.24) can be expressed for the general black hole mass case:

$$M\omega = 0.0437123 - \frac{i}{4}\left(\frac{1}{2}n + 0.5\right) + O[(n+1)^{-1/2}]. \tag{A.0.5}$$

The real part of (A.0.5) is related to the energy quanta exchanged at the $\tau \to 0$ limit. Then, Hod boldly regarded this value as $\mathrm{Re}(\omega) = 0.0437123 \approx \ln 3/8\pi$,[1]. Using this, the minimum value of the black hole area is estimated as follows:

$$\Delta A_{\min} = 32\pi\hbar\frac{\ln 3}{8\pi} = 4\hbar \ln 3 = 4\ell_p^2 \ln 3, \tag{A.0.6}$$

where

$$\ell_p = \sqrt{\hbar} \tag{A.0.7}$$

is the Planck length ($G = c = 1$). Here, we remember the relation between the entropy of the black hole and its area [70, 71, 72]:

$$S_{\mathrm{BH}} = \frac{\mathcal{A}}{4\hbar} = \frac{\mathcal{A}}{4\ell_p^2}, \tag{A.0.8}$$

and this entropy is assumed to be derived from the micro-states at the horizon,

$$S_{\mathrm{BH}} = \ln n = \frac{\mathcal{A}}{4\ell_p^2}, \tag{A.0.9}$$

$$\mathcal{A} = 4\ell_p^2 \ln 3, \tag{A.0.10}$$

where n is the number of micro-states of the black hole at the horizon. If we choose $n = 3$, the horizon area agrees with the result. It is surprising that

[1]This value is evaluated up to 50 digits as $\ln 3/8\pi = 0.04371239407075747224968391026484151146162986082014$0.

two results derived independently (A.0.6) and (A.0.10) are the same, but it is unclear why this unique value, $n = 3$, was selected.

One of the interpretations of this result was suggested by Dreyer [43]. He pointed out that there is some relation with the loop quantum gravity. Here, we simply introduce the result. In the loop quantum gravity, the spacetime is discretized, and the area also has a discrete value[2]:

$$\mathcal{A} = 8\pi\ell_p^2\gamma \sum_i \sqrt{j_i(j_i+1)} \tag{A.0.11}$$

where $j = 0, 1/2, 1, 3/2, \cdots$, and γ is the Immirzi parameter that arises in the loop quantum gravity, where there is no principle to determine to specific value [120]. It is also shown that the entropy of the black hole is given by the lowest possible spin [121, 122]:

$$S = \frac{A \ln(2j_{min}+1)}{8\pi\gamma\ell_p^2\sqrt{j_{min}(j_{min}+1)}}. \tag{A.0.12}$$

Then, we assume that the smallest area (smallest j) corresponds to the smallest area of the black hole:

$$\mathcal{A}_{\min} = \Delta\mathcal{A} = 8\pi\ell_p^2\gamma \sum_i \sqrt{j_{\min}(j_{\min}+1)}. \tag{A.0.13}$$

By comparing (A.0.13) with (A.0.10), we can obtain the Immirzi parameter using j_{min}:

$$\gamma = \frac{\ln 3}{2\pi\sqrt{j_{min}(j_{min}+1)}}. \tag{A.0.14}$$

Substituting this into (A.0.12),

$$S = \frac{A}{4\ell_p^2}\frac{\ln(2j_{min}+1)}{\ln 3}, \tag{A.0.15}$$

and supposing that this is equal to the Beckenstein entropy (A.0.8),

$$j_{\min} = 1, \tag{A.0.16}$$

[2]A spin network provides the basis of the Hilbert space of the loop quantum gravity, and the representation of the gauge group labels the edge of the graphs. Here, we use the result that the group is SU(2).

is derived. This is also surprising because the results of two different derivations coincide. Naively, $j_{\min} = 1/2$ is preferable, but there is no unified understanding of this and it still remains as an open question. In addition to this result, Tamaki et al. investigated the quasi-normal modes of the GM-GHS solution and showed that the asymptotic value is the same as that in the 4D Schwarzschild case [44].

A.1 Asymptotic value of real part

In this section we give some arguments of the asymptotic value of real part. The thermodynamics of a Kerr-AdS$_5$ black hole give the following relation [116]:

$$\Delta\mathcal{M} = T_{\mathrm{H}}\frac{\Delta A}{4G} + \sum_{i=1}^{2}\Omega_i \Delta J_i. \tag{A.1.1}$$

Remembering the correspondence of the asymptotic value of the quasi-normal modes and the quantization of the black hole area:

$$\Delta M = \lim_{n\to\infty} \mathrm{Re}(\omega). \tag{A.1.2}$$

Assuming that $\Delta J_i = m_i$, we naively combining these formulas produces the following relation:

$$T_{\mathrm{H}}\frac{\Delta A}{4G} = 0. \tag{A.1.3}$$

This result shows that in the case of $T_H \neq 0$, the horizon spacing is zero, but we have no further understanding of this result and we have just shown up to $n = 5$, so the higher modes may behave differently. In addition, an ultra-spinning Kerr-AdS$_4$ black hole can have a singular horizon [123, 124, 125], and a similar situation can be realized for a Kerr-AdS$_5$ back hole. Thus, further analysis is needed to obtain a certain result for area quantization. Anyway we show an initial insight into area quantization for a Kerr-AdS$_5$ black hole.

Bibliography

[1] A. Zhidenko, *Quasinormal modes of Schwarzschild de Sitter black holes*, *Class. Quant. Grav.* **21** (2004) 273 [gr-qc/0307012].

[2] Planck collaboration, *Planck 2018 results. VI. Cosmological parameters*, *Astron. Astrophys.* **641** (2020) A6 [1807.06209].

[3] A. Starobinsky, *A new type of isotropic cosmological models without singularity*, *Physics Letters B* **91** (1980) 99.

[4] K. Sato, *First-order phase transition of a vacuum and the expansion of the Universe*, *Monthly Notices of the Royal Astronomical Society* **195** (1981) 467.

[5] D. Kazanas, *Dynamics of the Universe and Spontaneous Symmetry Breaking*, *Astrophys. J. Lett.* **241** (1980) L59.

[6] A.H. Guth, *The Inflationary Universe: A Possible Solution to the Horizon and Flatness Problems*, *Phys. Rev. D* **23** (1981) 347.

[7] A.D. Linde, *A New Inflationary Universe Scenario: A Possible Solution of the Horizon, Flatness, Homogeneity, Isotropy and Primordial Monopole Problems*, *Phys. Lett. B* **108** (1982) 389.

[8] A.D. Linde, *Chaotic Inflation*, *Phys. Lett. B* **129** (1983) 177.

[9] A. Albrecht and P.J. Steinhardt, *Cosmology for Grand Unified Theories with Radiatively Induced Symmetry Breaking*, *Phys. Rev. Lett.* **48** (1982) 1220.

[10] K. Freese, J.A. Frieman and A.V. Olinto, *Natural inflation with pseudo - Nambu-Goldstone bosons*, *Phys. Rev. Lett.* **65** (1990) 3233.

[11] A.D. Linde, *Hybrid inflation*, *Phys. Rev. D* **49** (1994) 748 [astro-ph/9307002].

[12] D. Polarski and A.A. Starobinsky, *Spectra of perturbations produced by double inflation with an intermediate matter dominated stage*, *Nucl. Phys. B* **385** (1992) 623.

[13] E. Silverstein and D. Tong, *Scalar speed limits and cosmology: Acceleration from D-cceleration*, *Phys. Rev. D* **70** (2004) 103505 [hep-th/0310221].

[14] Supernova Search Team collaboration, *Observational evidence from supernovae for an accelerating universe and a cosmological constant*, *Astron. J.* **116** (1998) 1009 [astro-ph/9805201].

[15] Supernova Cosmology Project collaboration, *Measurements of Ω and Λ from 42 high redshift supernovae*, *Astrophys. J.* **517** (1999) 565 [astro-ph/9812133].

[16] W. Lerche, D. Lust and A.N. Schellekens, *Chiral Four-Dimensional Heterotic Strings from Selfdual Lattices*, *Nucl. Phys. B* **287** (1987) 477.

[17] L. Susskind, *The Anthropic landscape of string theory*, hep-th/0302219.

[18] S. Kachru, R. Kallosh, A.D. Linde and S.P. Trivedi, *De Sitter vacua in string theory*, *Phys. Rev. D* **68** (2003) 046005 [hep-th/0301240].

[19] V. Balasubramanian, P. Berglund, J.P. Conlon and F. Quevedo, *Systematics of moduli stabilisation in Calabi-Yau flux compactifications*, *JHEP* **03** (2005) 007 [hep-th/0502058].

[20] H. Ooguri and C. Vafa, *On the Geometry of the String Landscape and the Swampland*, *Nucl. Phys. B* **766** (2007) 21 [hep-th/0605264].

[21] N. Arkani-Hamed, L. Motl, A. Nicolis and C. Vafa, *The String landscape, black holes and gravity as the weakest force*, *JHEP* **06** (2007) 060 [hep-th/0601001].

[22] G. Obied, H. Ooguri, L. Spodyneiko and C. Vafa, *De Sitter Space and the Swampland*, 1806.08362.

[23] H. Ooguri, E. Palti, G. Shiu and C. Vafa, *Distance and de Sitter Conjectures on the Swampland*, *Phys. Lett. B* **788** (2019) 180 [1810.05506].

[24] A. Bedroya and C. Vafa, *Trans-Planckian Censorship and the Swampland*, *JHEP* **09** (2020) 123 [1909.11063].

[25] S. Banerjee, U. Danielsson, G. Dibitetto, S. Giri and M. Schillo, *de Sitter Cosmology on an expanding bubble*, *JHEP* **10** (2019) 164 [1907.04268].

[26] W. Israel, *Singular hypersurfaces and thin shells in general relativity*, *Nuovo Cim. B* **44S10** (1966) 1.

[27] P. Bizon and A. Rostworowski, *On weakly turbulent instability of anti-de Sitter space*, *Phys. Rev. Lett.* **107** (2011) 031102 [1104.3702].

[28] O.J.C. Dias, G.T. Horowitz and J.E. Santos, *Gravitational Turbulent Instability of Anti-de Sitter Space*, *Class. Quant. Grav.* **29** (2012) 194002 [1109.1825].

[29] R. Penrose and R. Floyd, *Extraction of rotational energy from a black hole*, *Nature Physical Science* **229** (1971) 177.

[30] Y.B. Zel'Dovich, *Generation of Waves by a Rotating Body*, *Soviet Journal of Experimental and Theoretical Physics Letters* **14** (1971) 180.

[31] C.W. Misner, *Interpretation of gravitational-wave observations*, *Phys. Rev. Lett.* **28** (1972) 994.

[32] A.A. Starobinsky, *Amplification of waves reflected from a rotating "black hole".*, *Sov. Phys. JETP* **37** (1973) 28.

[33] V. Cardoso and O.J.C. Dias, *Small Kerr-anti-de Sitter black holes are unstable*, *Phys. Rev. D* **70** (2004) 084011 [hep-th/0405006].

[34] J. Barragán Amado, B. Carneiro Da Cunha and E. Pallante, *Scalar quasinormal modes of Kerr-AdS$_5$*, *Phys. Rev. D* **99** (2019) 105006 [1812.08921].

[35] B.C. da Cunha and J.a.P. Cavalcante, *Teukolsky master equation and Painlevé transcendents: Numerics and extremal limit*, *Phys. Rev. D* **104** (2021) 084051 [2105.08790].

[36] J.B. Amado, B. Carneiro da Cunha and E. Pallante, *Vector perturbations of Kerr-AdS$_5$ and the Painlevé VI transcendent*, *JHEP* **04** (2020) 155 [2002.06108].

[37] J. Barragán Amado, B. Carneiro da Cunha and E. Pallante, *Remarks on holographic models of the Kerr-AdS$_5$ geometry*, *JHEP* **05** (2021) 251 [2102.02657].

[38] J.B. Amado, B.C. da Cunha and E. Pallante, *QNMs of scalar fields on small Reissner-Nordström-AdS$_5$ black holes*, 2110.08349.

[39] I. Koga, N. Oshita and K. Ueda, *Global study of the scalar quasinormal modes of Kerr-AdS5 black holes: Stability, thermality, and horizon area quantization*, *Phys. Rev. D* **105** (2022) 124044 [2201.07267].

[40] H.-P. Nollert, *Quasinormal modes of Schwarzschild black holes: The determination of quasinormal frequencies with very large imaginary parts*, *Phys. Rev. D* **47** (1993) 5253.

[41] L. Motl and A. Neitzke, *Asymptotic black hole quasinormal frequencies*, *Adv. Theor. Math. Phys.* **7** (2003) 307 [hep-th/0301173].

[42] S. Hod, *Bohr's correspondence principle and the area spectrum of quantum black holes*, *Phys. Rev. Lett.* **81** (1998) 4293 [gr-qc/9812002].

[43] O. Dreyer, *Quasinormal modes, the area spectrum, and black hole entropy*, *Phys. Rev. Lett.* **90** (2003) 081301 [gr-qc/0211076].

[44] T. Tamaki and H. Nomura, *The Universal area spectrum in single-horizon black holes*, *Phys. Rev. D* **70** (2004) 044041 [hep-th/0405191].

[45] J.M. Maldacena, *The Large N limit of superconformal field theories and supergravity*, *Adv. Theor. Math. Phys.* **2** (1998) 231 [hep-th/9711200].

[46] E. Witten, *Anti-de Sitter space and holography*, *Adv. Theor. Math. Phys.* **2** (1998) 253 [hep-th/9802150].

[47] D. Birmingham, I. Sachs and S.N. Solodukhin, *Conformal field theory interpretation of black hole quasinormal modes*, *Phys. Rev. Lett.* **88** (2002) 151301 [hep-th/0112055].

[48] S.R. Coleman, *The Fate of the False Vacuum. 1. Semiclassical Theory*, *Phys. Rev. D* **15** (1977) 2929.

[49] C.G. Callan, Jr. and S.R. Coleman, *The Fate of the False Vacuum. 2. First Quantum Corrections*, *Phys. Rev. D* **16** (1977) 1762.

[50] S.R. Coleman and F. De Luccia, *Gravitational Effects on and of Vacuum Decay*, *Phys. Rev. D* **21** (1980) 3305.

[51] W.A. Hiscock, *CAN BLACK HOLES NUCLEATE VACUUM PHASE TRANSITIONS?*, *Phys. Rev. D* **35** (1987) 1161.

[52] V.A. Berezin, V.A. Kuzmin and I.I. Tkachev, *O(3) Invariant Tunneling in General Relativity*, *Phys. Lett. B* **207** (1988) 397.

[53] R. Gregory, I.G. Moss and B. Withers, *Black holes as bubble nucleation sites*, *JHEP* **03** (2014) 081 [1401.0017].

[54] P. Burda, R. Gregory and I. Moss, *Vacuum metastability with black holes*, *JHEP* **08** (2015) 114 [1503.07331].

[55] N. Oshita, K. Ueda and M. Yamaguchi, *Vacuum decays around spinning black holes*, *JHEP* **01** (2020) 015 [1909.01378].

[56] D. Saito and C.-M. Yoo, *Stationary Vacuum Bubble in a Kerr-de Sitter Spacetime*, 2208.07504.

[57] D. Saito and C.-M. Yoo, *False vacuum decay in rotating BTZ spacetimes*, *Phys. Rev. D* **104** (2021) 124037 [2109.04051].

[58] P. Burda, R. Gregory and I. Moss, *The fate of the Higgs vacuum*, *JHEP* **06** (2016) 025 [1601.02152].

[59] K. Kohri and H. Matsui, *Electroweak Vacuum Collapse induced by Vacuum Fluctuations of the Higgs Field around Evaporating Black Holes*, *Phys. Rev. D* **98** (2018) 123509 [1708.02138].

[60] I. Koga, S. Kuroyanagi and Y. Ookouchi, *Instability of Higgs Vacuum via String Cloud*, *Phys. Lett. B* **800** (2020) 135093 [1910.02435].

[61] I. Koga and Y. Ookouchi, *Catalytic creation of baby bubble universe with small positive cosmological constant*, *JHEP* **10** (2019) 281 [1909.03014].

[62] I. Koga and Y. Ookouchi, *Catalytic creation of a bubble universe induced by quintessence in five dimensions*, *Phys. Rev. D* **104** (2021) 126015 [2011.07437].

[63] I. Koga, N. Oshita and K. Ueda, *dS_4 universe emergent from Kerr-AdS_5 spacetime: bubble nucleation catalyzed by a black hole*, 2209.05625.

[64] T. Banks, C.M. Bender and T.T. Wu, *Coupled anharmonic oscillators. 1. Equal mass case*, *Phys. Rev. D* **8** (1973) 3346.

[65] T. Banks and C.M. Bender, *Coupled anharmonic oscillators. ii. unequal-mass case*, *Phys. Rev. D* **8** (1973) 3366.

[66] S.R. Coleman, V. Glaser and A. Martin, *Action Minima Among Solutions to a Class of Euclidean Scalar Field Equations*, *Commun. Math. Phys.* **58** (1978) 211.

[67] R.L. Arnowitt, S. Deser and C.W. Misner, *Dynamical Structure and Definition of Energy in General Relativity*, *Phys. Rev.* **116** (1959) 1322.

[68] N. Hidekazu, *On a new cosmological solution of Einstein's field equations of gravitation*, *Sci. Rep. Tohoku Univ. Eighth Ser.* **35** (1951) 46.

[69] H. Nariai, *On some static solutions of Einstein's gravitational field equations in a spherically symmetric case*, *Sci. Rep. Tohoku Univ. Eighth Ser.* **34** (1950) 160.

[70] J.D. Bekenstein, *Black holes and entropy*, *Phys. Rev. D* **7** (1973) 2333.

[71] J.D. Bekenstein, *Generalized second law of thermodynamics in black hole physics*, *Phys. Rev. D* **9** (1974) 3292.

[72] S.W. Hawking, *Black Holes and Thermodynamics*, *Phys. Rev. D* **13** (1976) 191.

[73] U.H. Danielsson and T. Van Riet, *What if string theory has no de Sitter vacua?*, *Int. J. Mod. Phys. D* **27** (2018) 1830007 [1804.01120].

[74] P.S. Letelier, *CLOUDS OF STRINGS IN GENERAL RELATIVITY*, *Phys. Rev. D* **20** (1979) 1294.

[75] J. Stachel, *THICKENING THE STRING. I. THE STRING PERFECT DUST*, *Phys. Rev. D* **21** (1980) 2171.

[76] S. Chakrabortty, *Dissipative force on an external quark in heavy quark cloud*, *Phys. Lett. B* **705** (2011) 244 [1108.0165].

[77] S. Banerjee, U. Danielsson and S. Giri, *Dark bubbles and black holes*, *JHEP* **09** (2021) 158 [2102.02164].

[78] L. Randall and R. Sundrum, *A Large mass hierarchy from a small extra dimension*, *Phys. Rev. Lett.* **83** (1999) 3370 [hep-ph/9905221].

[79] L. Randall and R. Sundrum, *An Alternative to compactification*, *Phys. Rev. Lett.* **83** (1999) 4690 [hep-th/9906064].

[80] S. Banerjee, U. Danielsson and S. Giri, *Bubble needs strings*, *JHEP* **21** (2020) 250 [2009.01597].

[81] U. Danielsson, D. Panizo and R. Tielemans, *Gravitational waves in dark bubble cosmology*, *Phys. Rev. D* **106** (2022) 024002 [2202.00545].

[82] U.H. Danielsson, D. Panizo, R. Tielemans and T. Van Riet, *Higher-dimensional view on quantum cosmology*, *Phys. Rev. D* **104** (2021) 086015 [2105.03253].

[83] J.D. Brown and C. Teitelboim, *Neutralization of the Cosmological Constant by Membrane Creation*, *Nucl. Phys. B* **297** (1988) 787.

[84] G. D'Amico, R. Gobbetti, M. Kleban and M. Schillo, *D-brane scattering and annihilation*, *JHEP* **01** (2015) 050 [1408.2540].

[85] G. D'Amico, R. Gobbetti, M. Kleban and M. Schillo, *Unwinding Inflation*, *JCAP* **03** (2013) 004 [1211.4589].

[86] T. Regge and J.A. Wheeler, *Stability of a Schwarzschild singularity*, *Phys. Rev.* **108** (1957) 1063.

[87] E.W. Leaver, *An Analytic representation for the quasi normal modes of Kerr black holes*, *Proc. Roy. Soc. Lond. A* **402** (1985) 285.

[88] W. Gautschi, *Computational aspects of three-term recurrence relations*, *SIAM Review* **9** (1967) 24 [https://doi.org/10.1137/1009002].

[89] H. Suzuki, E. Takasugi and H. Umetsu, *Perturbations of Kerr-de Sitter black hole and Heun's equations*, *Prog. Theor. Phys.* **100** (1998) 491 [gr-qc/9805064].

[90] Y. Hatsuda, *Quasinormal modes of Kerr-de Sitter black holes via the Heun function*, *Class. Quant. Grav.* **38** (2020) 025015 [2006.08957].

[91] S.A. Teukolsky, *Rotating black holes - separable wave equations for gravitational and electromagnetic perturbations*, *Phys. Rev. Lett.* **29** (1972) 1114.

[92] E.J. Copeland, M. Sami and S. Tsujikawa, *Dynamics of dark energy*, *Int. J. Mod. Phys. D* **15** (2006) 1753 [hep-th/0603057].

[93] S. Tsujikawa, *Quintessence: A Review*, *Class. Quant. Grav.* **30** (2013) 214003 [1304.1961].

[94] V.V. Kiselev, *Quintessence and black holes*, *Class. Quant. Grav.* **20** (2003) 1187 [gr-qc/0210040].

[95] J. de M. Toledo and V.B. Bezerra, *Black holes with cloud of strings and quintessence in Lovelock gravity*, *Eur. Phys. J. C* **78** (2018) 534.

[96] M. Chabab and S. Iraoui, *Thermodynamic criticality of d-dimensional charged AdS black holes surrounded by quintessence with a cloud of strings background*, *Gen. Rel. Grav.* **52** (2020) 75 [2001.06063].

[97] R.C. Myers and M.J. Perry, *Black Holes in Higher Dimensional Space-Times*, *Annals Phys.* **172** (1986) 304.

[98] S.W. Hawking, C.J. Hunter and M. Taylor, *Rotation and the AdS / CFT correspondence*, *Phys. Rev. D* **59** (1999) 064005 [hep-th/9811056].

[99] G.W. Gibbons, H. Lu, D.N. Page and C.N. Pope, *Rotating black holes in higher dimensions with a cosmological constant*, *Phys. Rev. Lett.* **93** (2004) 171102 [hep-th/0409155].

[100] T. Delsate, J.V. Rocha and R. Santarelli, *Collapsing thin shells with rotation*, *Phys. Rev. D* **89** (2014) 121501 [1405.1433].

[101] J.V. Rocha, *Gravitational collapse with rotating thin shells and cosmic censorship*, *Int. J. Mod. Phys. D* **24** (2015) 1542002 [1501.06724].

[102] L. Herrera, A. Di Prisco, J. Ibáñez and J. Ospino, *Dissipative collapse of axially symmetric, general relativistic, sources: A general framework and some applications*, *Phys. Rev. D* **89** (2014) 084034 [1404.1176].

[103] Z.C. Wu, *Creation of Kerr-de Sitter black hole in all dimensions*, *Phys. Lett. B* **613** (2005) 1 [gr-qc/0412041].

[104] W.H. Press and S.A. Teukolsky, *Floating Orbits, Superradiant Scattering and the Black-hole Bomb*, *Nature* **238** (1972) 211.

[105] V. Cardoso, O.J.C. Dias, J.P.S. Lemos and S. Yoshida, *The Black hole bomb and superradiant instabilities*, *Phys. Rev. D* **70** (2004) 044039 [hep-th/0404096].

[106] T. Damour, N. Deruelle and R. Ruffini, *On Quantum Resonances in Stationary Geometries*, *Lett. Nuovo Cim.* **15** (1976) 257.

[107] S.L. Detweiler, *KLEIN-GORDON EQUATION AND ROTATING BLACK HOLES*, *Phys. Rev. D* **22** (1980) 2323.

[108] T.J.M. Zouros and D.M. Eardley, *INSTABILITIES OF MASSIVE SCALAR PERTURBATIONS OF A ROTATING BLACK HOLE*, *Annals Phys.* **118** (1979) 139.

[109] H. Furuhashi and Y. Nambu, *Instability of massive scalar fields in Kerr-Newman space-time*, *Prog. Theor. Phys.* **112** (2004) 983 [gr-qc/0402037].

[110] G.T. Horowitz and V.E. Hubeny, *Quasinormal modes of AdS black holes and the approach to thermal equilibrium*, *Phys. Rev. D* **62** (2000) 024027 [hep-th/9909056].

[111] V. Cardoso, R. Konoplya and J.P.S. Lemos, *Quasinormal frequencies of Schwarzschild black holes in anti-de Sitter space-times: A Complete study on the asymptotic behavior*, *Phys. Rev. D* **68** (2003) 044024 [gr-qc/0305037].

[112] V. Cardoso and J.P.S. Lemos, *New instability for rotating black branes and strings*, *Phys. Lett. B* **621** (2005) 219 [hep-th/0412078].

[113] S.W. Hawking and H.S. Reall, *Charged and rotating AdS black holes and their CFT duals*, *Phys. Rev. D* **61** (2000) 024014 [hep-th/9908109].

[114] V. Cardoso and S. Yoshida, *Superradiant instabilities of rotating black branes and strings*, *JHEP* **07** (2005) 009 [hep-th/0502206].

[115] O.J.C. Dias, *Superradiant instability of large radius doubly spinning black rings*, *Phys. Rev. D* **73** (2006) 124035 [hep-th/0602064].

[116] G.W. Gibbons, M.J. Perry and C.N. Pope, *The First law of thermodynamics for Kerr-anti-de Sitter black holes*, *Class. Quant. Grav.* **22** (2005) 1503 [hep-th/0408217].

[117] S. Hollands, A. Ishibashi and D. Marolf, *Comparison between various notions of conserved charges in asymptotically AdS-spacetimes*, *Class. Quant. Grav.* **22** (2005) 2881 [hep-th/0503045].

[118] R. Olea, *Regularization of odd-dimensional AdS gravity: Kounterterms*, *JHEP* **04** (2007) 073 [hep-th/0610230].

[119] A.N. Aliev and O. Delice, *Superradiant Instability of Five-Dimensional Rotating Charged AdS Black Holes*, *Phys. Rev. D* **79** (2009) 024013 [0808.0280].

[120] G. Immirzi, *Quantum gravity and Regge calculus*, *Nucl. Phys. B Proc. Suppl.* **57** (1997) 65 [gr-qc/9701052].

[121] C. Rovelli and L. Smolin, *Discreteness of area and volume in quantum gravity*, *Nucl. Phys. B* **442** (1995) 593 [gr-qc/9411005].

[122] A. Ashtekar and J. Lewandowski, *Quantum theory of geometry. 1: Area operators*, *Class. Quant. Grav.* **14** (1997) A55 [gr-qc/9602046].

[123] D. Klemm, *Four-dimensional black holes with unusual horizons*, *Phys. Rev. D* **89** (2014) 084007 [1401.3107].

[124] R.A. Hennigar, D. Kubizňák, R.B. Mann and N. Musoke, *Ultraspinning limits and super-entropic black holes*, *JHEP* **06** (2015) 096 [1504.07529].

[125] R.A. Hennigar, D. Kubizňák and R.B. Mann, *Entropy Inequality Violations from Ultraspinning Black Holes*, *Phys. Rev. Lett.* **115** (2015) 031101 [1411.4309].